ΕΘΝΙΚΟ ΜΕΤΣΟΒΙΟ ΠΟΛΥΤΕΧΝΕΙΟ
Εργαστήριο Ατμοκινητήρων & Λεβήτων
Τομέας Θερμότητας της Σχολής Μηχανολόγων Μηχανικών

ΔΙΠΛΩΜΑΤΙΚΗ ΕΡΓΑΣΙΑ

«EXPERIMENTAL PERFORMANCE INVESTIGATION OF GAS COOLER USED IN A SUPERCRITICAL CO_2 CYCLE»

«ΠΕΙΡΑΜΑΤΙΚΗ ΜΕΛΕΤΗ ΛΕΙΤΟΥΡΓΙΑΣ ΨΥΚΤΗ ΚΥΚΛΟΥ ΥΠΕΡΚΡΙΣΙΜΟΥ CO_2»

Του Φοιτητή
Αλεξόπουλου Χαράλαμπου

Επιβλέπων

Σωτήριος Καρέλλας, Καθηγητής,
Σχολή Μηχανολόγων Μηχανικών, ΕΜΠ

Αθήνα, Φεβρουάριος 2020

Περίληψη

Αυτή η διπλωματική εργασία αποτελεί μέρος ενός project στο Πανεπιστήμιο του Bayreuth. Το project αποσκοπεί στην μελέτη ενός αποδοτικού συστήματος κλιματισμού για οικιακές εφαρμογές με την χρήση φυσικών ψυκτικών υγρών. Το σύστημα στοχεύει στην κάλυψη των απαιτούμενων φορτίων κλιματισμού για πολυκατοικίες σε τέσσερις ευρωπαϊκές χώρες: Γερμανία (88 W/m²), Ισπανία (120 W/m²), Ελλάδα (143 W/m²), Κύπρος (180 W/m²). Με βάση αυτά τα φορτία, τρία συστήματα κλιματισμού ερευνήθηκαν, χρησιμοποιώντας διοξείδιο του άνθρακα (CO_2) για ψυκτικό μέσο.

Το CO_2 είναι ένα φυσικό, χαμηλού κόστους, μη εύφλεκτο, μη τοξικό ψυκτικό με καλές θερμοδυναμικές ιδιότητες. Για αυτό το λόγο έχει αναδειχθεί ως ένα αξιόπιστο φυσικό μέσο για την αντικατάσταση των HFCs. Τα συστήματα ψύξης με CO_2 χαρακτηρίζονται από τις υψηλές σχετικά πέσεις, επιβάλλοντας ιδιαίτερη προσοχή στον σχεδιασμό τέτοιων συστημάτων. Ιδιαίτερη προσοχή απαιτεί ο σχεδιασμός του συμπυκνωτή (gas cooler) που αποτελεί ένα από τα πιο κρίσιμα στοιχεία αυτών των συστημάτων. Ένας από τους πιο διαδεδομένους και καθιερωμένους τύπους εναλλάκτη για αυτές τις εφαρμογές είναι ο τύπος σωλήνων με πτερύγια.

Σε αυτή τη διατριβή, πραγματοποιήθηκε μια ανάλυση σχεδιασμού ενός οικονομικά αποδοτικού και αξιόπιστου εναλλάκτη τύπου σωλήνων με πτερύγια. Οι οριακές συνθήκες του συστήματος έχουν καθοριστεί με την χρήση του προγράμματος Aspen και με βάση αυτών, καθορίστηκε το σημείο σχεδιασμού του συστήματος. Επιπλέον, δύο διαφορετικά σημεία σχεδιασμού καθορίστηκαν με βάση την ύπαρξη inverter. Για τον σχεδιασμό του συμπυκνωτή (gas cooler) γράφτηκε κώδικας στην Matlab R2019a μελετώντας τρεις διαφορετικούς σωλήνες με πτερύγια και δύο αριθμούς σειρών. Τα αποτελέσματα δείχνουν ότι το σύστημα με inverter χρειάζεται μεγαλύτερο εναλλάκτη σε σχέση με το σύστημα χωρίς inverter. Εκτός αυτού, χρησιμοποιεί σωλήνες με πτερύγια με μεγαλύτερη εξωτερική διάμετρο. Πιο συγκεκριμένα, συμπυκνωτής με επιφάνεια συναλλαγής 2.106 m² και ένας σωλήνας με εξωτερική διάμετρο d_o = 0.0185 m υπολογίστηκε για το σύστημα με inverter. Για το σύστημα χωρίς inverter υπολογίστηκε συμπυκνωτής με επιφάνεια συναλλαγής 1.1697 m² και ένας σωλήνας με εξωτερική διάμετρο d_o = 0.00735 m.

Στην συνέχεια της διατριβής αυτής, πραγματοποιήθηκε μια ανάλυση της απόδοσης των εναλλακτών που σχεδιάστηκαν με βάση το σημείο σχεδιασμού. Οι υπολογισμοί έγιναν με την χρήση ενός κώδικα που δημιουργήθηκε στην Matlab R2019a. Ο κώδικας αυτός επικυρώθηκε με ένα πείραμα που πραγματοποιήθηκε στο Πανεπιστήμιο του Bayreuth. Για το πείραμα χρησιμοποιήθηκε ένα test-rig που βρισκόταν στο Πανεπιστήμιο. Η πειραματική διάταξη αποτελούταν από έναν συμπυκνωτή, θερμαντήρα, βαλβίδα ροής μάζας με κατάλληλο μετρητικό εξοπλισμό και νερό για ψυκτικό μέσο. Επιπλέον, τα πειράματα πραγματοποιήθηκαν για διαφορετικές θερμοκρασίες εισόδου νερού, συχνότητες ανεμιστήρα και παροχής μάζας νερού. Με αυτόν τον τρόπο, διεξήχθησαν αποκλίσεις μεταξύ των πειραματικών αποτελεσμάτων και των υπολογισμών και μεταξύ των σχέσεων για τους συντελεστές μεταφοράς θερμότητας για αέρα και ψυκτικό υγρό. Συγκεκριμένα για το συντελεστή μεταφορά θερμότητας από την πλευρά του ψυκτικού υγρού

χρησιμοποιήθηκαν οι σχέσεις του Gnielinski και του Dittus Boelter, ενώ για τον αέρα οι σχέσεις του VDI-Heat Atlas, Gianolo and Cuti, και Schmidt. Τα αποτελέσματα έδειξαν ότι οι αποκλίσεις μεταξύ των σχέσεων για την πλευρά του ψυκτικού υγρού είναι περίπου 1 %. Όσον αφορά τις αποκλίσεις μεταξύ των σχέσεων για την πλευρά του αέρα, η σχέση του VDI-Heat Atlas έδειξε τα πιο ακριβή αποτελέσματα, ενώ για την σχέση του Gianolo and Cuti έδειξαν σημαντική διαφορά. Συνολικά, τα πιο ακριβή αποτελέσματα ελήφθησαν εφαρμόζοντας τις σχέσεις VDI-Heat Atlas και Gnielinski για την πλευρά του αέρα και του ψυκτικού υγρού, αντίστοιχα. Τα αποτελέσματα, επίσης έδειξαν ότι οι αποκλίσεις επηρεάζονται ιδιαίτερα από την συχνότητα περιστροφής του ανεμιστήρα. Τελικά, οι υπολογισμοί του κώδικα προσεγγίζουν ικανοποιητικά τα πειραματικά αποτελέσματα για συχνότητες του ανεμιστήρα από 60 - 80 Hz. Οι αποκλίσεις σε αυτό το εύρος συχνοτήτων είναι περίπου 8 %.

Το τελευταίο κεφάλαιο της διατριβής αυτής εμπεριέχει την ανάλυση του συμπυκνωτή σε διαφορετικές συνθήκες από τις συνθήκες σχεδιασμού. Τα αποτελέσματα έδειξαν ότι ο COP του συστήματος με inverter είναι σημαντικά μεγαλύτερος. Πιο συγκεκριμένα, ο COP του συστήματος με inverter για θερμοκρασία περιβάλλοντος T_{amb} = 20 ° C είναι 4.6, ενώ ο COP του συστήματος χωρίς inverter είναι 4.3. Επιπλέον, το σύστημα χωρίς inverter δεν μπορεί να ακολουθήσει τα ευρωπαϊκά πρότυπα χωρίς άλλες εφαρμογές, όπως την ρύθμιση της πίεσης λειτουργίας του συστήματος. Από την άλλη πλευρά, το σύστημα με inverter συμβαδίζει με τα ευρωπαϊκά πρότυπα και επιτυγχάνει ευρωπαϊκό λόγο εποχιακής ενεργειακής απόδοσης (ESEER) 4.11. Αυτό σημαίνει ότι το σύστημα με inverter χαρακτηρίζεται από την κατηγορία A.

Abstract

This thesis is a part of a large project initiated by the University of Bayreuth, Energy Department. The project aims to develop an efficient air conditioning system for residential applications based on natural working fluids. The target of the system is to cover the required air conditioning loads for multi-family houses in four European countries: Germany (88 W/m²), Spain (120 W/m²), Greece (143 W/m²), Cyprus (180 W/m²). Based on those loads, three different refrigeration cycles for an air-conditioning system were investigated that use carbon dioxide (CO_2) as a working fluid.

CO_2 is a natural, low cost, non-flammable, non-toxic refrigerant with good thermophysical properties. Even if it has emerged as a credible natural refrigerant to replace HFCs, CO_2 refrigeration systems operate at relatively high pressures and this imposes special design and control considerations. The gas cooler is a very crucial component of these systems and can have a significant influence on their performance. The finned tube type for gas coolers is well established in the HVAC and refrigeration industries.

In this thesis, an on-design analysis of a cost-efficient and reliable detailed air finned gas cooler design has been carried out. The boundary conditions of the system have been defined and based on those, two different concepts have been investigated with respect to the use of an inverter. For both of them, the on-design point has been determined and thus a gas cooler's design has been defined. For this purpose, a script in Matlab R2019a has been created. The investigation included three potential finned tubes and two potential numbers of rows. The results show that the system with an inverter needs a bigger gas cooler as the gas cooler's duty is bigger. Besides, it uses finned tubes with bigger outside diameter. More specifically, a gas cooler with a bundle area of 2.106 m² and a finned tube with an outside diameter of d_o = 0.0185 m was defined for the system including an inverter. On the other hand, for the no-inverter system a gas cooler with a bundle area of 1.1697 m² and a finned tube with an outside diameter of d_o = 0.00735 m was defined.

Another aspect of the thesis is an analysis of the off-design performance of the gas coolers. A script in Matlab R2019a has been created and validated with an experiment carried out at the University of Bayreuth. A test rig was used consisting of a condenser, a heater, a mass flow valve and, appropriate measurements. The water was used as a refrigerant and the experiments were carried out for different water inlet temperatures, fan frequencies, and water mass flows. The off-design script was run regarding the experimental values and the deviations between the model and the experimental results were extracted. Besides that, a comparison between potential heat transfer correlations for the air side as well as the refrigerant side heat transfer coefficient has been extracted. Particularly, the Gnielinski and Dittus-Boelter correlation were used for the refrigerant side heat transfer coefficient and the VDI-Heat Atlas, Gianolo and Cuti and Schmidt correlations were used for the air side heat transfer coefficient. The results showed that the deviations between the refrigerant heat transfer correlations are about 1 %. As far as the deviations between the air-side heat transfer correlations, the VDI-Heat Atlas showed the most accurate results, while the Gianolo and Cuti showed significantly bigger deviations. The most accurate results were

obtained using the VDI-Heat Atlas and Gnielinski correlation for the air and refrigerant side, accordingly. The results showed that the deviations are highly-affected by the fan frequency and the script can approach adequately the experiments for fan frequencies from 60 – 80 Hz. The deviations in that fan frequency range are about 8 %.

The off-design performance for the two concepts has been investigated. The results showed that the COP of the system with an inverter is significantly higher. The COP of the inverter system for an ambient temperature of T_{amb} = 20 °C is 4.6 while the no-inverter system's COP is 4.3. Furthermore, the no-inverter system cannot follow the European seasonal energy efficiency standards without investigating other processes such as the regulation of the system's pressure process. On the other hand, the inverter system follows adequately the European seasonal energy efficiency standards with a European seasonal energy efficiency ratio of 4.11. That means the inverter system is characterized by the A energy efficient class.

Preface

This master's thesis has been a part of a project initiated by the University of Bayreuth, Center of Energy Technology (ZET).

First of all, I would like to express my sincere gratitude to Prof. Dr. –Ing. Sotirios Karellas, Professor at the National Technical University of Athens and to Dr. –Ing. Florian Heberle, Managing Director at the Center for Energy Technology (ZET), the University of Bayreuth for their support throughout this project, as well as, their advices have strongly inspired me.

Secondly, I would like to thank Tryfonas Roumpedakis and Aljolani, Osama Atef Ishaq for their assistance, great guidance and support.

Table of Contents

List of Figures

List of Tables

Nomenclature

A	*Total surface*	$[m^2]$
A_{bundle}	*Bundle area*	$[m^2]$
A_f	*Total area of the fins per tube*	$[m^2]$
A_{fin}	*Fin surface*	$[m^2]$
A_i	*Inside surface of tubes*	$[m^2]$
A_{inflow}	*Inflow cross-sectional area*	$[m^2]$
A_R	*Required exchanged area*	$[m^2]$
$A_{smallest}$	*Smallest cross-sectional area between fins*	$[m^2]$
A_t	*Total external area of the tube*	$[m^2]$
A_{t0}	*Surface of the base tube*	$[m^2]$
a_a	*Air heat transfer coefficient*	$\left[\frac{W}{m^2 \cdot K}\right]$
a_c	*Refrigerant heat transfer coefficient*	$\left[\frac{W}{m^2 \cdot K}\right]$
$a\_virtual$	*Virtual heat transfer coefficient*	$\left[\frac{W}{m^2 \cdot K}\right]$
C_{bend}	*Bend coefficient*	-
Cp	*Specific heat capacity*	$\left[\frac{J}{kg \cdot K}\right]$
D	*Diameter*	$[m]$
d_f	*Fin diameter*	$[m]$
d_i	*Inside diameter*	$[m]$
d_o	*Outside diameter*	$[m]$
d_r	*Fin thickness*	$[m]$
F	The logarithmic temperature difference correction	-
f	*Friction factor*	-
G	*Mass velocity*	$\left[\frac{kg \cdot m^2}{s}\right]$

h	*Enthalpy*	$\left[\frac{kJ}{kg}\right]$
h_f	*Height of fin*	$[m]$
k	*Thermal Conductivity*	$\left[\frac{W}{m \cdot K}\right]$
L	*Length*	$[m]$
L_{pass}	*Length of the pass*	$[m]$
m	*Pitch fin*	$[m]$
$\dot{m}$	*Mass flow rate*	$\left[\frac{kg}{s}\right]$
N_{fins}	*Number of fins*	-
NR	*Number of rows*	-
N_t	*Number of tubes*	-
N_{trow}	*Number of tubes per row*	-
N_p	*Number passes*	-
Nu	*Nusselt*	-
P	*Pressure*	$[bar]$
Pr	*Prandtl*	-
$\dot{Q}$	*Heat transfer rate*	$[Watt]$
$\dot{Q}_c$	*Cooling capacity*	$[Watt]$
$\dot{Q}_H$	*Rejected heat transfer rate*	$[Watt]$
Re	*Reynolds*	-
S	*Entropy*	$\left[\frac{J}{kg \cdot K}\right]$
s_1	*Spacing longitudinal*	$[m]$
s_2	*Spacing transversal*	$[m]$
T	*Temperature*	$[K]$
T_{ai}	*Air inlet temperature*	[°C]
T_{ao}	*Air outlet temperature*	$[K]$

T_C	*Low temperature*	$[K]$
T_H	*High temperature*	$[K]$
T_{ri}	*Refrigerant inlet temperature*	$[K]$
T_{ro}	*Refrigerant outlet temperature*	$[K]$
U	*Overall heat transfer coefficient*	$\left[\frac{W}{m^2 \cdot K}\right]$
$\dot{V}$	*Volumetric flow rate*	$\left[\frac{m^3}{s}\right]$
$\dot{W}$	*Work*	$[Watt]$
w_o	*Velocity*	$\left[\frac{m}{s}\right]$
w_s	*Velocity in the smallest cross-section*	$\left[\frac{m}{s}\right]$

Greek Symbols

ε	Effectiveness	-
η	Efficiency	-
η_{is}	Isentropic efficiency	-
μ	Viscosity	$\left[\frac{kg}{m \cdot s}\right]$
ξ	Drag coefficient	-
ρ	Density	$\left[\frac{kg}{m^3}\right]$
ΔT_{LM}	Logarithmic mean temperature	$[K]$

Abbreviations

ASHRAE	American Society of Heating, Refrigerating and Air-Conditioning Engineers
CFC	Chlorofluorocarbons
COP	Coefficient of Performance
COP_{carnot}	Coefficient of Performance for the reversible Carnot cycle

EER	Energy Efficiency Ratio
ESEER	European Seasonal Energy Efficiency Ratio
GWP	Global Warming Potential
HCFC	Hydrochlorofluorocarbons
HFC	Hydrofluorocarbons
HVAC	Heating, Ventilation and Air Conditioning
IHX	Internal Heat Exchanger
LMTD	Logarithmic Mean Temperature Difference
ODP	Ozone Depletion Potential
R134a	1.1.1.2-Tetrafluoroethane
R152a	Difluorethane
R744	Carbon dioxide

Subscript

a	Air
amb	Ambient
b	Bulk
CO_2	carbon dioxide
lam	Laminar
$mean$	Mean
pc	Pseudocritical
r	Refrigerant
$turb$	Turbulent
w	Wall
wa	Water

Chapter 1. Introduction

1.1. Introduction in refrigeration and air-conditioning

Cooling is generally the process of removing heat from a matter. The matter can be a solid, a liquid or a gas. When heat is removed from the matter, it lowers its temperature. As it is well-known, two common methods of refrigeration are natural and mechanical. Natural refrigeration has been known since ancient times, therefore, it is still widely used. Mechanical refrigeration uses a substance, which called refrigerant and it is capable to absorb and reject heat. Absorption of heat occurs at low temperatures and pressures while rejecting occurs at high temperatures and pressures.

In the ideal case, the cooling is the reverse process of a thermal machine which consists of two isothermal processes and between them two adiabatic processes. This process can be characterized by reverse Carnot. The Figure 1.1 below shows the basic refrigeration T-s diagram of a refrigerant.

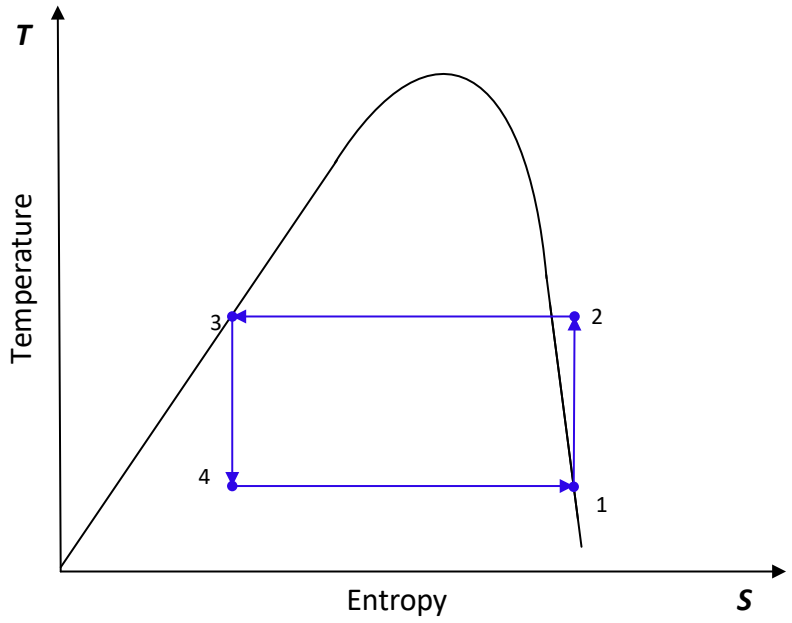

Figure 1.1: T-s diagram of the reverse Carnot process for refrigeration.

The heat that is rejected in the environment, $\dot{Q}_H$, is calculated as follows:

$$\dot{Q}_H = \dot{m} \cdot (h_2 - h_3) \quad 1.1$$

The cooling capacity of the cycle, $\dot{Q}_C$, is calculated as follows:

$$\dot{Q}_C = \dot{m} \cdot (h_1 - h_4) \quad 1.2$$

The work consumed at the compressor, $\dot{W}$, is calculated as follows:

$$\dot{W} = \dot{m} \cdot (h_2 - h_1) \quad 1.3$$

The coefficient of performance (COP), measures the efficiency of a cooling system and is calculated as follows:

$$COP = \frac{heat\_absorbed\_at\_the\_low\_temperature\_T_C}{work\_consumed} \quad 1.4$$

$$COP = \frac{|\dot{Q}|}{|\dot{W}|} \quad 1.5$$

The coefficient of performance for the reversible Carnot cycle, $(\mathrm{COP_{Carnot}})$, is calculated as follows:

$$COP_{carnot} = \frac{T_C}{T_H - T_C} \quad 1.6$$

Nowadays cooling technologies are generally separated into two categories:

1. Air-conditioning and
2. Refrigeration applications

Air-conditioning is a process that controls the temperature, humidity, air movement, air cleanliness, and pressure differential within predetermined limits in order to maintain acceptable thermal comfort conditions for people and equipment. The basic components of an air-conditioning system are:

- Circulation fan
- Compressor
- Condenser
- Dryer
- Evaporator
- Supply Duct
- Supply outlet
- Return outlet
- Filters

Refrigeration is the process that a refrigerant extracts heat from a lower temperature heat source, rejecting it to a higher temperature heat sink. The basic components of a refrigeration system are:

- Compressor
- Cooler or heat exchanger
- Expander
- Refrigerator

1.2. Refrigeration technologies

Refrigeration technologies have the main goal to remove the heat from a heat source which has a low temperature and to transfer it to a higher temperature medium. In these systems, the refrigerant is the medium that is used to transfer the heat. The main refrigeration technology is the vapor-compression which includes: the evaporator, the compressor, the condenser, and the expansion valve. Other technologies have been investigated but the main idea is the same. The differences can be another way of compression and different types of refrigerants.

1.2.1 Vapor-compression cooling

Oliver Evans described a vapor-compression refrigeration cycle in order to produce ice in 1805. Furthermore, Jacob Jenkins was the first man who built a working vapor-compression refrigeration system in 1834. The vapor-compression cooling is the most commonly used refrigeration process which uses a circulating liquid that named as a refrigerant and is the medium that absorbs and rejects heat. The cycle of this process is approximately a Rankine cycle run in reverse. The heat is removed from the area to be cooled and is rejected in the atmosphere. Vapor compression cooling systems employ a compressor. In a vapor-compression refrigeration cycle, four major thermal processes take place as follows:

- Evaporation
- Compression
- Condensation
- Expansion

Compression

The system begins with the compressor. In this stage, the refrigerant enters the compressor in a thermodynamic state known as a saturated vapor (that happens only in the ideal case) and is compressed adiabatically to a higher pressure, thus the refrigerant is also in higher temperature.

Condensation

The high pressure, high temperature vapor (superheated vapor) is at a stage at which it can be condensed and thus to reject heat in the atmosphere. As the heat is removed the energy stored in the high-pressure gas is released and the refrigerant gives up its latent heat and as it reverts to a saturated liquid. So, the refrigerant leaves as a high pressure liquid.

Expansion

The next step is the expansion valve or throttling. In this stage, the liquid undergoes a throttling causing the liquid to expand. The refrigerant now has lower pressure and lower temperature. The expansion valve ensures that adequate pressure is retained for heat transfer.

Evaporation

The low pressure, low temperature medium enters the evaporator where interacts with the (secondary) medium to be cooled. Hence, the liquid absorbs heat from the secondary medium and evaporates. The heat is absorbed from the refrigerant through phase change heat transfer and the low temperature, low pressure gas then enters the compressor completing the cycle. The Figure 1.2 and 1.3 shows the vapor-compression refrigeration system and the T-s, P-h diagram, respectively.

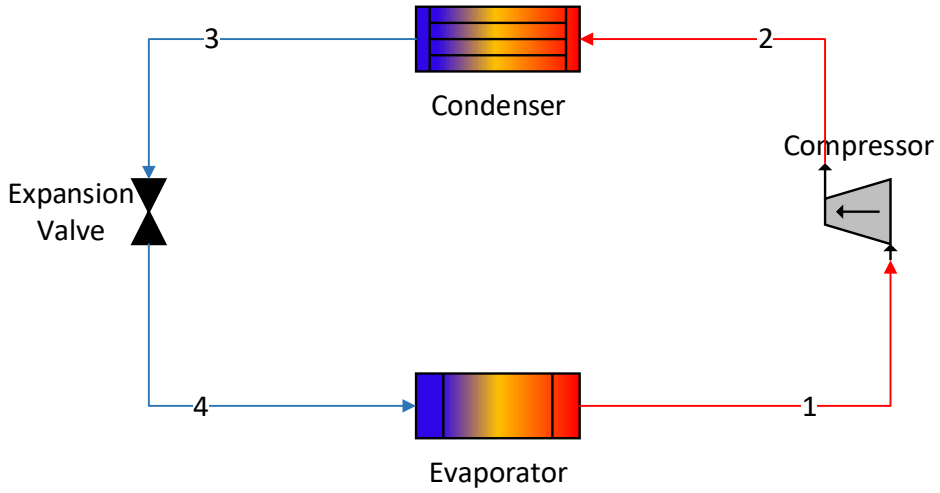

Figure 1.2: Vapor-compression refrigeration system.

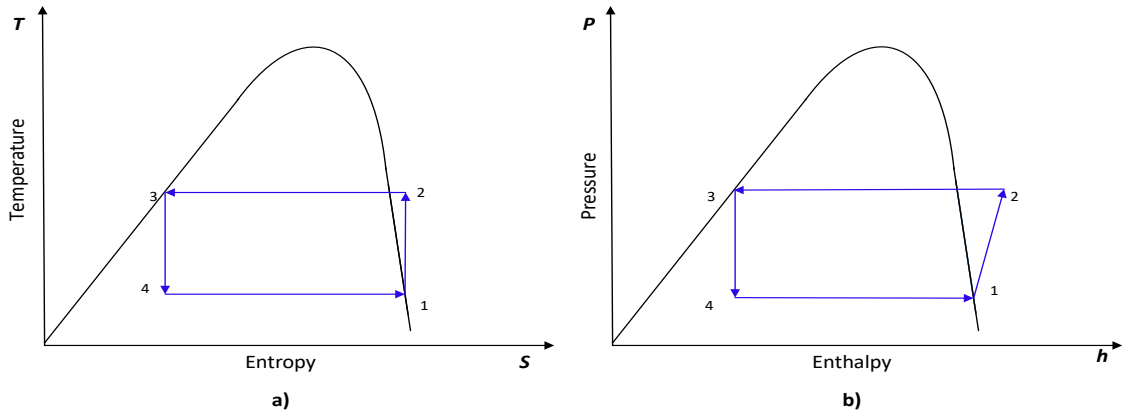

Figure 1.3: a) T-s diagram b) P-h diagram for an ideal VCC.

1.2.2 Absorption cooling

The absorption process is to separate and recombine the refrigerant and the absorbent in order to produce cooling. The cooling effect is again produced in the evaporator of the system. The basic idea of absorption cooling is to replace the mechanical compression with the creation of a liquid solution with the refrigerant that can be pumped to a higher pressure. This pumping process is a replacement of the mechanical compression. The process starts at the generator where heat is input. The heat source produces ammonia vapor from the solution, then passes to the condenser where rejected heat leaves the system. After cooling it goes through a throttle valve (expansion valve), so the pressure and the temperature are reduced. The next step is the evaporator which is the process where

the refrigerant absorbs heat and then leaves as a saturated vapor. The solution flows towards the absorber where heat is rejected. It is subsequently passed to the heat exchanger where it can return to the generator. Usually, absorption chillers are either NH_3-H_2O cycle or H_2O-LiBr cycle. In the NH_3-H_2O cycle, water acts as the absorbent while ammonia as the refrigerant. In the latter cycle, the lithium bromide is the absorbent and the water is the refrigerant. The absorption refrigeration system is depicted in the Figure 1.4 below.

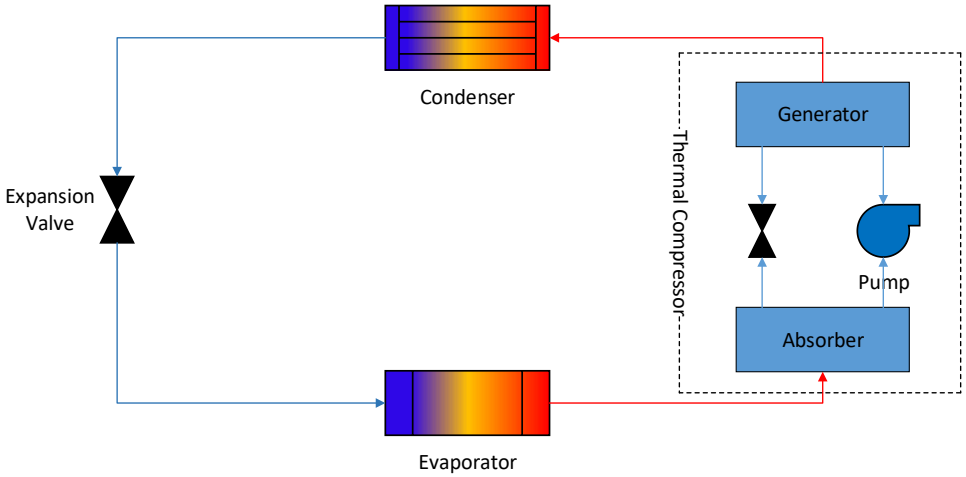

Figure 1.4: Absorption refrigeration system.

1.2.3 Adsorption cooling

Adsorption cooling technologies are also thermally driven systems such as absorption cooling technologies. In the case of adsorption, the sorbent is solid material and is used to adsorb the refrigerant and increase its pressure. The adsorption is a highly exothermal reaction; thus, a secondary stream has to absorb the produced heat. When the sorbent is heated, it desorbs the refrigerant vapor at the condenser pressure. The vapor is then liquefied in the condenser, flows through an expansion valve and enters the evaporator. The liquefied refrigerant in the evaporator absorbs heat and vaporizes, producing a cooling effect. The adsorption cooling system is depicted in the Figure 1.5 below.

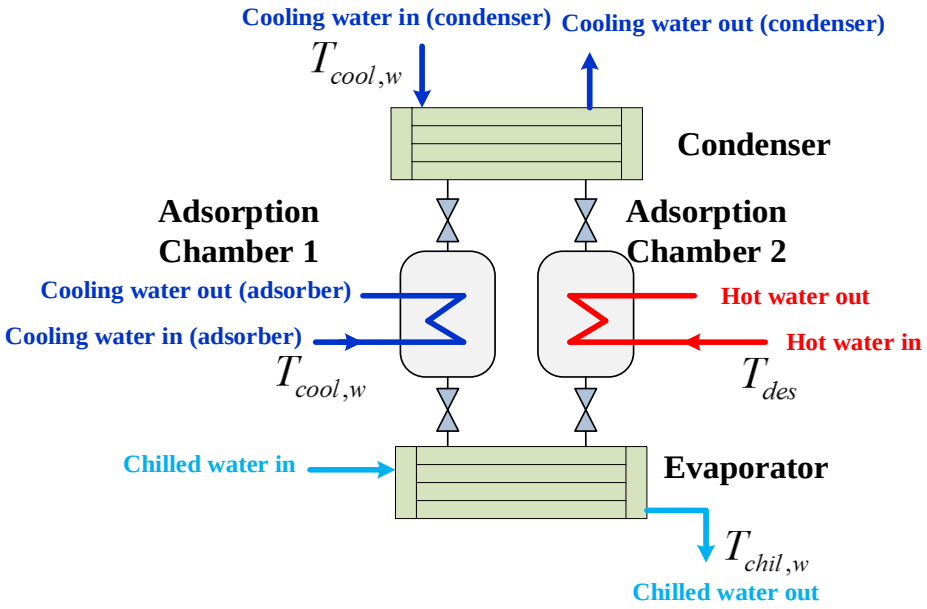

Figure 1.5: Adsorption cooling.

1.3. Carbon dioxide air conditioning systems

The operation of the carbon dioxide air conditioning system is the same as the vapor-compression cooling. The refrigerant which is used is the CO_2 named as R744, based on ASHRAE's designation. CO_2 has emerged as a credible natural refrigerant to replace HFCs. It is non-flammable and non-toxic, it has zero Ozone Depletion Potential (ODP) and negligible Global Warming Potential (GWP=1). It has favorable thermophysical properties such as high density, specific heat, volumetric cooling capacity, latent heat, and thermal conductivity. CO_2 distinguishes from other refrigerants due to its critical point with a relatively low temperature of 31.0 °C and high pressure of 73.8 bar, as shown in Figure 1.6.

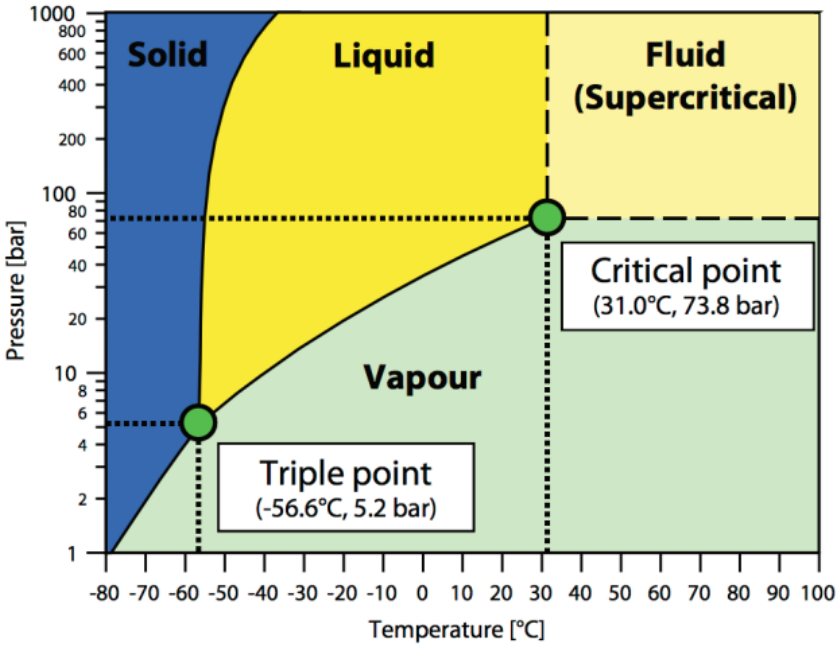

Figure 1.6: Phase diagram of CO_2 [1].

As it is shown in the Figure 1.7 below the CO_2 has a much higher working pressure than other refrigerants.

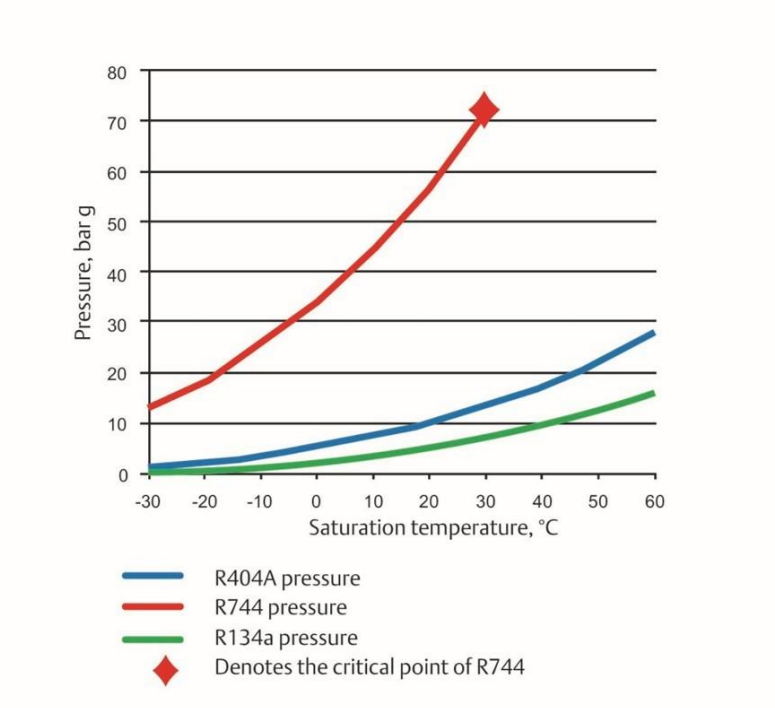

Figure 1.7: Saturation pressure versus temperature for selected refrigerants [1].

Two significant thermophysical advantages for the refrigeration cycle result from the high working pressure. Firstly, the high working pressure results in high vapor density. Consequently, for refrigerants with similar values of latent heat of vaporization/condensation, the volumetric refrigerating effect will be higher. The second

main advantage associated with the high working pressure is the low vapor pressure drop which means that smaller components and distribution lines can be used.

As it is referred the CO_2 has a low critical temperature, which means in order to reject heat by condensation it must be established at temperatures up to 31 °C. This temperature is indeed much lower than necessary for rejecting heat to the atmosphere. Furthermore, the ambient temperature for many applications exceeds a level of 25 °C, which is necessary for condensation, making it practically impossible to reject heat by condensation. However, this does not mean that carbon dioxide cannot be used as a refrigerant in these applications. Carbon dioxide can be used for these applications but the heat rejection process must be based on a different process than condensation. This process is known as a gas cooling and the condenser is replaced by the gas cooler. These applications described as supercritical systems. The P-h diagram for subcritical and supercritical systems is depicted in the Figure 1.8 below.

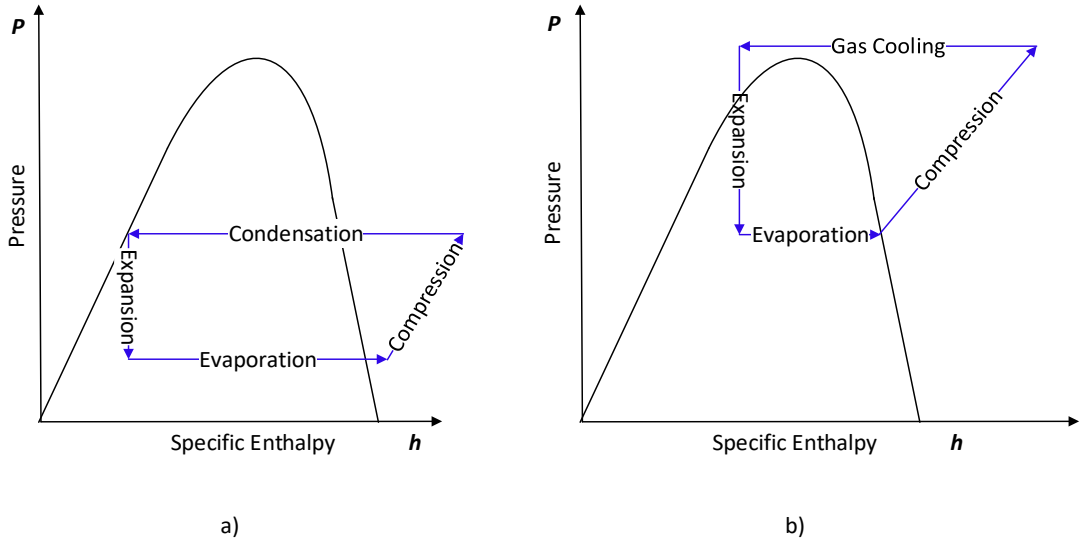

Figure 1.8: P-h diagram of a) subcritical system b) supercritical system.

In a conventional subcritical cycle, the low critical temperature is a disadvantage because it limits the operating temperature range; heat cannot be delivered at temperatures greater than the critical temperature. The transcritical operation is the most prevalent, due to the temperature of the heat sink being too high for subcritical operation.

1.4. Literature review

The supply of CO_2 systems is increasing rapidly, especially in the northern and southern parts of Europe. There is a clear tendency towards developing all-natural solutions for warm climates in order to expand the uptake of CO_2 in commercial refrigeration to the southern part of Europe. It is a fact that refrigeration systems represent a great part of today's energy consumption and optimization of these systems can play an important role in reaching the climate targets in Europe, but also in other continents.

A review of the most promising technologies for CO_2 systems is provided below.

1.4.1 Suction line heat exchanger

The internal heat exchanger brings the discharge vapor of the gas cooler into a thermal exchange with the discharge vapor of the evaporator, as it is shown in the Figure 1.9 below. The Figure 1.10 depicts the P-h diagram.

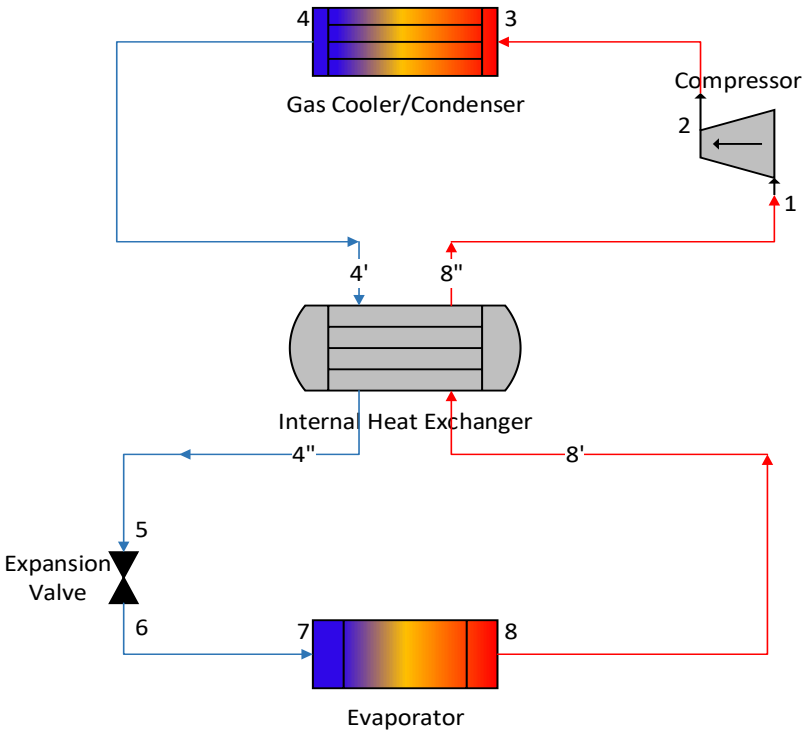

Figure 1.9: Transcritical cycle with an internal heat exchanger scheme.

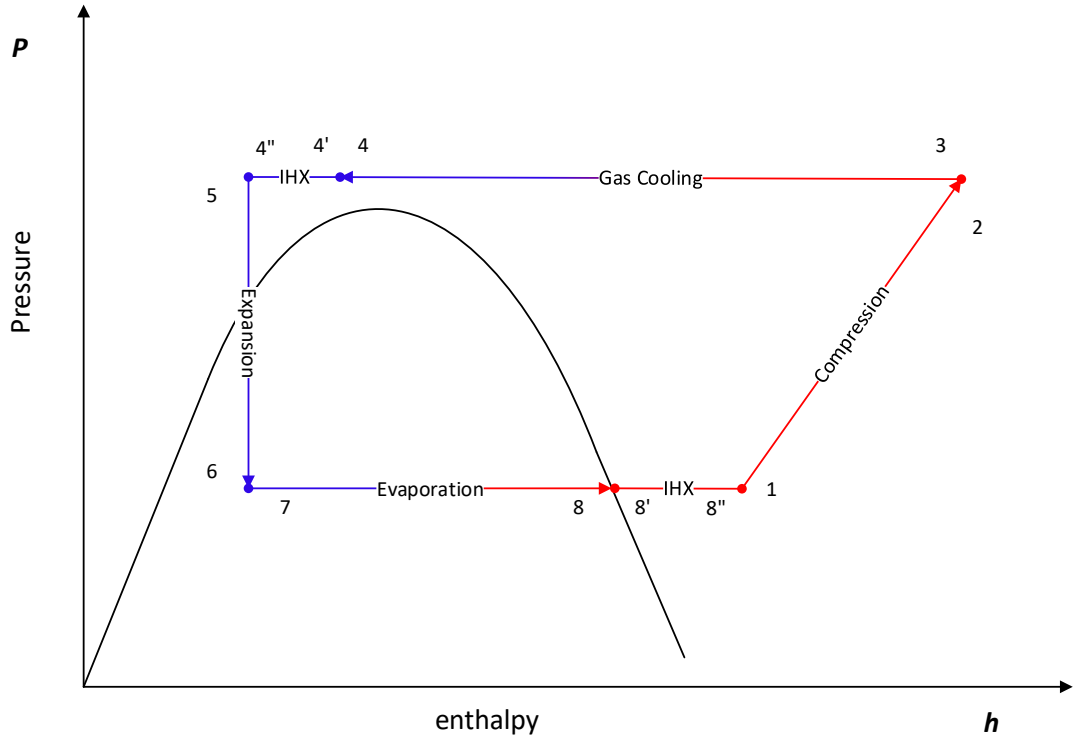

Figure 1.10: P-h process diagram.

The implementation of this exchanger has two offsetting effects; increased the refrigeration capacity due to subcooling (4'-4'') and increased compression work due to higher suction temperature (8'-8''). The influences on the system's overall efficiency depend on the operating conditions and working fluids. However, for CO_2 the benefits are significant. The optimum pressure is lower when an internal heat exchanger is present and throttling losses are reduced. It is confirmed experimentally that efficiency and cooling capacity increased with the use of the IHX. Measures have shown cooling capacity can be increased by 12 % and the efficiency of the system by up to 12 %. However, it has been noticed an increase in compressor discharge temperature of 10 °C at the evaporating temperature of -15.0 °C, which limits the operation of the plant at low evaporating levels [2]. As it is mentioned the influence of IHX changes according to the operating conditions. The internal heat exchanger has a negative impact in the case of the carbon dioxide cycle replace the throttling valve with the expander. Results have indicated that using a heat exchanger in the cycle with an expander reduces COP and exergy efficiency while using a heat exchanger in the cycle with the throttling valve increases COP and exergy efficiency [3]. Moreover, at higher ambient conditions the implementation of the internal heat exchanger improves the COP in a range from 2 to 4 % for the conventional R744 cycle [4].

1.4.2 Cascade systems

A lot of industrial applications require simultaneous refrigeration and heating, of up to -50 °C and 100 °C, respectively. Refrigerants in a single-stage system do not have the ability to work efficiently for so large temperature lifts. In this case, cascade systems offer feasible solutions. Cascade system uses two kinds of refrigerants, which run through their own independent cycle and are joined by a heat exchanger. The condenser of the lower cycle acts

as the evaporator for the cycle above. The overall cycle and the P-h diagram are shown in the Figures 1.11 and 1.12, respectively.

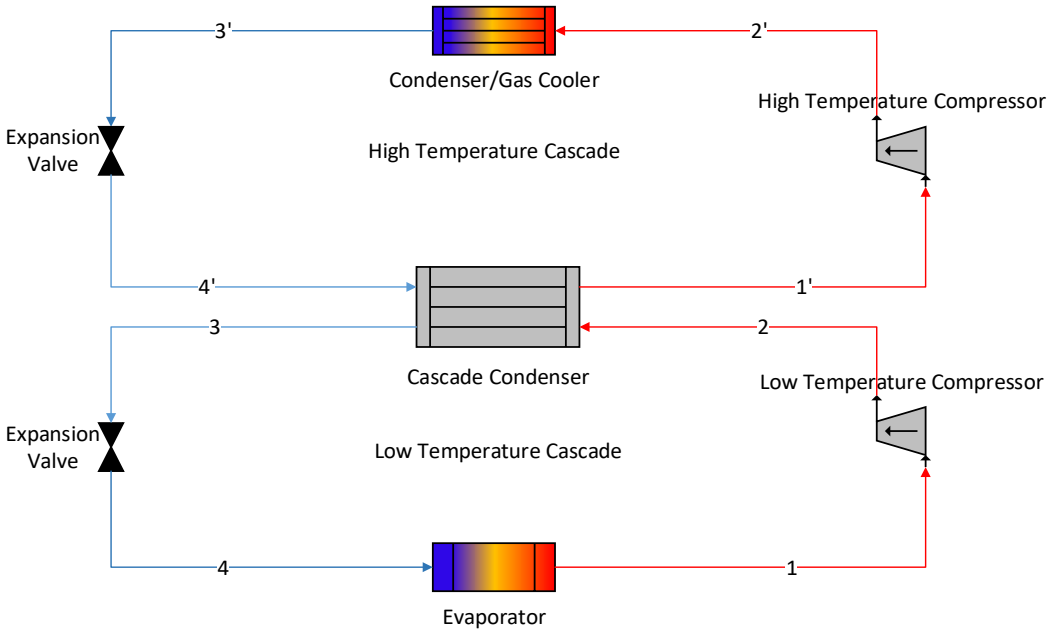

Figure 1.11: Schematic diagram of a cascade system.

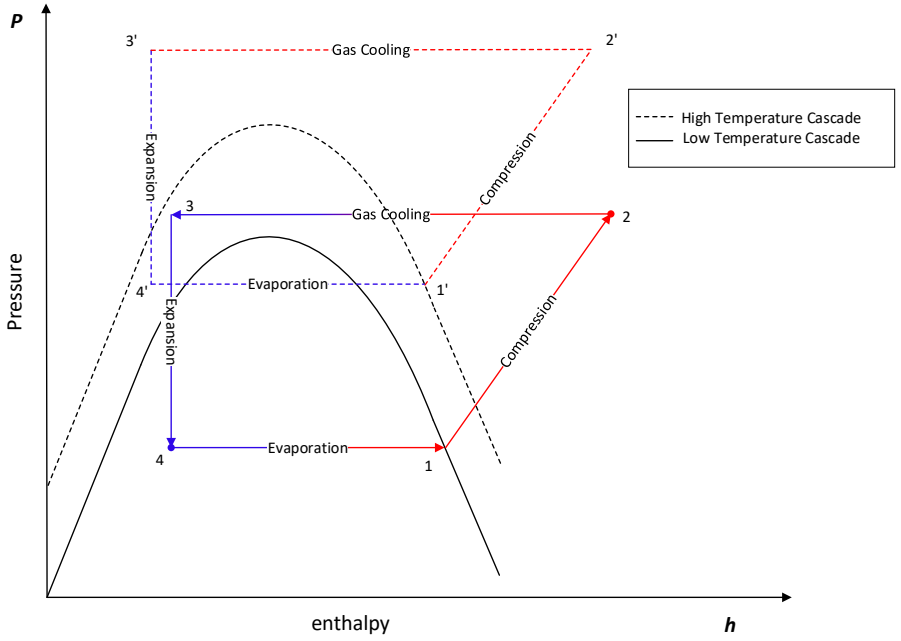

Figure 1.12: P-h process diagram.

Cascade systems are very attractive alternatives to conventional systems in hot climates. Furthermore, offers the opportunity to build CO_2 systems with low pressures. It is a fact that the COP and exergy efficiency of the combined system is significantly increased. Theoretical studies of a high temperature heat pump system of R152a heat pump and CO_2 transcritical cycle have indicated that the combined system has increased its COP and exergy efficiency, under the same conditions, by about 54.7 % and 175 % accordingly, as compared to the single of each one system [5].

1.4.3 Subcooling systems

In order to increase the efficiency of the overall system, you can also cool the refrigerant further to lower temperature than the gas cooler has achieved. This cycle operates in subcritical or transcritical conditions depending on the heat rejection temperature and the high pressure. Subcooling can be implemented in several ways which can be divided into internal or external methods. Moreover, in transcritical conditions, subcooling reduces the optimum working pressure and maximize improvement. Regarding internal methods such as internal heat exchanger, COP can be incremented up to 20 % or even more. Another way of internal subcooling is the economization of CO_2 cycles. With economizer, COP has been improved up to 15.2 %, the implementation also of integrated mechanical subcooling systems has shown COP improvements up to 17.5 %. External subcooling systems include: dedicated mechanical subcooling systems having achieved COP improvements up to 28.8 %. Thermoelectric subcooling systems have increased the COP approximately 20 % [6]. The Figures 1.13 and 1.14 shows the subcooling system and the P-h diagram, accordingly.

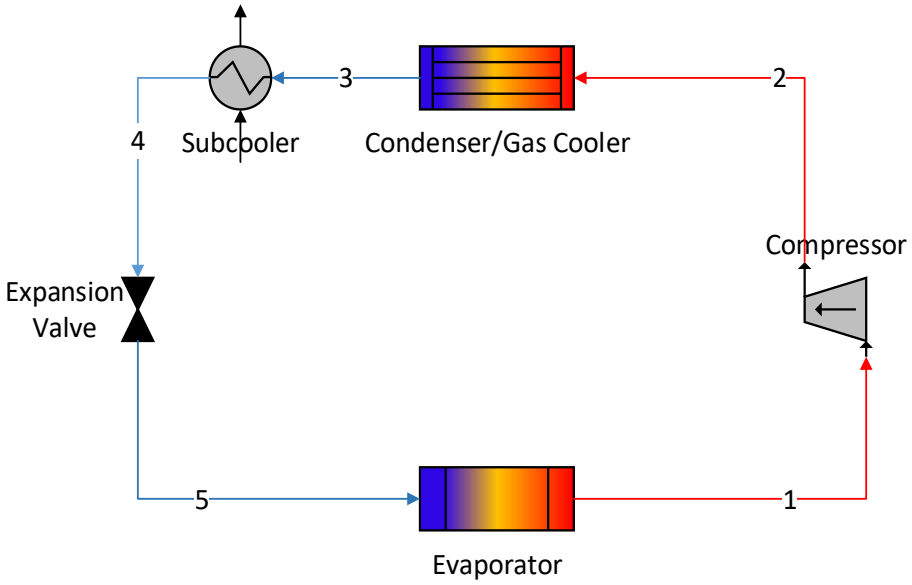

Figure 1.13: Schematic diagram of a subcooling system.

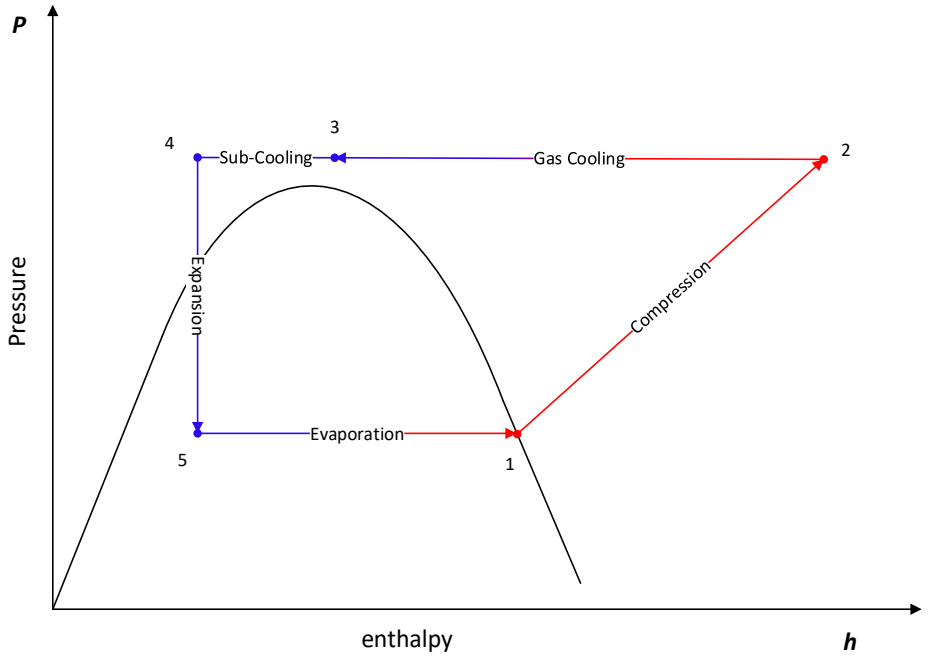

Figure 1.14: Pressure-enthalpy diagram of the mechanical sub-cooling cycle in transcritical conditions.

1.4.4 Expanders

CO_2 cycles are distinguished by their greater throttling loss compared to conventional refrigerants, as the Figure 1.15 shows below. In the expansion process, also, it is noticeable the large pressure change.

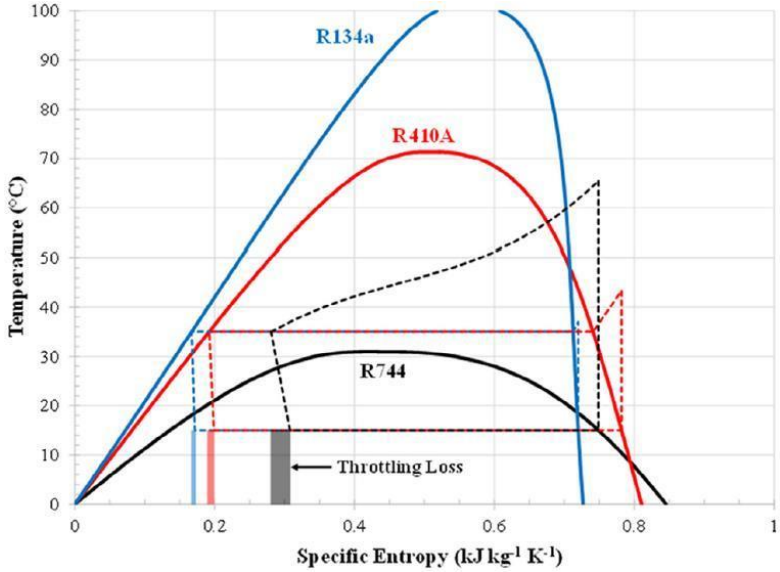

Figure 1.15: Vapor-compression cycle with isenthalpic expansion shown on temperature-specific entropy diagram for R744, R410A, and R134a [7].

Investments have shown that a system including an expander has a greater impact than systems with other components. The improvement of refrigeration capacity is one of the advantages of this cycle. Furthermore, the advantages include decreased compression work as a result of recovered expansion work. The isentropic efficiency of the expander plays a crucial role in the amount of recovered work. It is also important to refer that in supercritical

conditions the efficiency is better than subcritical because most of the expansion occurs in the dense gas phase where the friction is less than in the two-phase region. The Figure 1.16 below shows the system, which the throttling valve has been replaced by an expander.

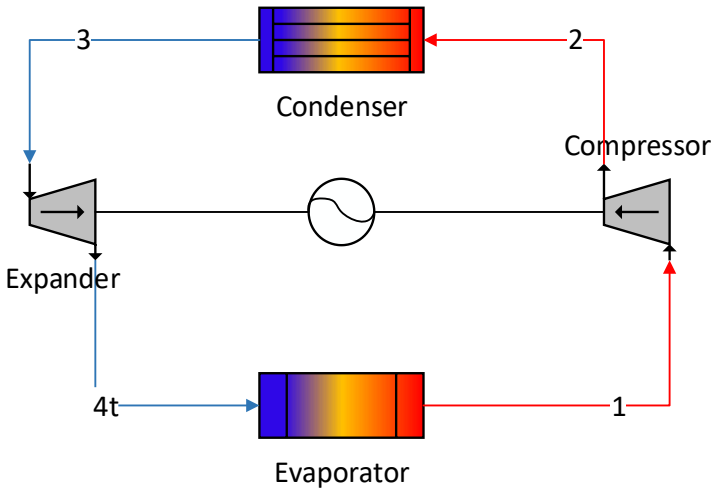

Figure 1.16: Conventional system with expander.

The comparison of four compression evaporative refrigeration cycles indicates that the cycle with the expander has the highest COP and exergy efficiency. From an energy point of view, when evaporation temperature is kept at 5 °C, the pressure is optimized and gas cooler outlet temperature is 40 °C, COP of a cycle with an expander is 3.2 and COP of a cycle with throttling valve is 2.5 [3].

1.4.5 Indirect systems

Indirect systems tend to replace systems with direct expansion, mainly, in commercial supermarket applications. Furthermore, they have long been used for systems with many units to be cooled, such as butcheries and dairies. Indirect systems are also noticeable at freezer applications where the secondary refrigerant ensures the appropriate temperature of goods.

Indirect systems use two different circuits a primary circuit and a secondary circuit. In many applications are needed two secondary circuits, one on the evaporator side and one on the condenser as the Figure 1.17 shows below.

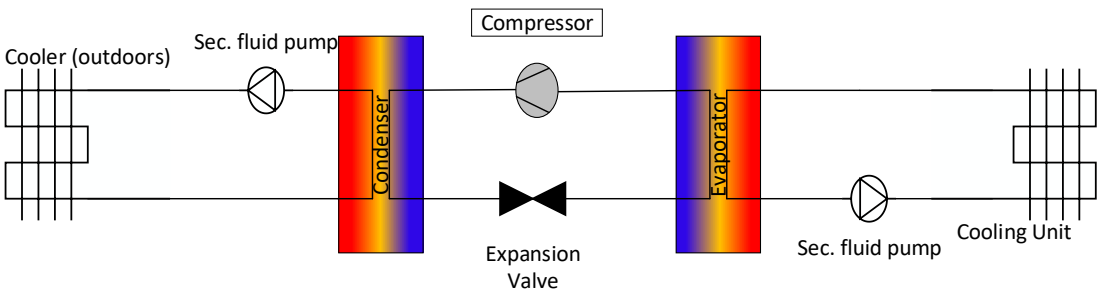

Figure 1.17: Indirect refrigeration system.

Carbon dioxide is usually used as a secondary fluid since it is non-flammable and non-toxic. Moreover, the pumping power for CO_2 is lower than for other fluids due to the low-pressure drop and small volume flow rate.

1.4.6 Booster systems

A conventional CO_2 booster refrigeration system is depicted in the Figure 1.18 below. The typical booster system has four pressure regions: high, intermediate, medium and low with two-stage compressors and two evaporating systems. The system also includes two by-pass valves. The first by-pass valve mixes the expanded fluid from the saturated vapor with refrigerant from the low stage compressor and MT evaporator. The second valve is added to by-pass the refrigerant from the internal heat exchanger, in case the designed hot side fluid temperature is lower than that of the cold side. The Figure 1.19 depicts the P-h diagram of this system.

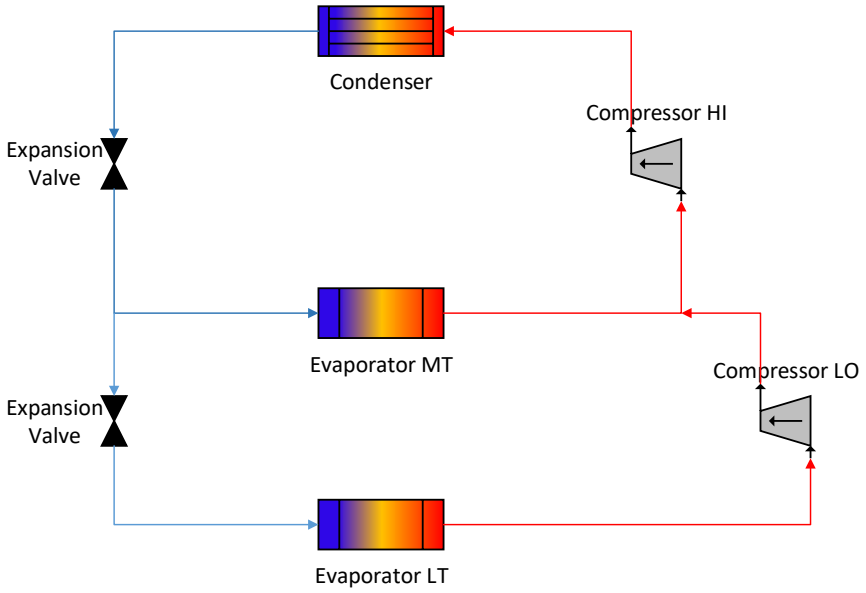

Figure 1.18: A typical CO_2 booster system applied in the supermarket refrigeration system

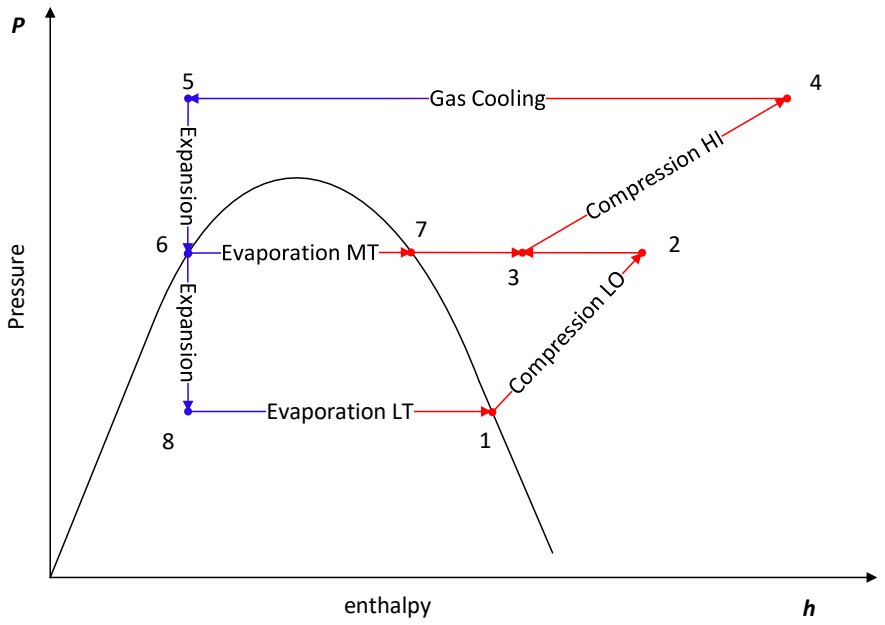

Figure 1.19: P-h diagram of the transcritical cycle in the CO_2 booster system.

The coefficient of performance of the booster system depends on the ambient temperature as the Figure 1.20 below shows. The optimum discharge pressure increases at higher ambient temperature in order to get maximize COP. Moreover, in order to increase the cooling COP, the intermediate pressure and HT compressor efficiency ratio should be as low as possible [8].

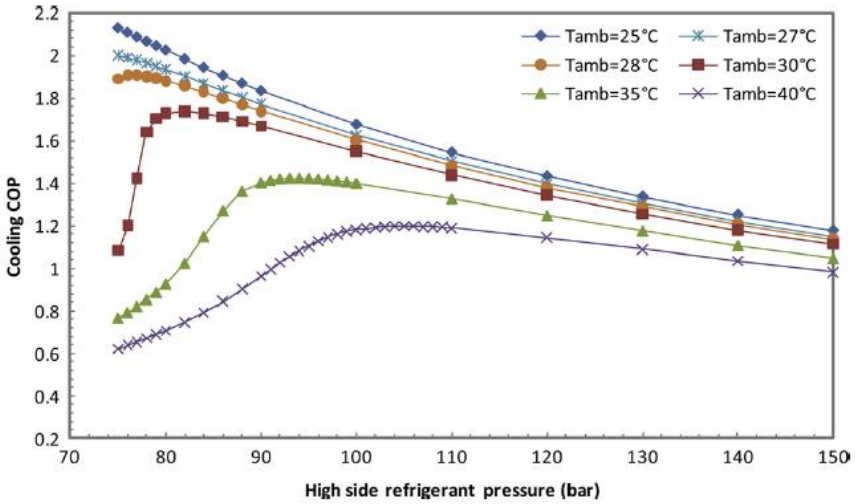

Figure 1.20: Variation of COP with high side refrigerant pressure and ambient air temperature for the transcritical CO_2 booster system [8].

1.4.7 Ejectors

The pressure difference between discharge and evaporating pressure causes large expansion loss in the supercritical CO_2 refrigeration system, and as a result, the performance of the system is low. In order to improve the performance, the expansion process takes place in an ejector. Replacing the throttling valve with an ejector, the system increases the

performance, especially when operates in warm climates. The Figures 1.21 and 1.22 presents an overview of the transcritical ejector system and the P-h diagram of this cycle.

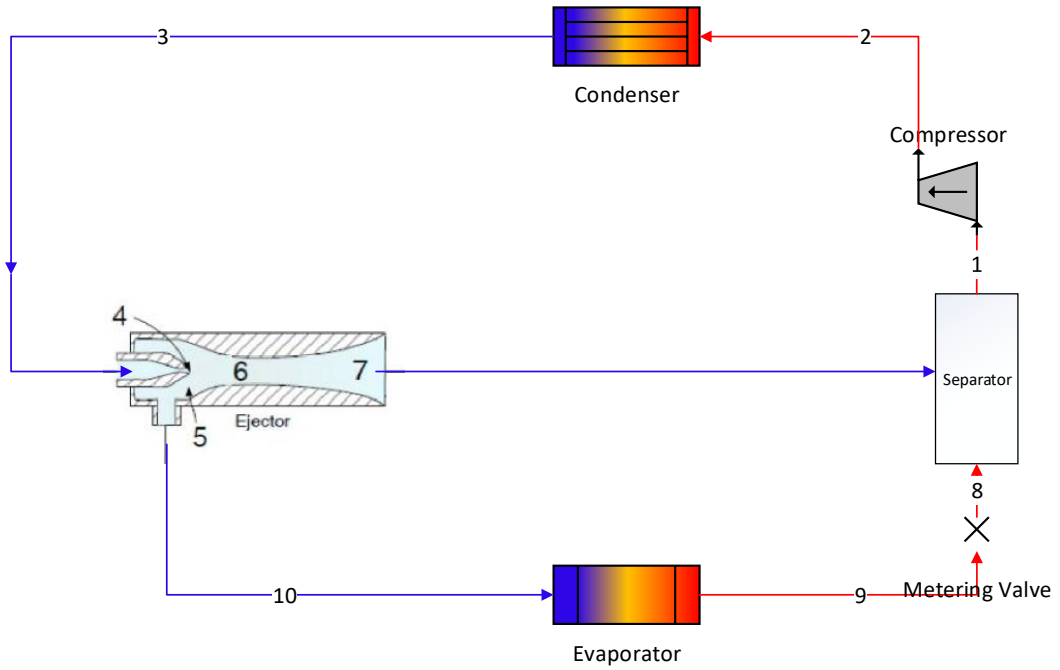

Figure 1.21: Transcritical R744 ejector system component layout.

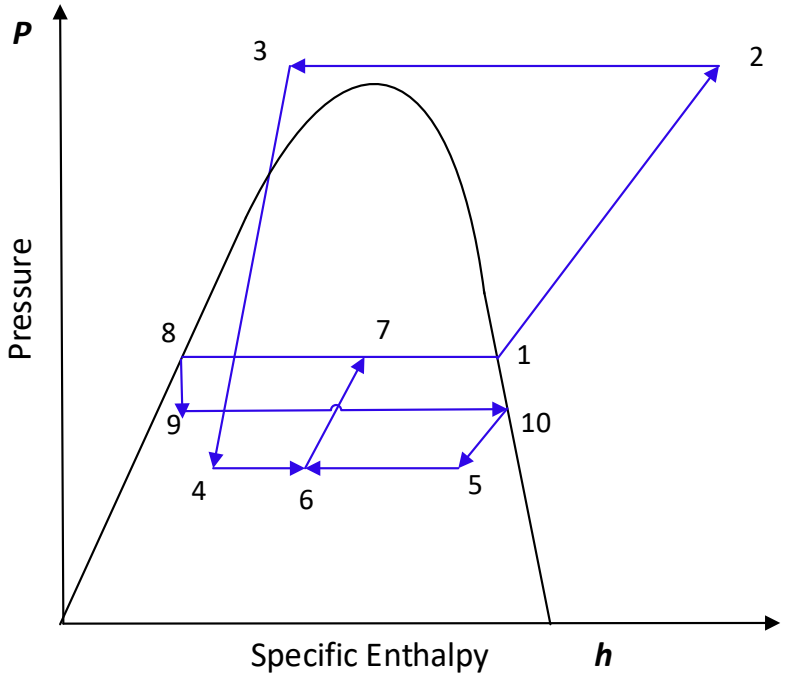

Figure 1.22: Corresponding pressure-specific enthalpy diagram.

Many investigations have shown that the system with an ejector, indeed, minimizes the expansions losses. Experiments have shown that the cooling capacity and COP can be improved simultaneously by up to 8 % and 7 %, accordingly. Moreover, the ejector is able to recover up to 14.5 % of the throttling losses [9]. Investigations, also, have shown that the

COP of the ejector refrigeration system can be improved by 16.7 % at -30 °C evaporation temperature compared with a normal refrigeration system. Nevertheless, if the evaporation temperature increases further, the ejector shows less influence on the system performance [10]. Another experiment that compared the standard CO_2 refrigeration system with the ejector refrigeration system has indicated that COP improvements of the ejector cycle of 17 % were reached with ejector efficiencies of up to 22 % [11]. Furthermore, ejector systems have combined with other components such as internal heat exchanger in order to be improved the performance of the system. Results have shown that the internal heat exchanger obviously increased the coefficient of the performance of the ejector system. Experimental analysis has indicated that the ejector system with a 60 cm internal heat exchanger provides the maximum COP improvement of up to 27 % compared to a similar conventional system [12].

Chapter 2. Gas cooler

2.1. Introduction to the gas cooler

As it is referred, the refrigeration system can operate in the subcritical or supercritical conditions depending on the ambient temperature. When the temperature is above from the critical temperature then the system works in the supercritical mode. In this case, the heat rejection takes place in the heat exchanger which is called gas cooler. The heat exchanging process is different from the condensation and it is observed single-phase heat transfer. In subcritical mode, the heat exchange takes place in the conventional condenser. There are many types of condensers based on a cooling medium such as water-cooled condensers, air-cooled condensers, and evaporative condensers. Furthermore, water-coolers can be separated into categories based on the type of the heat exchanger. There are different types of heat exchangers that can be determined by the cooling capacity, the stream conditions and the amounts of mediums required for the condensation. Especially, the design of the gas cooler needs special considerations due to the high operating pressure and the temperature glide during the cooling of CO_2. Many investigators consider the gas cooler as the main component of the CO_2 supercritical refrigeration system. Gas coolers can be classified into two main categories: the air gas coolers and the water gas coolers. The difference between these two types is the medium that cools the CO_2. As the name indicates the air-gas cooler uses ambient air while the water gas cooler uses water.

2.2. The importance of gas cooler

Gas cooler plays an important role in the COP of the system. In order to obtain the best COP and the highest capacity, the gas cooler outlet temperature of the CO_2 has to be as low as possible. More specifically, the approach temperature between the heat sink and refrigerant must be minimized. The capacity of the system depends on the efficiency of the gas cooler. The amount of heat rejection can be maximized by reducing the approach temperature. Furthermore, reducing the optimal operating pressure the gas cooler can achieve less compressor power.

2.3. Air cooled gas cooler

The vast majority of gas cooler applications use air-coupled gas coolers. There are two types that distinguish in CO_2 systems; the macro tube and micro-channel. Each type of gas cooler has advantages and disadvantages.

2.3.1 Micro-channel

The micro-channel gas cooler uses flow channels with a hydraulic diameter of less than 1 mm. This type offers the advantage of a higher heat transfer coefficient compared to conventional tube geometries, allowing a more compact design of heat exchanger. It shows a larger contact area with air and fluid per unit volume and yields a higher heat transfer coefficient.

On the other hand, micro-channels have very rigid construction, thus, it is difficult to have special circuits of large coils. It is observed also that they accumulate dirt in the air flow passages requiring frequent maintenance.

Although the additional contact area with the fluid increases the pressure drop in the micro-channels, CO_2 shows less pressure drop than other conventional refrigerants. The Figure 2.1 below shows a conventional micro-channel heat exchanger.

Figure 2.1: Micro-channel heat exchanger [13].

2.3.2 Macro tube

Macro-tube fin and tube exchangers have good reliability, low airflow resistance and low dirt accumulation in the field. They also offer manufacturing flexibility and reduced capital and maintenance costs compared to micro-channel gas coolers. The macro-finned tube gas cooler is the most favorable type in industrial applications compared to the micro-channel gas cooler. The air finned heat exchanger is the cheapest way of cooling and obviously easy to design it as it rejects the heat directly to the ambient air. However, the design of macro-finned tube gas coolers for CO_2 refrigeration systems has evolved from the design of standard finned tube HVAC coils and further research and development is required to optimize their design for operation in the condensing and gas cooling modes at high pressures for the unique properties of CO_2. The air heat exchanger has as main disadvantage because it has a low heat transfer coefficient larger equipment is required. The heat exchanging occurs when the refrigerant flows inside the finned tubes and the air is forced through the tube bundle. The Figure 2.2 below shows a conventional macro-finned tube.

Figure 2.2: Macro-finned tube [14].

There are many ways to circulate air through the tube bundle. Air-cooled heat exchangers can be categorized into three groups in which described the air provision: the forced draft, the induced draft, and the natural convection. The third group is rarely used. The vast majority of air-cooled exchangers are of forced draft construction because it is easier to manufacture and to maintain. As the Figure 2.3 shows below the tube bundle is mounted on top of the plenum, so it is easily removed. Forced draft constructions also require less power since the fan is moving a lower volume of air at the inlet than they would at the outlet. The forced draft units do not have the fans exposed to hot exhaust air, so they are a better choice in such cases. On the other hand, the induced draft unit has the advantage that there is a high exhaust air velocity through the top-mounted fan so it is certain that will not occur air recirculation. What is more, the plenum does not have to support the tube bundle so the weight is decreased. The induced draft is depicted in the Figure 2.4 below.

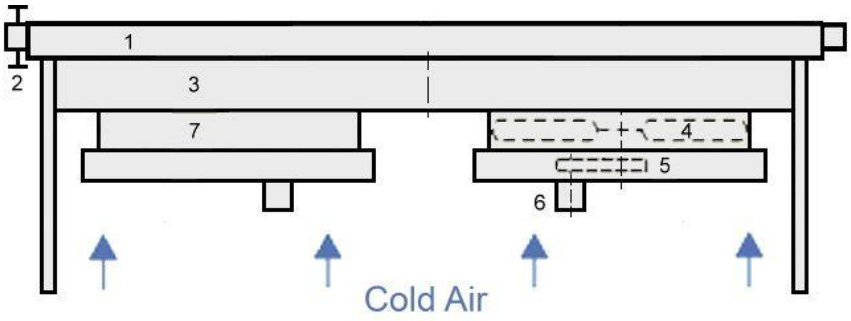

Figure 2.3: Forced Draft 1.Tube bundle, 2.Header, 3.Plenum, 4.Fan, 5.Belt Drive, 6.Motor, 7.Fan ring [15].

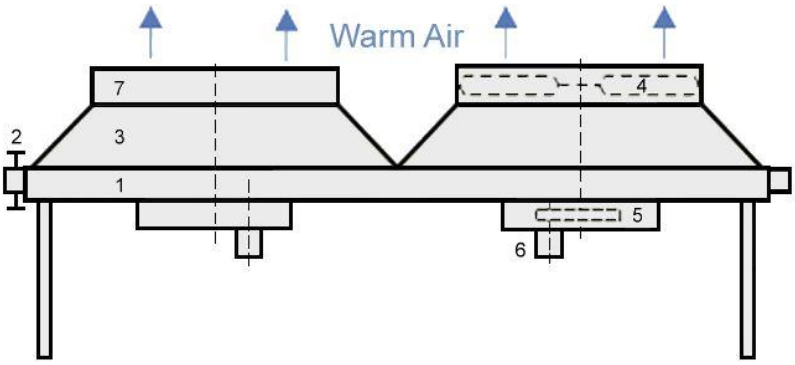

Figure 2.4: Induced Draft 1. Tube bundle, 2. Header, 3. Plenum, 4. Fan, 5. Belt Drive, 6. Motor, 7. Fan ring [15].

Another important thing is the configuration of the shape of the heat exchanger. There are four configurations that are mainly used. Each of these configurations can exist as a forced and induced draft. More specifically, the aforementioned types are; the vertical configuration, the horizontal configuration, V-type configuration, and the in-line configuration. The Figure 2.5 below shows the different types of configurations.

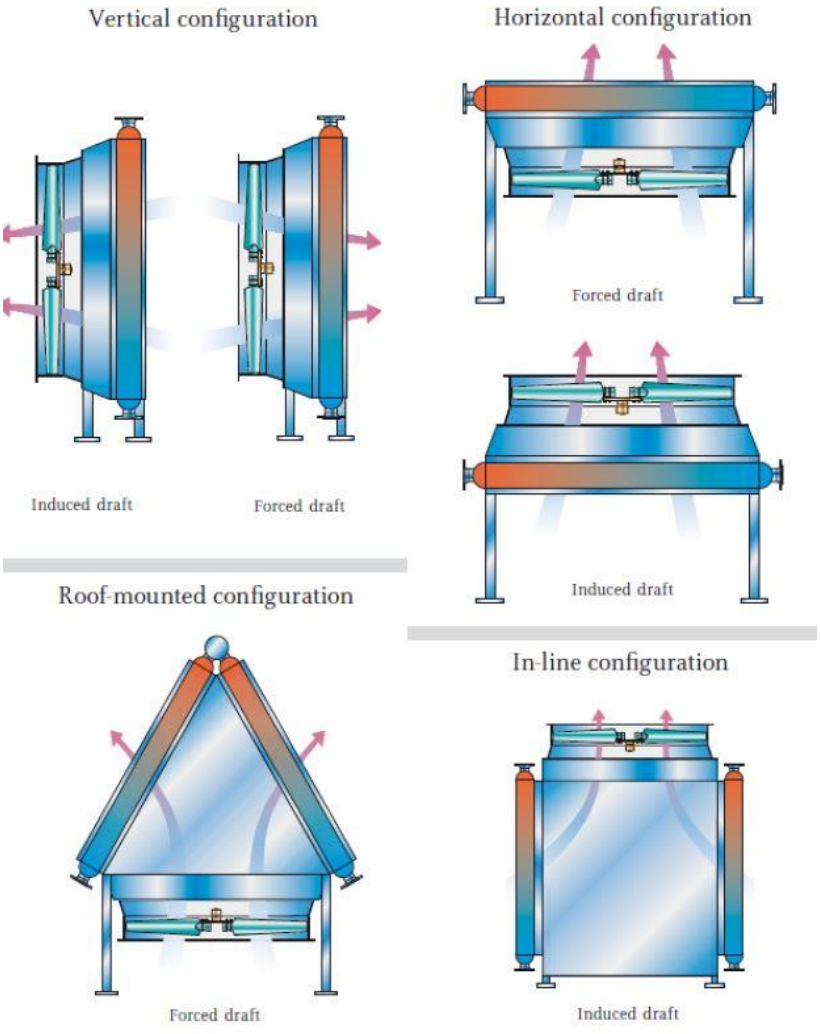

Figure 2.5: Air provision configurations [16].

2.4. Heat transfer coefficients and refrigerant pressure drop of supercritical CO_2

As far as the design of the gas coolers is concerned, it is acceptable to use the logarithmic mean temperature difference (LMTD) and effectiveness-heat transfer unit (ε-NTU) for the calculations. The implementation of these methods though has confused many investigators because of unique thermodynamic and transport properties, especially in the supercritical region. One of the most characteristic issues of supercritical fluids is that the properties change rapidly with temperature in an isobaric pressure, especially near the pseudocritical points. In order to use the ε-NTU method, it is necessary to assure that the specific heat is constant. Furthermore, there are three most important things that anyone must take into consideration: the air heat transfer coefficient, refrigerant side heat transfer coefficient and pressure drop. In fact, many investigations have been carried out about heat transfer coefficients and pressure drops. Many of them also include and experiments that show the accuracy of the theoretical studies. Below it is presented a review of some heat transfer coefficient and pressure drop correlations.

2.4.1 Tube side heat transfer coefficient

(Pitla, Groll et al.) presented a review of heat transfer and pressure drop characteristics in-tube flow. The new correlation is presented and it is seen that the majority of the numerical and experimental values are within $\pm$ 20 % [17].

$$Nu = \left(\frac{Nu_w + Nu_b}{2}\right)\frac{k_w}{k_b} \qquad 2.1$$

Where Nu_w and Nu_b are Nusselt numbers that are evaluated based on the thermophysical properties at the wall and bulk temperatures, respectively. In each case, the Gnielinski correlation is used to calculate the respective Nusselt number [18].

$$Nu = \frac{{}^{f}/_{8}\,(Re - 1000)Pr}{12.7\sqrt{{}^{f}/_{8}}\left(Pr^{2/3} - 1\right) + 1.07} \qquad 2.2$$

The above equation requires knowledge of the wall and bulk Reynolds numbers, the friction coefficient, f, and the Prandtl number.

The friction factor is calculated from the following equation:

$$f = [0.79ln(Re) - 1.64]^{-2} \qquad 2.3$$

(Jackson) modified the original correlation for forced-convective heat transfer in water and carbon dioxide at supercritical pressures [19].

$$Nu = 0.0183 \cdot Re^{0.82}Pr^{0.5}\left(\frac{\rho_w}{\rho_b}\right)^{0.3}\left(\frac{Cp_w}{Cp_b}\right)^{n} \qquad 2.4$$

Where:

$$Cp_m = \int_{T_b}^{T_w} \frac{C_p dT}{(T_w - T_b)} = \frac{h_w - h_b}{T_w - T_b} \quad 2.5$$

And

$$n = 0.4 \quad 2.6$$

$$for\ T_b < T_w < T_{pc}\ and\ for\ 1.2 \cdot T_{pc} \leq T_b < T_w$$

$$n = 0.4 + 0.2 \cdot \left(\frac{T_w}{T_b} - 1\right) \quad 2.7$$

$$for\ T_b \leq T_{pc} < T_w$$

$$n = 0.4 + 0.2\left(\frac{T_w}{T_b} - 1\right)\left[1 - 5\left(\frac{T_b}{T_{pc}} - 1\right)\right] \quad 2.8$$

$$for\ T_{pc} < T_b < 1.2 \cdot T_{pc}\ and\ T_b < T_w$$

The Dittus-Boelter equation is an explicit function for calculating the Nusselt number [20]. The equation is:

$$Nu = 0.023 Re^{4/5} Pr^n \quad 2.9$$

The Dittus-Boelter equation is valid for:

$$0.6 \leq Pr \leq 160 \quad 2.10$$

$$Re \geq 10000 \quad 2.11$$

$$\frac{L}{D} \geq 10 \quad 2.12$$

Where: D is the inside diameter of the circular duct, Pr is the Prandtl number. n=0.4 for the fluid being heated, and n=0.3 for the fluid being cooled.

2.4.2 Air Side Heat Transfer Coefficient

The VDI-Heat Atlas proposed the below correlation in order to calculate the Nusselt number [16].

$$Nu = C \cdot Re^{0.6} \left(\frac{A}{A_{t0}}\right)^{-0.15} Pr^{1/3} \quad 2.13$$

For in-line arrangement C=0.22, while for staggered banks C=0.38. The Figure 2.6 below shows the in-line arrangement and staggered banks.

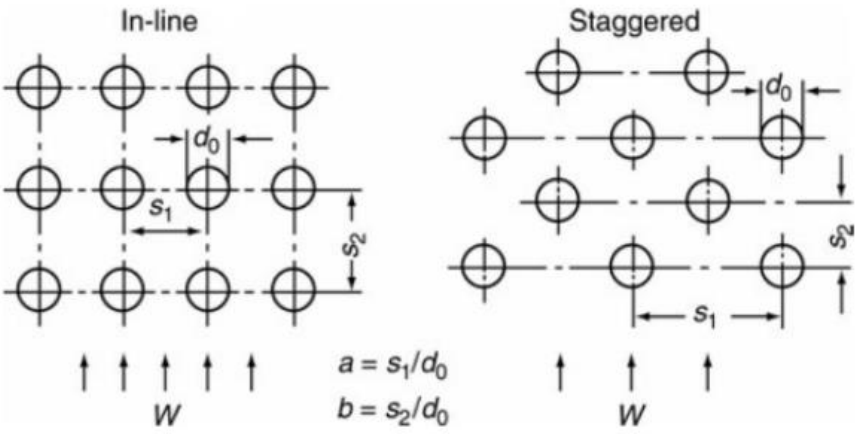

Figure 2.6: Schematic of (a) In-line arrangement (b) Staggered arrangement [16].

(Schmidt) presented a new correlation quite similar to the correlation of VDI-Heat Atlas [21].

$$Nu = C \cdot Re^{0.625} \cdot Pr^{1/3} \cdot \left(\frac{A}{A_{t0}}\right)^{-0.375} \quad 2.14$$

Where C=0.45 for Staggered arrangement and C=0.3 for in-line arrangement.

(Gianolio and Cuti) presented a new correlation for the heat transfer coefficient in the induced-draft mode for less than six rows [22].

$$Nu = 0.271 \cdot Re^{0.685} \cdot Pr^{0.33} \cdot \left(\frac{A}{A_{t0}}\right)^{-0.311} \cdot \left(\frac{n}{6}\right)^{-0.138} \quad 2.15$$

Where n=number of rows.

2.4.3 Pressure drop

Generally, the pressure drop increases as the mass flux increases and as the system pressure decreases. If the system pressure is higher, then the density of CO_2 is higher. The pressure drop, in turn, decreases as the density increases. Single-phase flow pressure drop is defined with the following equation:

$$\Delta P = f \frac{G^2}{2\rho} \frac{L}{D} \quad 2.16$$

where f is the friction factor. There are many correlations for the friction factor, such as the Filonenko correlation and the Blasius correlation [20].

Filolenko correlation:

$$f = [1.82ln(Re_b - 1.64)]^{-2} \quad 2.17$$

$$is\ used\ for\ 10^4 \leq Re_b \leq 5x10^6$$

The Blasius equation:

$$f = \frac{0.316}{Re_b{}^{1/4}} \qquad 2.18$$

$$is\ used\ for\ Re_b \leq 10^5$$

which is widely used for turbulent flow in smooth tubes. The Table 2.1 shows the already mentioned correlations.

Table 2.1: Heat Transfer Coefficient and pressure drop correlations.

	Author	Tube side Heat transfer Coefficient
1	Pitla, Groll et al. [17]	$Nu = \left(\frac{Nu_w + Nu_b}{2}\right)\frac{k_w}{k_b}$
2	Dittus-Boelter [20]	$Nu = 0.023Re^{4/5}Pr^n$
3	Gnielinski [18]	$Nu = \frac{{}^{f}/_{8}\,(Re - 1000)Pr}{12.7\sqrt{{}^{f}/_{8}}\left(Pr^{2/3} - 1\right) + 1.07}$
4	Jackson [19]	$Nu = 0.0183 \cdot Re^{0.82}Pr^{0.5}\left(\frac{\rho_w}{\rho_b}\right)^{0.3}\left(\frac{Cp_w}{Cp_b}\right)^n$
		Drop Correlation $\Delta P = f\frac{G^2}{2\rho}\frac{L}{D}$
1	Blasius [20]	$f = \frac{0.316}{Re_b{}^{1/4}}$
2	Filolenko [20]	$f = [1.82ln(Re_b - 1.64)]^{-2}$
		Air side Heat Transfer Coefficient
1	VDI-Heat Atlas [16]	$Nu = C \cdot Re^{0.6}\left(\frac{A}{A_{t0}}\right)^{-0.15}Pr^{1/3}$
2	Schmidt [21]	$Nu = C \cdot Re^{0.625} \cdot Pr^{1/3} \cdot \left(\frac{A}{A_{t0}}\right)^{-0.375}$
3	Gianolio and Cuti [22]	$Nu = 0.271 \cdot Re^{0.685} \cdot Pr^{0.33} \cdot \left(\frac{A}{A_{t0}}\right)^{-0.311} \cdot \left(\frac{n}{6}\right)^{-0.138}$

2.5. Literature review of the gas cooler

(Tsamos, Ge et al.) built two CO_2 finned-tube gas coolers with different structural designs and controls, connected with a test rig of a CO_2 booster refrigeration system. They carried out experiments at different operating conditions while they had developed models of the finned-tube CO_2 gas cooler. The analysis based on both the distributed and lumped methods. The former is a detailed model, wherein the heat exchanger is divided into a number of small segments with specified 3-D coordinates. For each piece, it is necessary to be derived and applied the equation of mass, momentum, and energy. Applying localized correlations of heat and mass transfer coefficients, the distributed method can predict the distribution profiles of temperature, pressure, and the heat transfer rate of hot and cold fluid along with the heat exchanger. The detailed model obviously is the most accurate method and is more suitable for the analysis and design of heat exchangers. However, the computation time that requires, many times it is not appropriate. The latter is a simple method, dividing into a very limited number of segments and each piece is described with the three basic equations; mass, momentum, and energy. The experiments are carried out in two finned-tube gas coolers. The larger one has 3 rows, 4 pipe circuits, 96 pipes in the total and an overall dimension of 1.6m*0.066m*0.82m while the other has 2 rows, 2 circuits, 64 pipes in the total and overall dimension of 1.6m*0.044m*0.82m. They both have a copper pipe with an inner diameter of 6.72mm, a 0.16mm thick aluminum fin with a density of 453 fins/m [23]. The Figure 2.7 shows the two tested finned-tube heat exchangers.

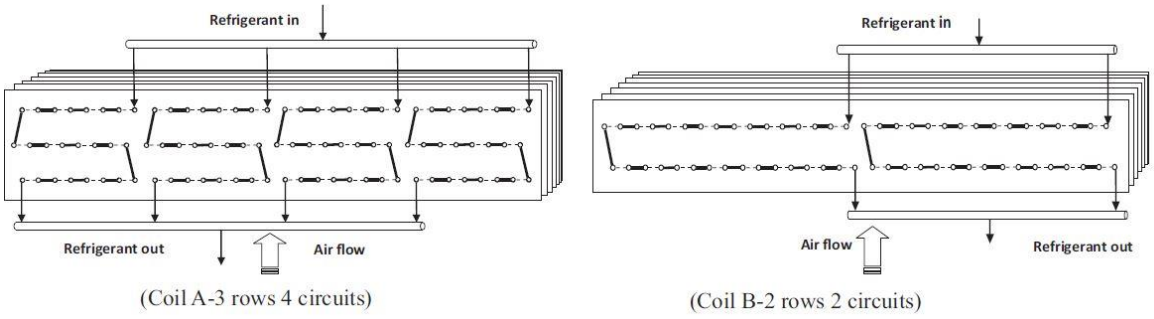

Figure 2.7: Two tested finned-tube CO_2 gas coolers/condensers [23].

They concluded that the heat exchanger designs can affect the performance of both the component and the integrated system and controls. The effect of heat exchanger sizes on system performance can be enhanced with fan speed controls. The Figure 2.8 shows the variations of the refrigerant outlet temperature according to the air flow rate.

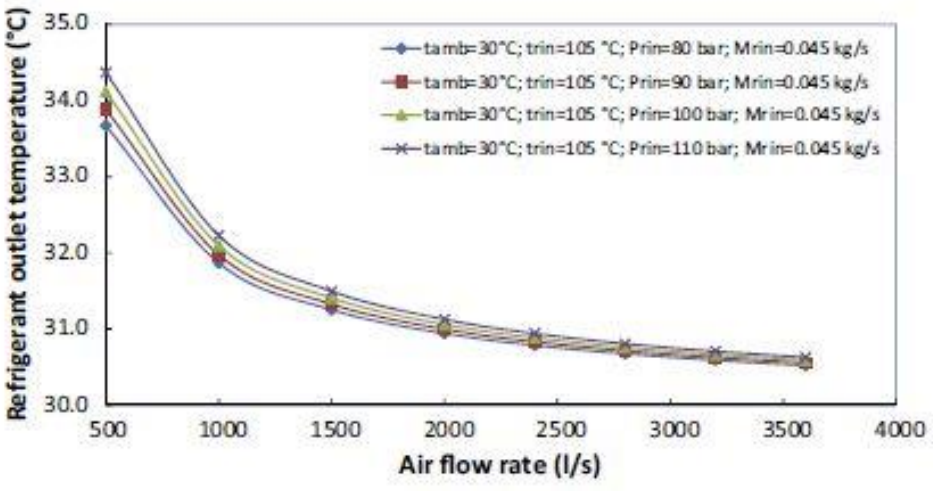

Figure 2.8: Variation of refrigerant temperature at the gas cooler (3-row) outlet air flow rate [23].

(Ge and Cropper) have conducted an investigation that presents a detailed mathematical model for air-cooled finned-tube CO_2 gas coolers. They use a distributed method in order to obtain more accurate refrigerant thermophysical properties and local heat transfer coefficients during cooling processes. The model compared with published test results. The comparison was between the gas temperature profiles along the coil pipes from refrigerant inlet to outlet at different operating states. They found that the approach temperature and the heat capacity are simultaneously increased with the increase of heat exchanger circuit numbers [24]. The Figure 2.9 depicts a comparison of simulation with test results of test conditions for refrigerant temperature profile.

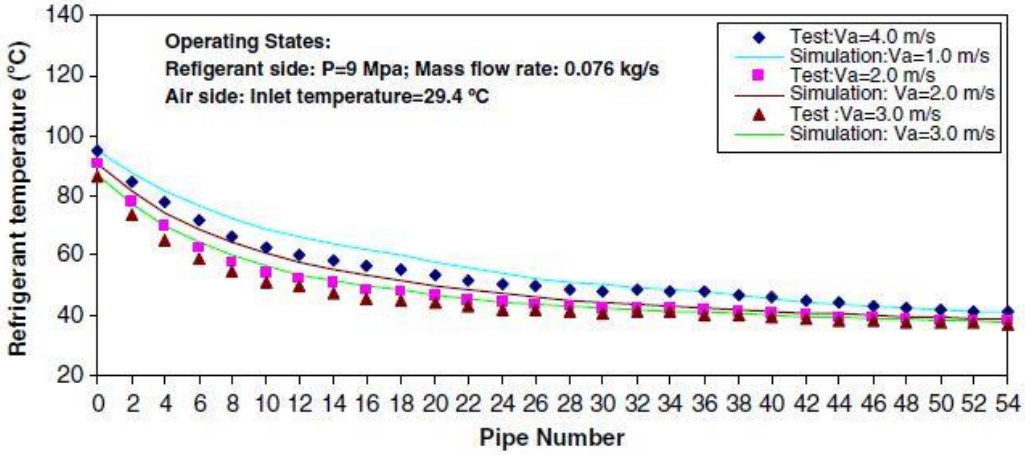

Figure 2.9: Comparison of simulation with test results of test conditions for refrigerant temperature profile [24].

(Han and Lee) have investigated experimentally the single-phase heat transfer and flow characteristics of micro-fin tubes. They used four different tubes to obtain heat transfer coefficients and friction factor with varying Reynold and Prandtl numbers. The micro-fin tubes show an outstanding achievement of the fully rough region which starts at the Re of 70 for the roughened surface tube. The approved that the tube with larger relative

roughness and smaller spiral angle showed better heat transfer performance than the tube with a larger spiral angle and smaller relative roughness as the Figure 2.10 depicts [25].

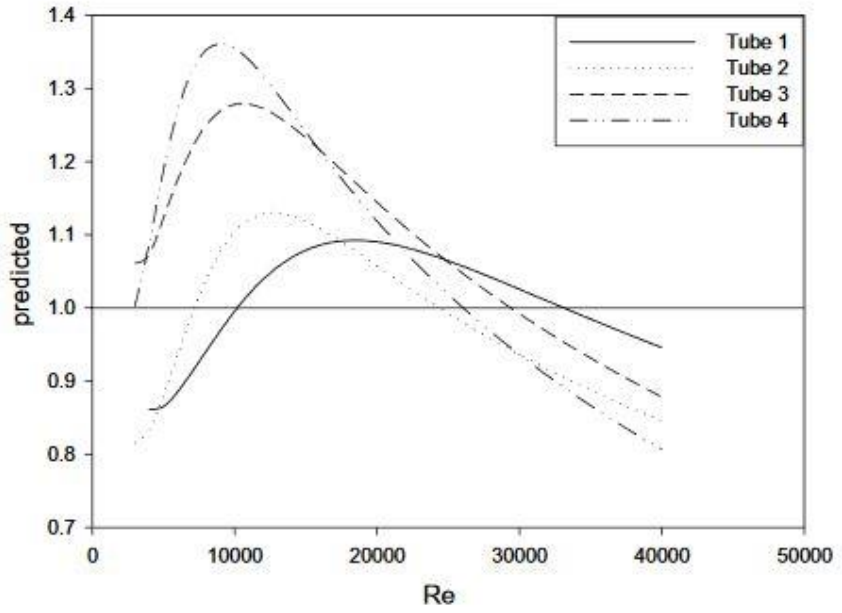

Figure 2.10: Calculated efficiency index versus Re [25].

2.6. Lubricant oil in CO_2

It is necessary to outline that practical air-conditioning, heat pump, and refrigeration systems encounter problems arising from the partial miscibility of lubricant oil in CO_2. The oil affects the heat transfer and pressure drop in which way decrease the former and increase the latter. Furthermore, it is argued that the following aspects should be considered in order to estimate the effects of the oil.

i. The partial miscibility of CO_2-lubricant oil mixtures at conditions of process operation.
ii. The densities of the continuous gas phase and the dispersed oil phase with dissolved gas.
iii. The viscosities of CO_2 and oil with dissolved gas.
iv. The interfacial tension between CO_2 and oil at operating conditions.

(Mori, Onishi et al.) studied heat transfer characteristics of cooling CO_2-oil mixtures in a macro-channel at supercritical pressures and found that oil resulted in significantly lower heat transfer coefficients. The Figure 2.11 below shows the comparison of the heat transfer coefficient for pure CO_2 and a CO_2 oil mixture [26].

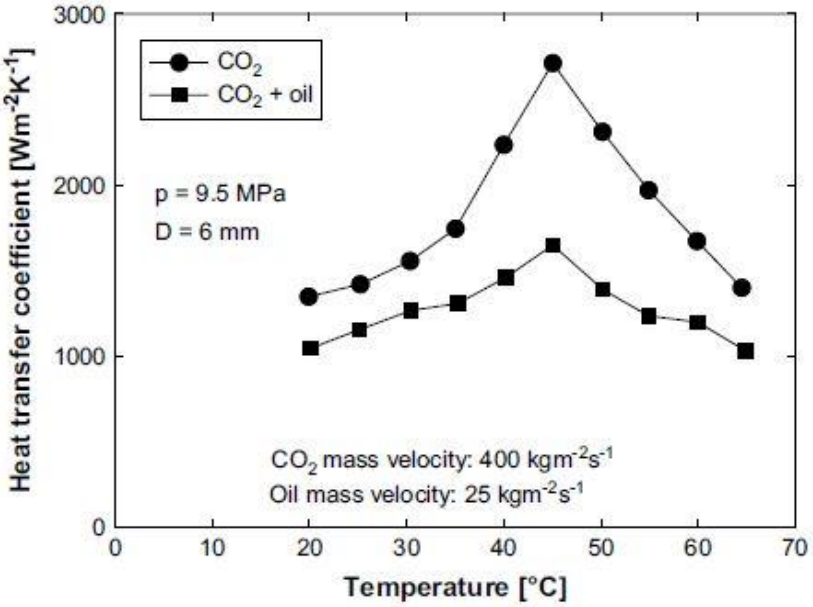

Figure 2.11: The effect of oil on heat transfer [26].

(Kuang, Ohadi) have studied the effect of oil on heat transfer and pressure drops in supercritical gas cooling in micro-channels. Three different oils were tested at oil concentrations from 0 to 5 wt % (two immiscible and one miscible). As far as the type of oil is concerned, the immiscible oils showed more negative influence than the miscible oil [27]. The Figure 2.12 and 2.13 below show the heat transfer and pressure drop, respectively.

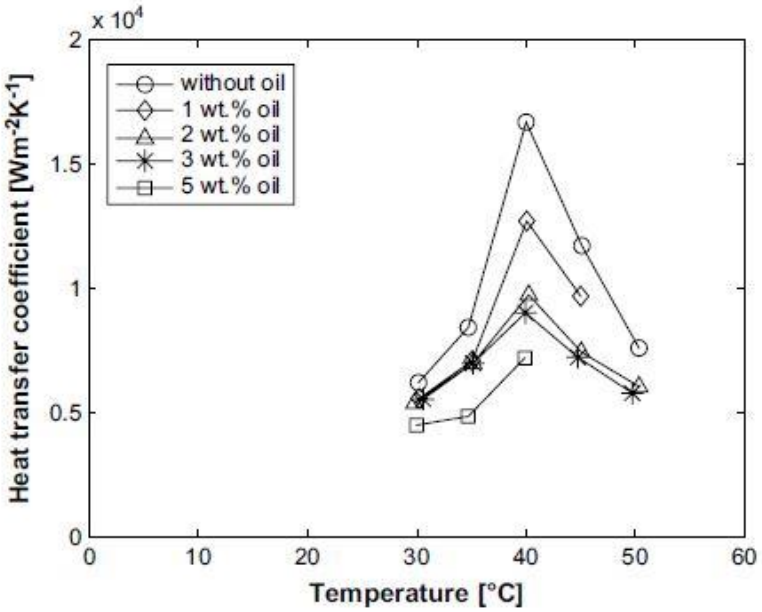

Figure 2.12: The effect of oil on heat transfer [27].

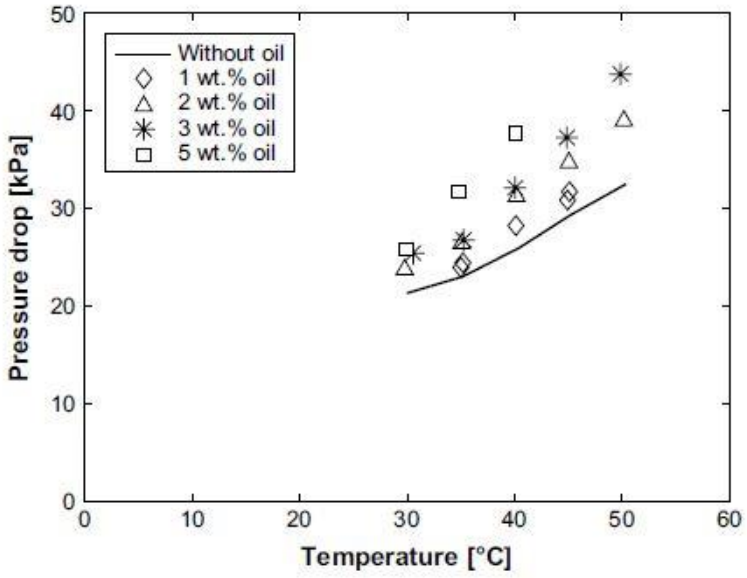

Figure 2.13: The effect of oil on pressure drops [27].

2.7. Thesis scope

For air-conditioning systems, the use of CO_2 as a working fluid is a promising step towards sustainable and climate friendly devices. In this context, it is important to design the components cost-efficient and reliable. The gas cooler plays a main role in the refrigeration cycle. Due to poor heat transfer characteristics in the gas cooler (air to supercritical CO_2) high heat transfer areas and high investment costs results. The objective of this work is to identify a compromise between pressure drop and required heat transfer area in the design point for the gas cooler. Based on the developed design model, off-design calculations should be performed. The corresponding part load conditions are related to a variety of ambient temperatures and this cold demand. The resulting overall heat transfer coefficients could be implemented to cycle simulations in order to predict the off-design behavior of the air-conditioning system. Furthermore, a comparison between an inverter and no-inverter system, a validation of the heat exchanger model and a comparison of potential heat transfer correlations are from interest.

Tasks:

- Definition of the gas cooler's design based on the on-design point for a system with respect to the use of an inverter.
- Off-design performance and thermodynamic analysis of the gas cooler for the defined off-designed conditions.
- Validation of the model and quantification of the deviations in the context of different heat transfer correlations.
- A comparison between an inverter and no-inverter system.

Chapter 3. CO_2 air-conditioning system

3.1. Air-conditioning system

This chapter shows the air-conditioning system and the boundary conditions of the CO_2 project which took place at the University of Bayreuth, Energy Department. In order to define the exact air-conditioning system, an investigation between three potential concepts was conducted. The investigation was carried out by the researchers at the University of Bayreuth. The system A, that is depicted in the Figure 3.1 below, is characterized by the internal heat exchanger which aims to enhance the performance of the system. The results showed a cooling capacity of 11.3 kW and a COP of 2.83.

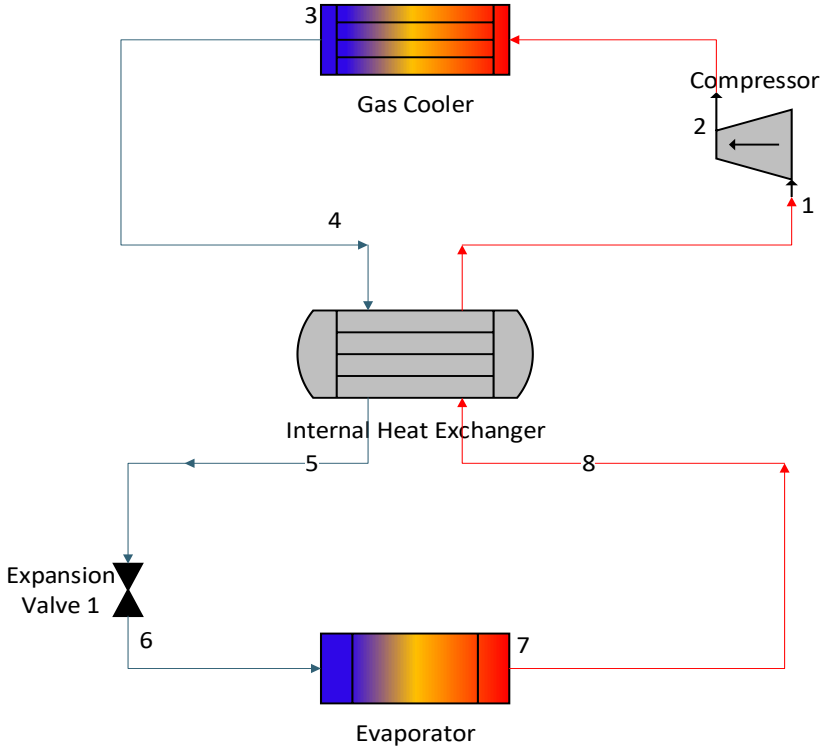

Figure 3.1: System A with an internal heat exchanger.

The second system studied the concept to separate part from the main CO_2 stream after the condenser. An identical performance was found with the first system while the cooling capacity and coefficient of performance were the same. The Figure 3.2 below shows the second system.

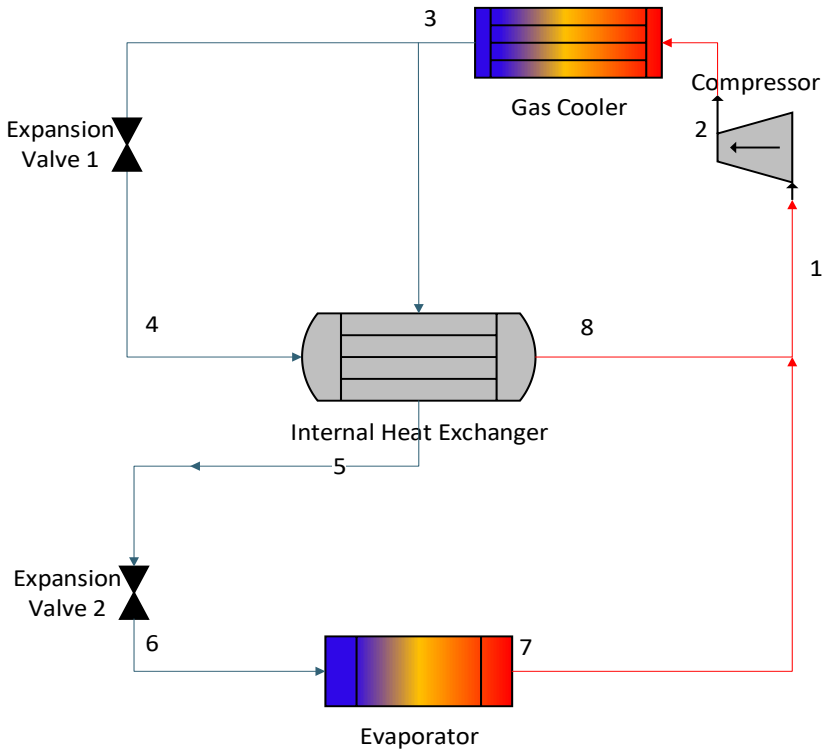

Figure 3.2: System B with a separation from the main CO_2 stream.

The third system incorporated into a second compressor and a second expansion valve and an additional storage tank. Incorporating two compressors, the system had nearly 30 kW cooling capacity but the lowest COP was 2.59. The Figure 3.3 shows the third system.

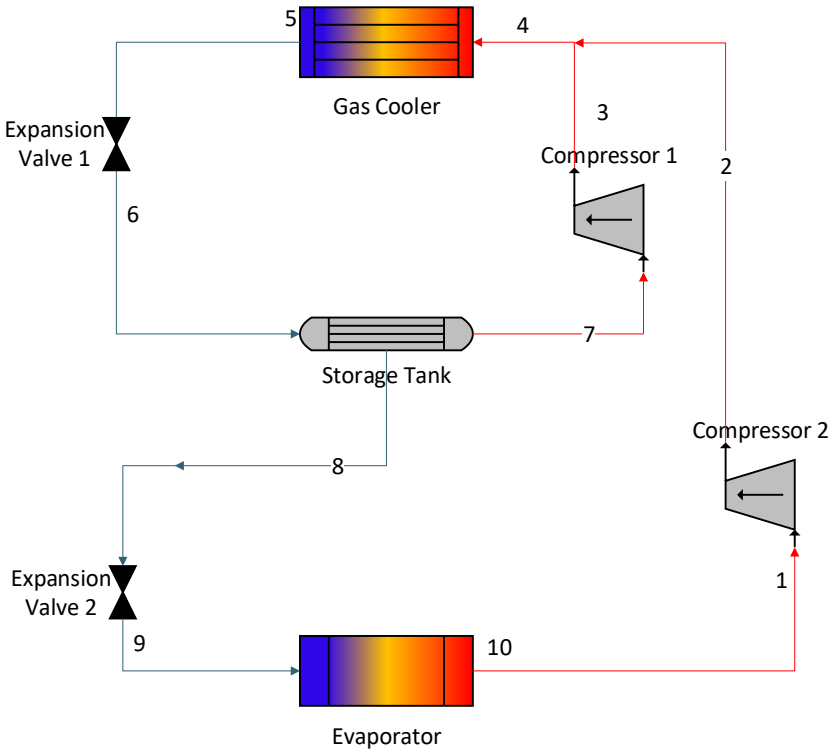

Figure 3.3: System C with two compressors and two expansion valves.

The first and the second system had the same COP of 2.83 while the third system had a COP equal to 2.59. Between the first and the second system, the first system was the simplest in terms of its controls and equipment. Based on that, the system A was chosen for further investigation. Further investigation showed that a second expansion valve was required in order to keep the refrigerant in an appropriate temperature and pressure before entering into the internal heat exchanger. In addition, the system included an accumulator for safety reasons. The final concept of the system is depicted in the Figure 3.4 below.

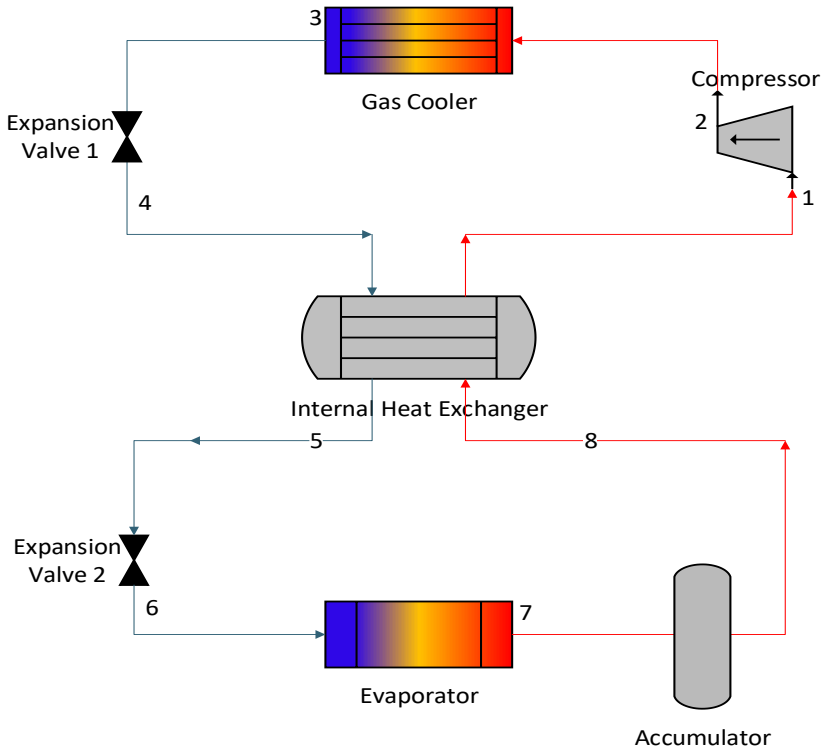

Figure 3.4: Final system with an IHX and two expansion valves.

An investigation for the boundary conditions was conducted and based on its results the experimental test rig will be developed. In order to have more accurate results and be able to control efficiently the conditions of the gas cooler, a water gas cooler was chosen. In actual test rigs, however, the system cannot include a water heat exchanger. For that reason, a study about the air-gas cooler was considered necessary. As it was mentioned previously, an investigation for the boundary conditions was conducted with Aspen. The boundary conditions, eventually for the project are depicted in the Table 3.1 below.

Table 3.1: Boundary Conditions.

High Pressure	93	bar
Middle Pressure	61.5	bar
Low Pressure	45	bar
Gas Cooler Outlet Temperature	38	°C
Evaporating Temperature	10	°C
Ambient Temperature	35	°C
Frequency range	30-75	Hz
Mass Flow Rate Range	184-525	kg/h
Cooling Capacity range	9.7-19.0	kW
Power Range	2.1-6.3	kW
Room Temperature	23	°C

Based on the boundary conditions more specific data was provided (Table 3.3). Using this data, the P-h and T-s diagrams were created in Matlab R2019a. The diagrams are depicted below in the Figures 3.5 and 3.6, respectively. Furthermore, the coefficient of performance and the cooling capacity were calculated. The results showed a cooling capacity of 16 kW and a COP of 2.96. It is important to mention that no pressure drop during the heat exchanging process was taken into consideration. Furthermore, typical values for isentropic efficiencies of the expansion valves and the compressor were considered. More specifically, isentropic efficiencies of 0.85 were assumed for both of the components.

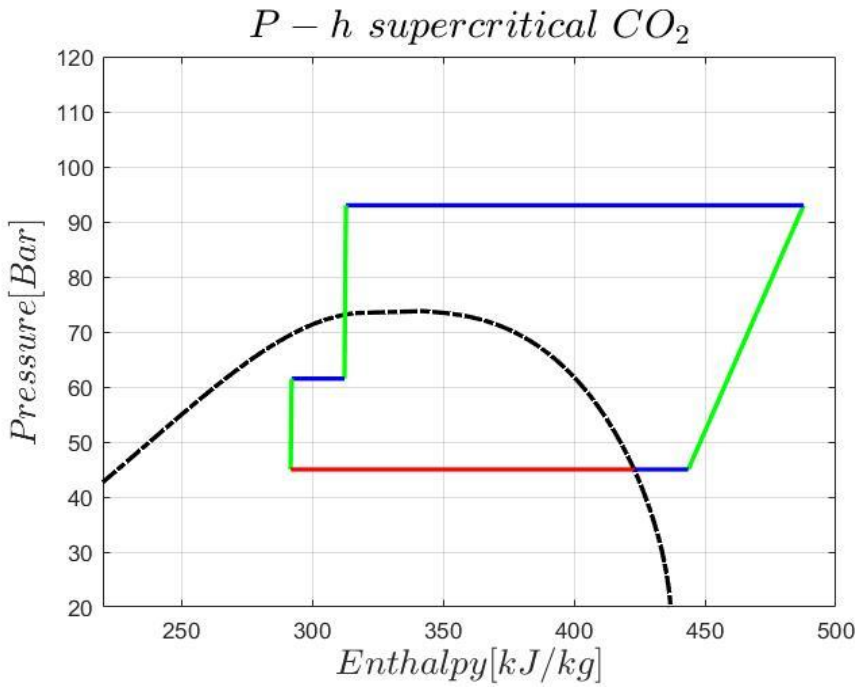

Figure 3.5: P-h process diagram.

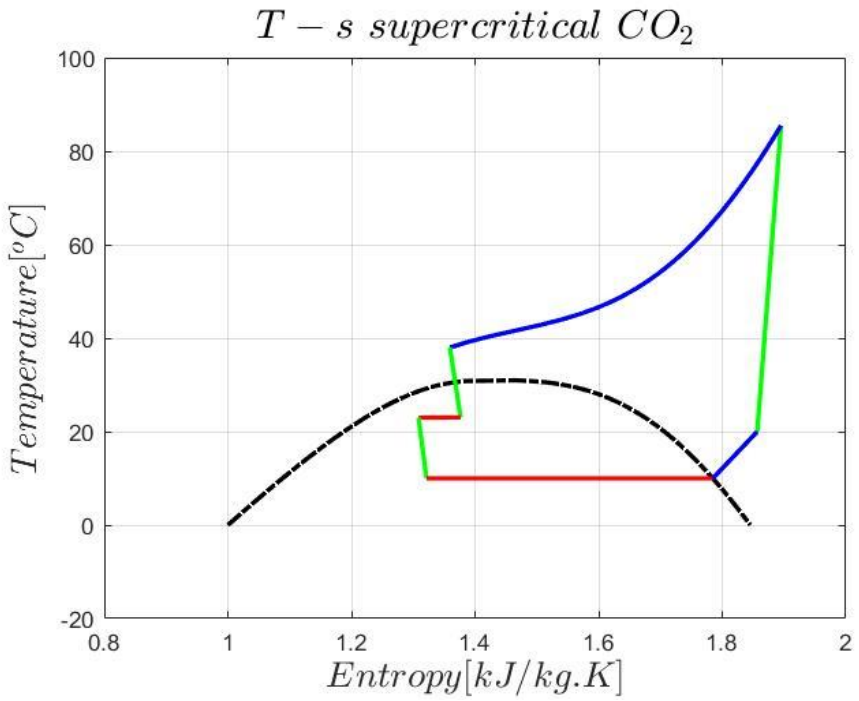

Figure 3.6: T-s process diagram.

The table 3.2 below shows the important quantities of the cycle.

Table 3.2: Important quantities.

Cooling Capacity [kW]	16.0
Compressor Duty [kW]	5.43
COP	2.96
COPcarnot	3.75
Exergy	0.79

The table 3.3 below shows the thermodynamic properties at each point of the cycle.

Table 3.3: Thermodynamic properties of the cycle.

		Gas cooler	**Exp 1**	**IHX 1**	**Exp 2**	**Evaporator**	**IHX 2**	**Compressor**
Inlet:	T [K]	358.64	311.15	296.15	296.15	283.15	283.15	293.15
	P [bar]	93.0	93.0	61.5	61.5	45.0	45.0	45.0
Outlet:	T [K]	311.15	296.15	296.15	283.15	283.15	293.15	358.64
	P [bar]	93.0	61.5	61.5	45.0	45.0	45.0	93.0

3.2. Inverter - no-inverter air-conditioning system.

It was considered reasonable to investigate the operation of the system with respect to the use of an inverter. An inverter is used to control the speed of the compressor based on the

ambient and indoor temperature. As the speed of the compressor is controlled, the refrigerant flow rate and the room temperature are controlled. Inverter air-conditioners operate at maximum capacity as soon as they start up. As a result, the set temperature can be reached quickly. When the indoor temperature approaches the set temperature, the speed of the compressor is changed to low capacity operation to maintain this temperature. An inverter air-conditioner is characterized by the energy saving can achieve compared to non-inverter operation. The addition of the inverter provides the advantage of a higher comfort level as they can eliminate any temperature fluctuations; non-inverter systems start and stop repeatedly in order to control the indoor temperature. The cooling or heating capacity is fixed and when the system restarts the power consumption rises sharply and thus it has high power consumption and temperature variations. The Figures 3.7 and 3.8 below show the differences between these systems.

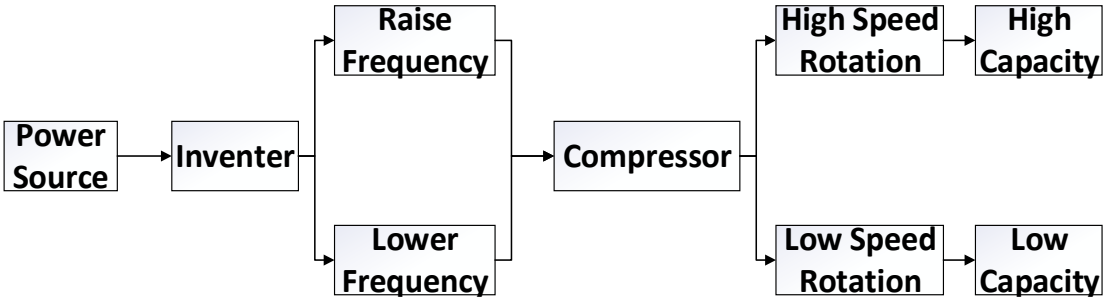

Figure 3.7: Inverter air-conditioning system.

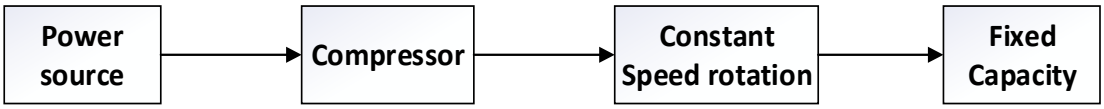

Figure 3.8: No- inverter air-conditioning system.

At that point, it is crucial to mention that in no-inverter air conditioners the refrigerant mass flow remains constant. On the other hand, an inverter air-conditioner regulates the refrigerant mass flow. For each of these systems, an appropriate on design point was found it out. Depending on whether the system includes inverter or not and based on the particular type of the compressor an appropriate compressor's frequency was defined. More specifically, a frequency of 50 Hz was defined for the no-inverter system while for the latter the range of the frequency was defined from 30 to 75 Hz. The on-design point for each of the systems is shown in the Table 3.4 below.

Table 3.4: On – design points.

	Inverter		No-Inverter	
CO_2				
P	93	bar	93	bar
T_{ri}	358.22	K	358.99	K
T_{ro}	311.15	K	311.15	K
m_c	0.146	kg/s	0.092	kg/s
Cooling Medium				
T_{ai}	308.15	K	308.15	K
T_{ao}	315.15	K	315.15	K
Duty	25382.5	Watt	16118.4	Watt

The differences between the duty of the gas coolers due to the refrigerant mass flow differences are noticeable.

Chapter 4. Gas cooler design

The on-design model is a model in which the thermodynamic properties are already defined along the cycle and based on this, the geometries of each component of the cycle are extracted. In this chapter, how the detailed gas cooler's design can be found in order to cover the demands of the system is described. Since there are two potential concepts, the same process was conducted twice. Below, the process in order to define an appropriate gas cooler design is described.

A computational model was created in Matlab R2019a so an appropriate gas cooler's design will be found. The script has as input the thermodynamic properties of the cooling medium, the refrigerant and the duty of the heat exchanger. The type of the heat exchanger was determined as an air finned type. The investigation for different diameters of the air finned tube was considered necessary. One of the most crucial parameters that should have been taken into consideration is that the design should be cost-efficient. That means the gas cooler should have as lower bundle area as possible. Another parameter was the pressure drop of the working fluid. More specifically, a permissible pressure drop of the working fluid was chosen; 0.4 bar for the refrigerant.

The criteria for an appropriate gas cooler's design are:

- Low bundle area.
- Refrigerant pressure drop lower than the permissible.

4.1. Type of the gas cooler

As it was mentioned before, the type of the gas cooler is an air finned tube. As the basic concept was chosen the next step is to determine the configuration of the air finned gas cooler. There are two basic categories:

Cross-flow configuration: In this concept, the refrigerant splits into the tubes which are connected to a common header. This configuration is characterized by large flows and large temperature differences. The cross-flow configuration is depicted in the Figure 4.1 below.

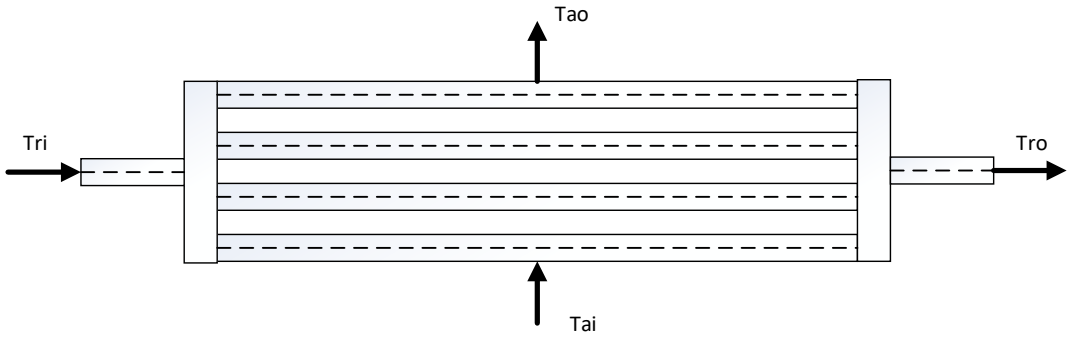

Figure 4.1: Cross-flow configuration.

Counter-current flow configuration (U-tube): In this concept, there is practically one long tube through which refrigerant flows. This configuration is characterized by small fluid

volumes and small temperature differences. The header also must be divided into compartments. The U-tube configuration is depicted in the Figure 4.2 below.

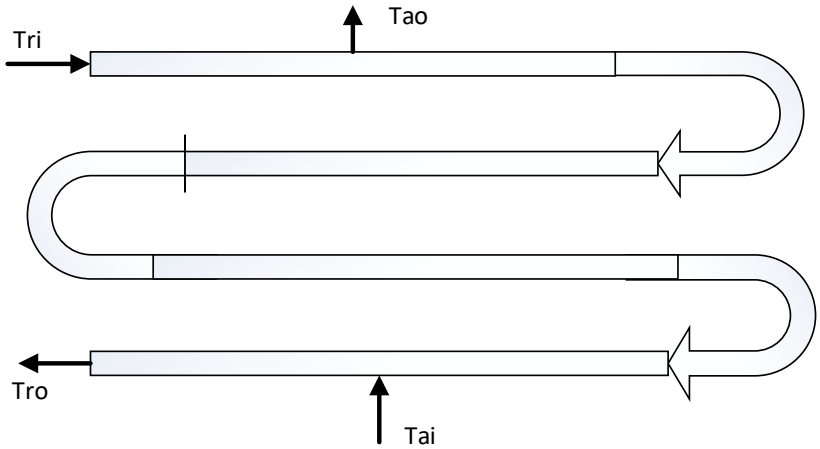

Figure 4.2: Counter-current flow configuration.

The cross-flow configuration was selected because of the capability to calculate the thermodynamic properties and pressure drops in an easier and more accurate way. Furthermore, the type of the fin is circular-round as it is highly used. The specifications of the finned tube obviously affect the efficiency and the overall heat transfer coefficient of the gas cooler. For that reason, different diameters of circular-round finned tubes were investigated. The table 4.1 below shows the different diameters of the finned tube that were investigated. For each tube, the Matlab R2019a code was run for different tube lengths. The data from the 1st tube is from the condenser used for the experiments (Appendix A). The data for the 2nd and the 3rd is from the GEWA.

Table 4.1: Finned tube data.

Finned Tube Datasheet			
	1st Tube	2nd Tube	3rd Tube
Di(m)	0.00685	0.01600	0.02250
Do(m)	0.00735	0.01850	0.02500
hf(m)	0.00700	0.01000	0.01000
dr(m)	0.00060	0.00060	0.00060
m(m)	0.00320	0.00320	0.00320

Where:

- h_f=fin height
- m=fin pitch
- d_r=fin thickness

The Figure 4.3 depicts the above values.

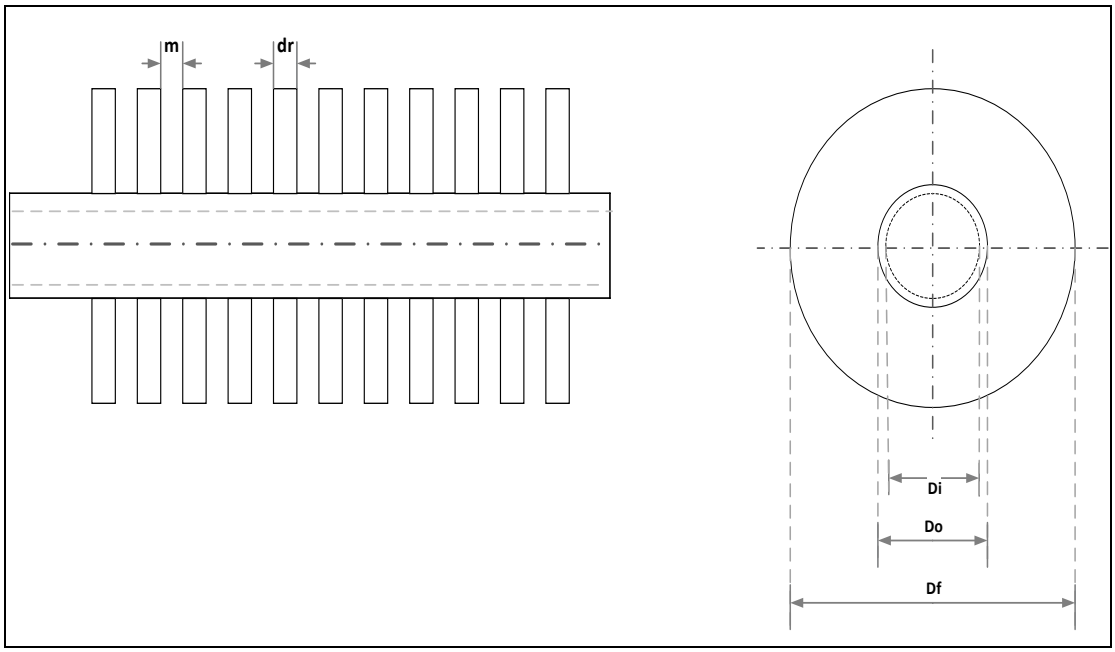

Figure 4.3: Air finned tube geometrical characteristics.

It was considered that aluminum alloys would be used so the thermal conductivity was equal to k=210 W/mK.

4.2. On-design model

The heat transfer in the finned tube mostly results from heat convection. There is also heat transfer from conduction but the amount of the energy interchanged is slightly compared to convection. The heat transfer rate is calculated by the equation according to the LMTD method:

$$\dot{Q} = U \cdot A_R \cdot \Delta T_{LM} \qquad 4.1$$

Where:

- U=overall heat transfer coefficient
- A_R=required exchanged area
- ΔT_{LM}=logarithmic mean temperature

Overall Heat Transfer Coefficient-U

The overall heat transfer coefficient is reciprocal to the total heat transfer resistance, consisting of the two heat transfer resistances due to convection at the internal area and external area of the tube and the conductive wall resistance. In order to have the overall heat transfer coefficient, we have to summarize these three resistances. So, the overall heat transfer coefficient is calculated from the following equation:

$$U = \left[\frac{1}{a\_a} + \frac{A \cdot ln\frac{d_o}{d_i}}{2 \cdot \pi \cdot L \cdot k} + \frac{A}{A_i} \cdot \frac{1}{a\_c} \right]^{-1} \quad 4.2$$

Where:

- A=total external area of the tube and total surface of fins.
- A_i=internal area of the tube
- a_a=air-side heat transfer coefficient
- a_c=refrigerant-side heat transfer coefficient

Total external area of the finned tube:

The external area of the finned tube consists of the total area of the fins A_f, and the total area of the tube A_t without the fins.

$$A = A_f + A_t \quad 4.3$$

The total area of the fins is calculated by multiplication of the number of fins and the area of the fin of each turn.

$$A_f = 2 \cdot A_{fin} \cdot N_{fins} \quad 4.4$$

Where the number of fins N_{fins} is calculated from the equation:

$$N_{fins} = \frac{L}{m} \quad 4.5$$

And the area of the fin:

$$A_{fin} = \pi \cdot \frac{\left({d_f}^2 - {d_o}^2\right)}{4} \quad 4.6$$

The external area of the tube that does not have fins is calculated from the equation:

$$A_t = \left(N_{fins} + 1\right) \cdot \pi \cdot d_o \cdot m \quad 4.7$$

Internal area of the tube:

The internal area of the tube is calculated from the equation:

$$A_i = \pi \cdot d_i \cdot L \quad 4.8$$

Air-side heat transfer coefficient:

As to obtain the air-heat transfer coefficient it is necessary to calculate first the Nusselt number. In fact, there are many correlations to obtain the Nusselt number of the air side. For this project the equation which is proposed from the VDI-Heat Atlas was considered the most appropriate correlation [16]:

$$Nu_{d_o} = C \cdot {Re_{d_o}}^{0.6} \left(\frac{A}{A_{to}}\right)^{-0.15} Pr^{1/3} \qquad 4.9$$

For in-line arrangement C = 0.22 according to the VDI-Heat Atlas [16].

For circular fins, the ratio A/A_{to} of the finned surface to the surface of the base tube becomes:

$$\frac{A}{A_{to}} = 1 + 2 \cdot \frac{h_{fin} \cdot \left(h_{fin} + d_o + d_r\right)}{m \cdot d_o} \qquad 4.10$$

The Reynolds number is calculated with the equation:

$$Re_{d_o} = \frac{\rho \cdot w_s \cdot d_o}{\mu} \qquad 4.11$$

where w_s, is the velocity in the smallest cross-section which is calculated from the velocity in the free flow w_o.

$$w_s = w_o \cdot \frac{A_{\mathrm{inf}low}}{A_{smallest}} \qquad 4.12$$

For in-line arrangement the ratio of inflow area to the smallest cross-sectional area is calculated with the equation:

$$\frac{A_{\mathrm{inf}low}}{A_{smallest}} = \frac{s_1 \cdot m}{m \cdot (s_1 - d_o) + \left(s_1 - d_f\right) \cdot d_r} \qquad 4.13$$

As all the variables for the Nusselt number could be found the air side heat transfer coefficient could be calculated from its definition as the following equations show.

$$Nu_{d_o} = \frac{a\_a \cdot k_{air}}{d_o} \qquad 4.14$$

$$a\_a = \frac{Nu_{d_o} \cdot k_{air}}{d_o} \qquad 4.15$$

Where k_{air}: is the air thermal conductivity.

Actually, having a finned tube it is necessary to calculate the fin efficiency. In this case, the air side heat transfer coefficient changes and becomes:

$$a_{virtual} = a\_a \cdot \left[1 - \left(1 - \eta_{fin}\right) \cdot \frac{A_{fin}}{A}\right] \qquad 4.16$$

With:

$$\frac{A_{fin}}{A} = \frac{2 \cdot \frac{\pi}{4} \cdot \left({d_f}^2 - {d_o}^2\right)}{\pi \cdot d_o \cdot (m - d_r) + 2 \cdot \frac{\pi}{4} \cdot \left({d_f}^2 - {d_o}^2\right)} \qquad 4.17$$

The fin efficiency is defined as the ratio of the heat removed by fin to heat removed by fin at wall temperature:

$$\eta_{fin} = \frac{\dot{Q}_{exchanged\_by\_fin}}{\dot{Q}_{exchanged\_if\_fin\_was\_at\_root\_temperature}} \quad 4.18$$

There is, also the fin effectiveness which is defined as the ratio of the heat removed by fin to heat removed by tube wall without fin:

$$\varepsilon_{fin} = \frac{\dot{Q}_{exchanged\_by\_fin}}{\dot{Q}_{exchanged\_by\_base\_of\_fin\_without\_fin}} \quad 4.19$$

The efficiency of the fin is calculated from the equation:

$$\eta_{fin} = \frac{tanhX}{X} \quad 4.20$$

With:

$$X = \varphi \cdot \frac{d_o}{2} \cdot \sqrt{\frac{2 \cdot a\_a}{k \cdot d_r}} \quad 4.21$$

For circular fins:

$$\varphi = \left(\frac{d_f}{d_o} - 1\right)\left[1 + 0.35ln\left(\frac{d_f}{d_o}\right)\right] \quad 4.22$$

It is necessary to mention that in order to calculate air properties the mean temperature of the air as the bulk temperature was used.

So, the equation of the heat transfer coefficient changes and becomes:

$$U = \left[\frac{1}{a_{virtual}} + \frac{A \cdot ln\frac{d_o}{d_i}}{2 \cdot \pi \cdot L \cdot k} + \frac{A}{A_i} \cdot \frac{1}{a\_c}\right]^{-1} \quad 4.23$$

Refrigerant-side heat transfer coefficient:

As it was mentioned, many investigators have proposed Nusselt correlations about supercritical carbon dioxide. In chapter 2, some of them were listed. For this project, Gnielinski's correlation was chosen in order to calculate the Nusselt number.

Gnielinski correlation:

$$Nu = \frac{{}^{f}/_{8}\,(Re - 1000)Pr}{12.7\sqrt{{}^{f}/_{8}}\left(Pr^{2/3} - 1\right) + 1.07} \quad 4.24$$

Where:

$$f = [0.79ln(Re) - 1.64]^{-2} \quad 4.25$$

As the Nusselt number was calculated the refrigerant side heat transfer coefficient could be found.

$$Nu = \frac{a\_c \cdot k_{co2}}{d_o} \quad 4.26$$

$$a\_c = \frac{Nu \cdot k_{co2}}{d_o} \quad 4.27$$

The next parameter from the equation 4.1 is the Logarithmic mean temperature and can be calculated from the following equation:

$$\Delta T_{LM} = F \cdot \Delta T_M \quad 4.28$$

Where F: the logarithmic temperature difference correction for cross-flow.

With:

$$\Delta T_M = \frac{(T_{ri} - T_{ao}) - (T_{ro} - T_{ai})}{ln\left(\frac{T_{ri} - T_{ao}}{T_{ro} - T_{ai}}\right)} \quad 4.29$$

- T_{ri}= inlet refrigerant temperature
- T_{ro}= outlet refrigerant temperature
- T_{ai}= inlet air temperature
- T_{ao}= outlet air temperature

Since the heat transfer rate $\dot{Q}$ was given, the required exchanged area could be calculated and then the required number of tubes could be calculated from the following equation:

$$N_t = \frac{A_R}{A} \quad 4.30$$

In order to find the optimal design for our application, it is necessary to calculate other parameters that affect the overall efficiency of the system. For that reason, the drop pressure on both sides (air and refrigerant) and the power fan consumption were found. Below it is displayed thoroughly how these parameters were calculated.

Drop Pressure:

These systems are characterized by their pressure drop, especially on the refrigerant side. Despite the necessity to investigate the refrigerant side pressure drop, it was also necessary to investigate the air side pressure drop.

Air Side:

For the air side pressure drop the methodology of the VDI Heat Atlas was conducted [16]:

As it was mentioned, the in-line arrangement was chosen so the pressure drop was given by the equation:

$$\Delta P = \xi \cdot n_{MR} \cdot \frac{\rho \cdot {w_s}^2}{2} \qquad 4.31$$

Where:

- ξ=drag coefficient
- n_{MR}=the number of main resistances in the flow direction
- ρ=density
- w_s= *Velocity in the smallest cross-section*

For in-line tube arrangement, the number of the main resistances in the flow direction n_{MR} is identical with the number of the tube rows NR.

As far as the drag coefficient is concerned, it is a function of the Reynolds number. In order to calculate the drag coefficient, an ideal tube bundle with in-line tube arrangement was assumed, so we used the below equation:

$$\xi = \xi_{lam} + \xi_{turb} \cdot F_f \qquad 4.32$$

With

$$F_f = 1 - exp\left(-\frac{Re + 1000}{2000}\right) \qquad 4.33$$

The drag coefficient ξ_{lam} for laminar flow is given by

$$\xi_{lam} = \frac{f_{a,l,f}}{Re} \qquad 4.34$$

With

$$f_{a,l,f} = \frac{280 \cdot \pi \cdot [(b^{0.5} - 0.6)^2 + 0.75]}{(4ab - \pi)a^{1.6}} \qquad 4.35$$

The drag coefficient ξ_{turb} for turbulent flow is given by

$$\xi_{turb} = \frac{f_{a,t,f}}{Re^{0.1(\frac{b}{a})}} \qquad 4.36$$

With

$$f_{a,t,f} = \left[0.22 + 1.2\frac{\left(1-\frac{0.94}{b}\right)^{0.6}}{(a-0.85)^{1.3}}\right] x10^{0.47[(b/a)-1.5]} + [0.03(a-1)(b-1)] \quad 4.37$$

Refrigerant Side:

For the calculation of the refrigerant pressure drop, the most highly used correlation was chosen. Generally, for the pressure drop as it was referred and previously is calculated for the equation:

$$\Delta P = f\frac{G^2}{2\rho}\frac{L}{D} \quad 4.38$$

The variable that changed accordingly is the drag coefficient f. So, for the refrigerant side, the following equations were used:

$$f = [1.82ln(Re_b - 1.64)]^{-2} \quad 4.39$$

$$is\ used\ for\ 10^4 \leq Re_b \leq 5x10^6$$

$$f = \frac{0.316}{Re_b^{\,1/4}} \quad 4.40$$

$$is\ used\ for\ Re_b \leq 10^5$$

Which are Filolenko and Blasius correlations, accordingly [20].

At that point, it is crucial to mention that the design of the gas cooler should be as compact as possible. That means, we chose 1.2 m as a length of each pass. For that reason, when the length of the tube is more than 1.2, U-bend (Figure 4.2) is implemented and as a result, each tube has more than one passes depending on its length. As the tube is bending then it is necessary to recalculate the new pressure drop and the bundle area.

More specifically, the new pressure drop was calculated based on the VDI-Heat Atlas that proposes a factor for each U-bend [16]. In this case, a factor of 1.2 for each U-bend was implemented so the new pressure drop was calculated with the following equation:

$$\Delta P = C_{bend} \cdot N_p \cdot f\frac{G^2}{2\rho}\frac{L}{D} \quad 4.41$$

Where:

- C_{bend}= 1.2
- N_p= Number of passes.

In addition, a distance equal to the transversal distance of the tubes was considered for each U-bend. The bundle area is calculated from the equation below:

$$A_{bundle} = s_1 \cdot N_p \cdot N_{trow} \cdot L_{pass} \quad 4.42$$

Where:

- s_1 = Trasversal distance
- N_p = Number of passes
- N_{trow} = Number of tubes per row
- L_{pass} = 1.2 (Length of each pass).

Fan power:

For the estimation of the fan power consumption, it was assumed a fan efficiency of 50 %. The fan power consumption is calculated by:

$$\dot{W}_{fan} = \frac{w_o \cdot (s_1 \cdot A_{bundle} \cdot \Delta P)}{\eta_{fan}} \quad 4.43$$

For the thermodynamic properties of the carbon dioxide and the air, the REFPROP 10 was used.

The flowchart which is depicted in the Figure 4.4 below shows how the above equations were used in order to obtain the results.

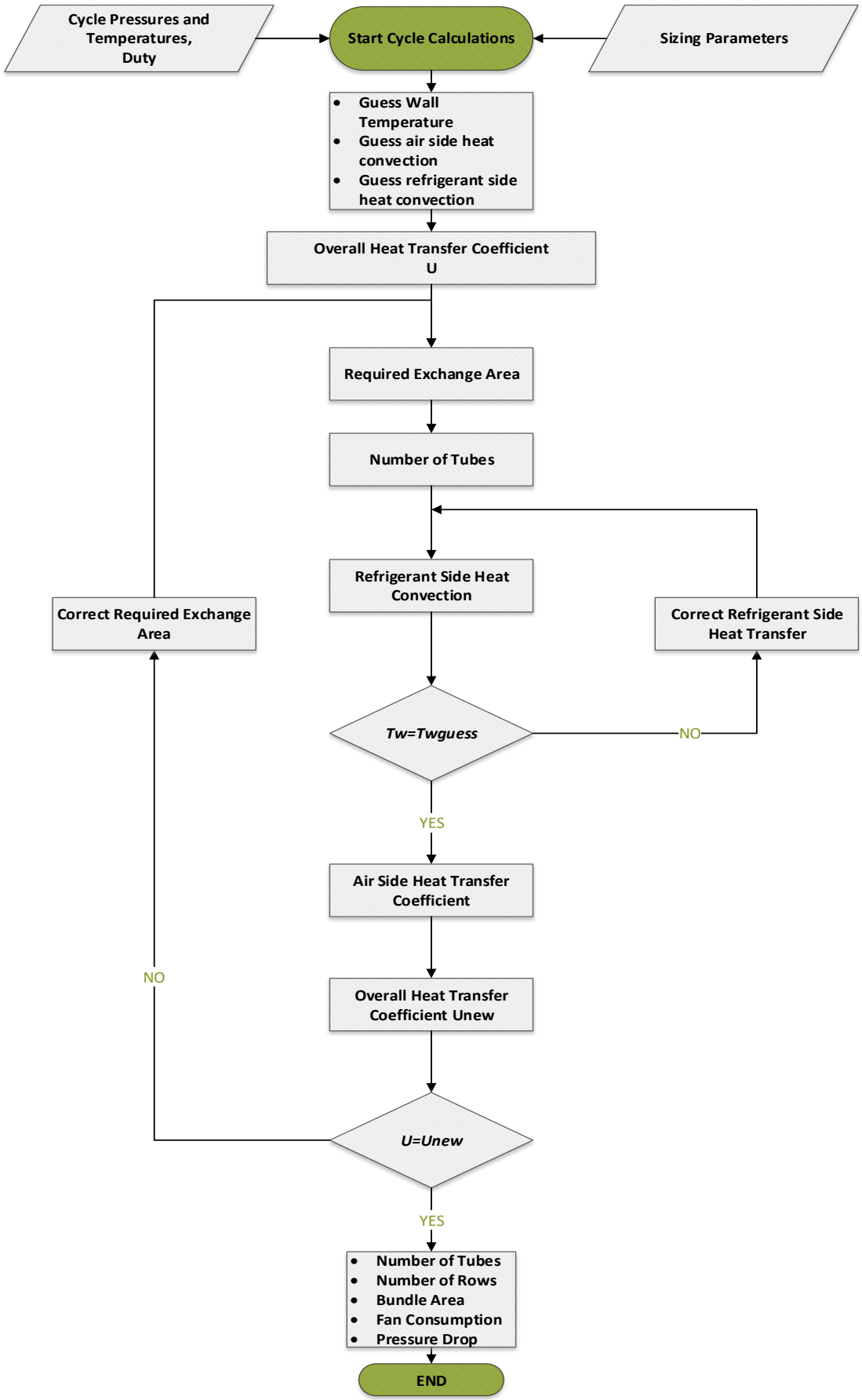

Figure 4.4: On – design model flowchart.

4.3. Results and discussion

4.3.1 Inverter

Below, the results of the gas cooler's model are presented for the inverter. Different diameters were investigated for different lengths of the tube and different numbers of rows (NR). A compromise between the bundle area and the pressure drop was necessary in order to find an appropriate gas cooler's design. The Figures 4.5, 4.6 and 4.7 below show the bundle area of the heat exchanger according to the length of the tube.

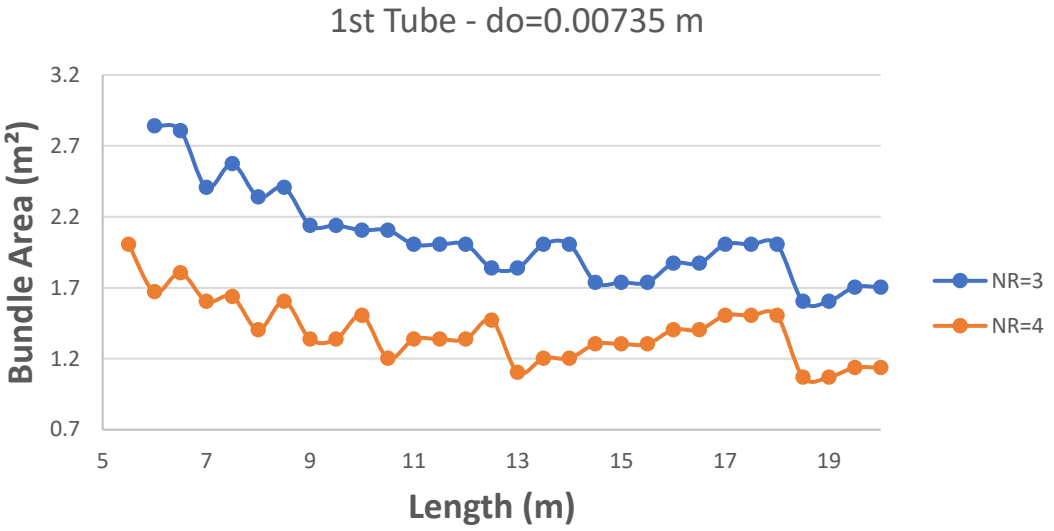

Figure 4.5: Bundle area according to the length of the tube with d_o = 0.00735 m - Inverter.

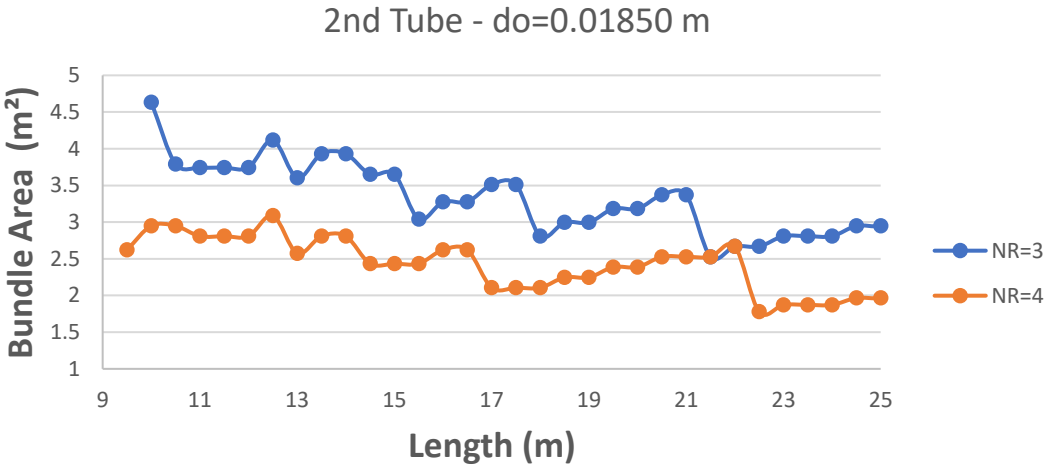

Figure 4.6: Bundle area according to the length of the tube with d_o = 0.01850 m - Inverter.

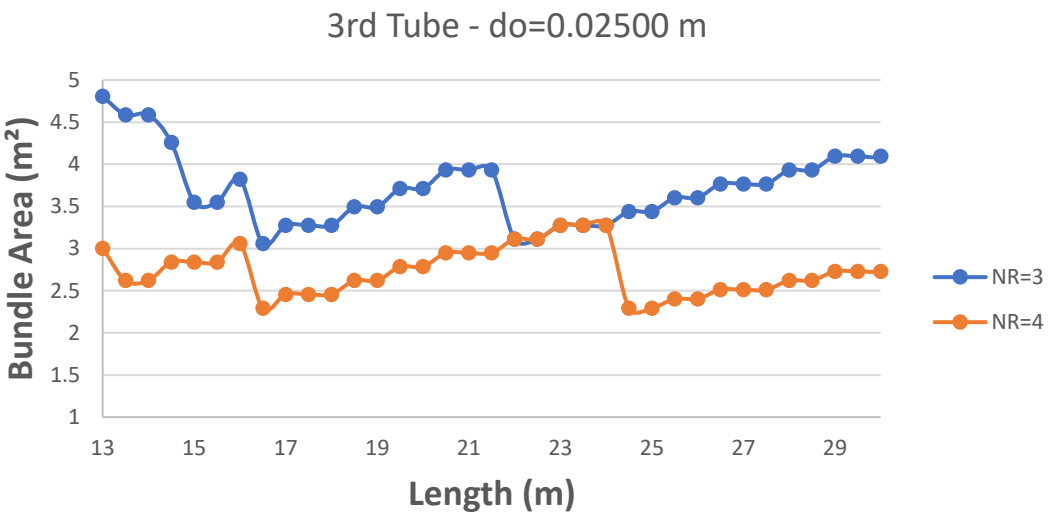

Figure 4.7: Bundle area according to the length of the tube with d_o = 0.02500 m - Inverter.

First of all, the above Figures 4.5, 4.6 and, 4.7 show a not linear correlation between the bundle area and the length of the tube that can be justified by the three different stages of the flow; laminar, transition and turbulent. Secondly, it is noticeable that for each tube, the heat exchanger with 4 numbers of rows has a smaller bundle area than with 3 number of rows. Since the heat exchanger with 4 numbers of rows has the smallest bundle area, it was reasonable to focus on this. The Figure 4.8 below depicts that the tube with the smallest diameter has the smallest bundle area.

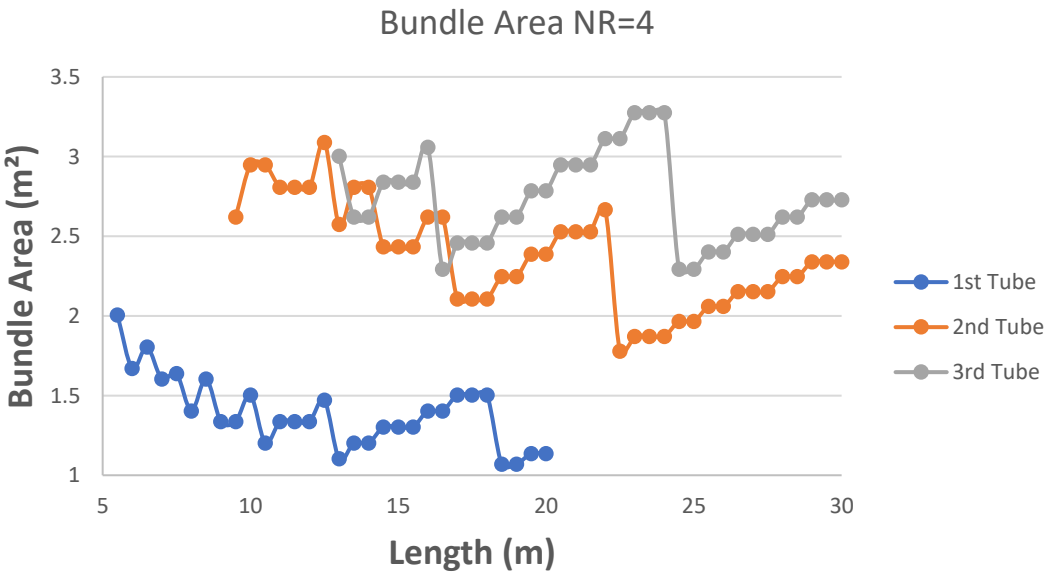

Figure 4.8: A comparison between the bundle area according to the length of the tube for 4 number of rows - Inverter.

However, the pressure drop should be taken into consideration. As it was mentioned previously, the permissible pressure drop for the refrigerant is 0.4 bar. The Figure 4.9 below

shows that the 1st tube with the smallest diameter has a higher pressure drop than the permissible.

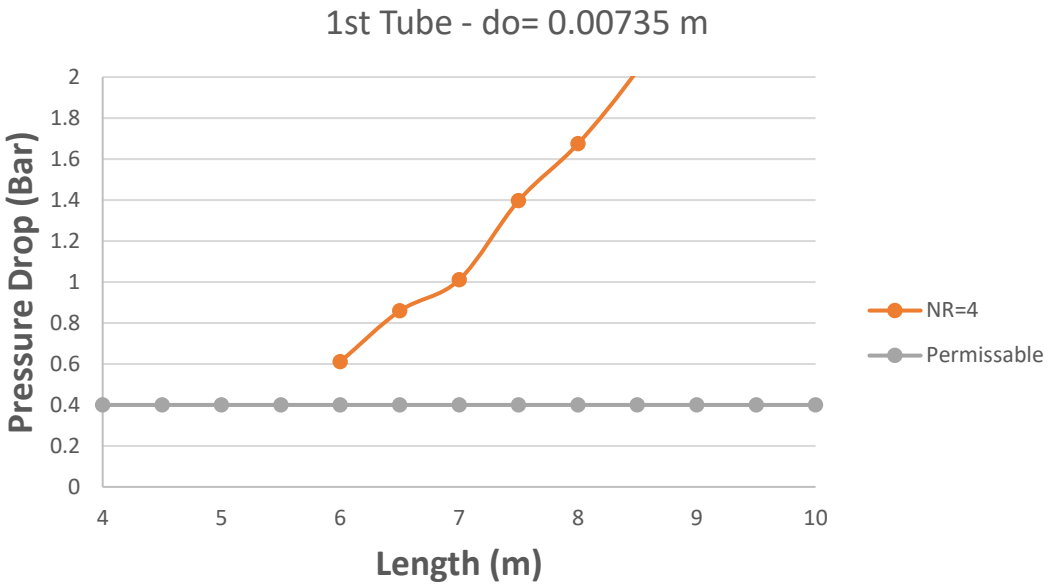

Figure 4.9: Pressure drop according to the length of the tube for the 1st tube and NR = 4 - Inverter.

For that reason, the 1st tube even though it had a smaller bundle area it was not acceptable to use it. Since the 1st tube cannot be selected, the 2nd or the 3rd tube should be selected instead. The pressure drop for both of the tubes is smaller than the permissible. That means, the 2nd tube with the smallest bundle area can be used.

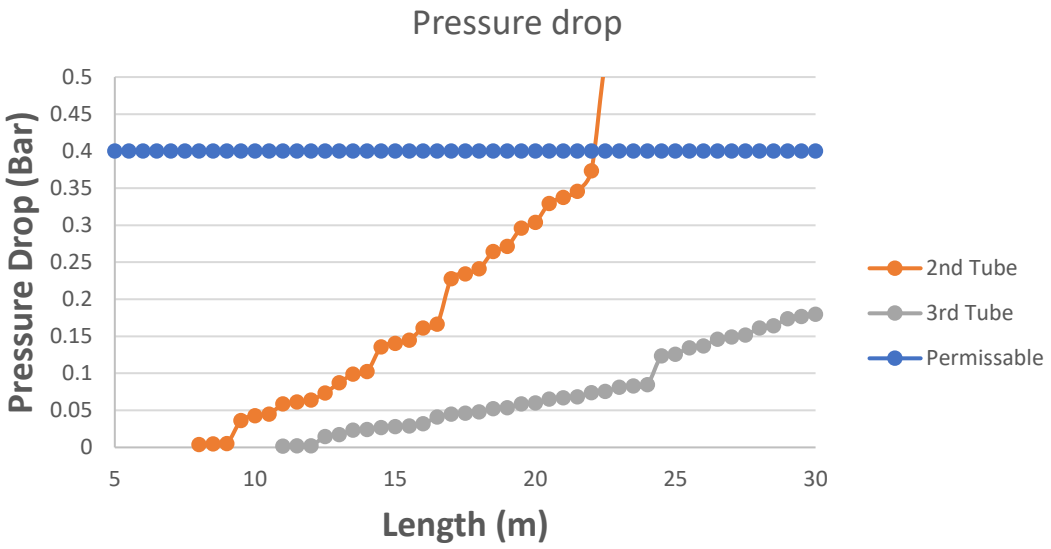

Figure 4.10: Pressure drop according to the length of the 2nd and 3rd tube NR = 4 - Inverter.

More specifically, the smallest bundle area with pressure drop lower than the permissible is with 17 m length of the tube. The design of the gas cooler is designed based on that tube. Specifications about the final gas cooler design are provided in the Table 4.2 below.

Table 4.2: Gas cooler specifications – Inverter system.

Gas Cooler Specifications	
Total Length of Tube [m]	17
Number of Passes per tube	14
Number of Passes	43
Length of each pass [m]	1.2
Number of Rows	4
Number of Tubes per Row	3
Bundle Area [m²]	2.106
Refrigerant Pressure Drop [bar]	0.22769345
Air Pressure Drop [Pascal]	6.4722
Air Finned Tube Specifications	
Outside diameter [m]	0.0185
Wall thickness [m]	0.00125
Fin height [m]	0.01
Fin Pitch [m]	0.0032
Tube Pitch [m]	0.039

4.3.2 No-inverter

The same process was carried out in order to define the gas cooler design according to the no-inverter system. Different diameters were investigated for different lengths of the tube and different numbers of rows. The Figures 4.11, 4.12 and, 4.13 below show the bundle area of the heat exchanger according to the length of the tubes.

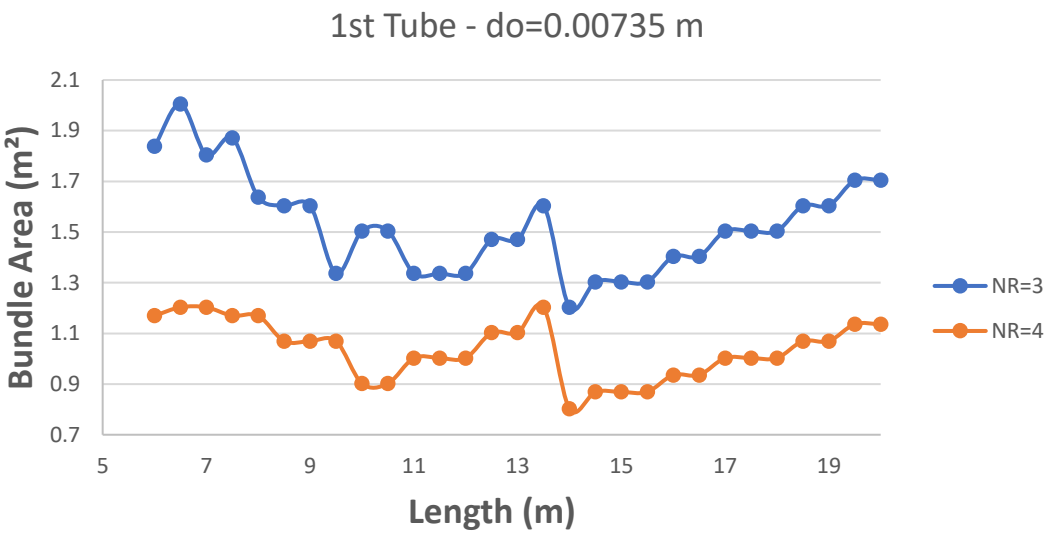

Figure 4.11: Bundle area according to the length of the 1st tube d_o = 0.00735 m - No - Inverter.

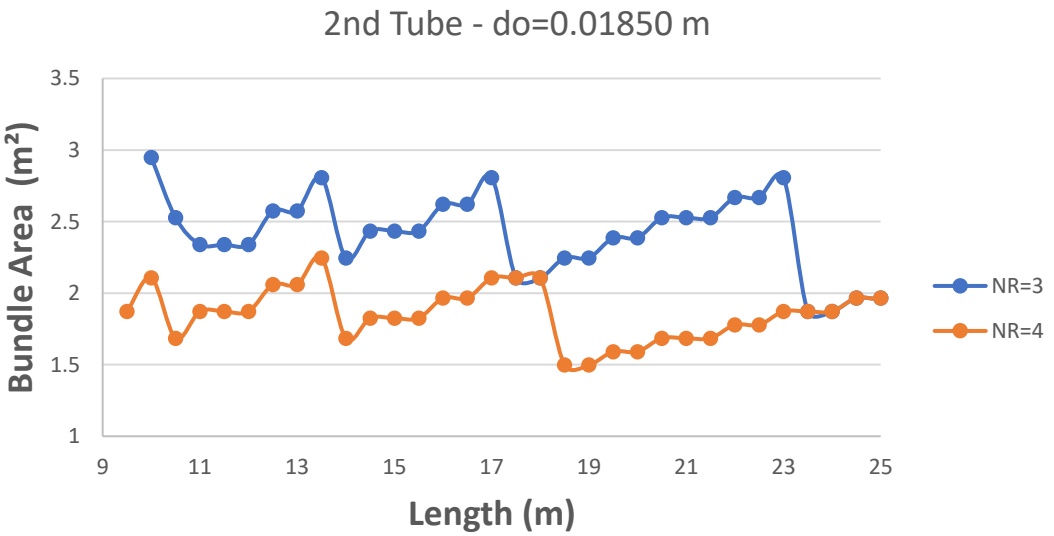

Figure 4.12: Bundle area according to the length of the 2nd tube with d_o = 0.01850 m - No - Inverter.

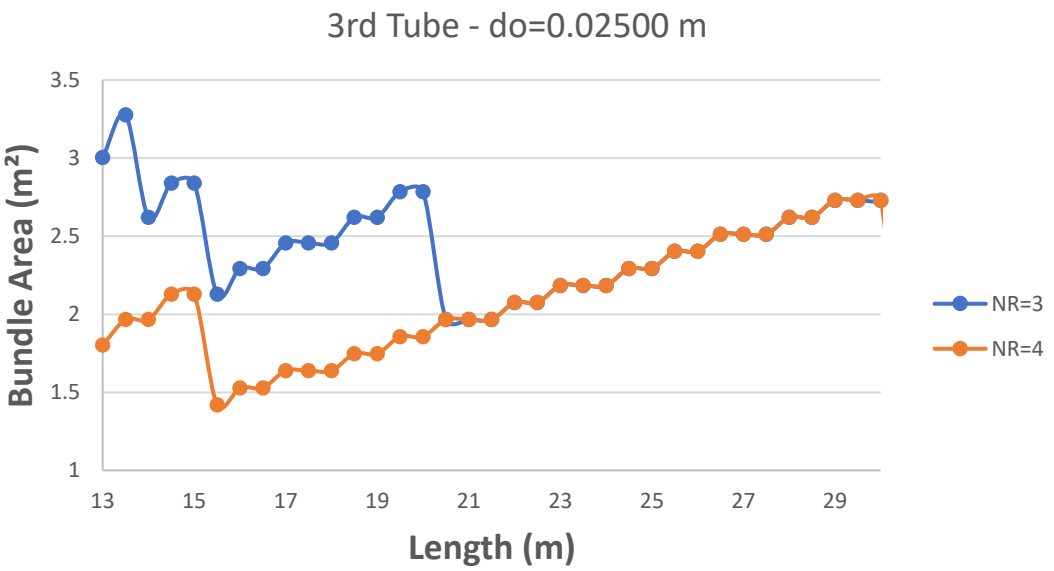

Figure 4.13: Bundle area according to the length of the 3rd tube with d_o = 0.02500 m No - Inverter.

First of all, the above Figures 4.11, 4.12 and, 4.13 show a not linear correlation between the bundle area and the length of the tube that can be justified by the three different stages of the flow; laminar, transition and turbulent. Secondly, it is noticeable that for each tube the heat exchanger with 4 number of rows has a minimum bundle area. Since the heat exchanger with 4 numbers of rows has the smallest bundle area, it was reasonable to focus on this. The Figure 4.14 below depicts that the tube with the smallest diameter has the smallest bundle area.

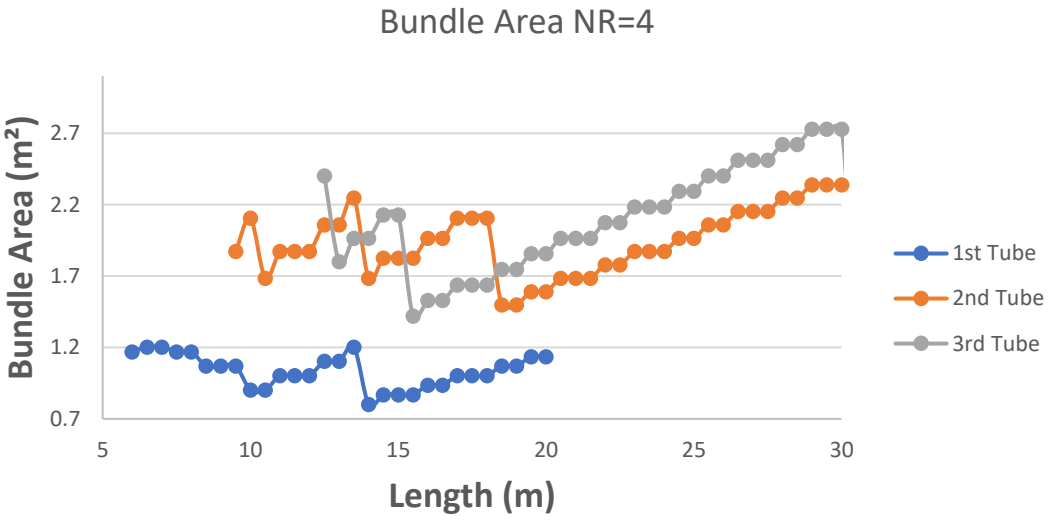

Figure 4.14: Bundle area according to the length of the tube and NR=4 – No - Inverter.

However, the pressure drop should be taken into consideration. The Figure 4.15 below shows that the 1st tube with the smallest diameter has a larger pressure drop than the permissible for each length of the tube except the tube with a length of L = 6 m.

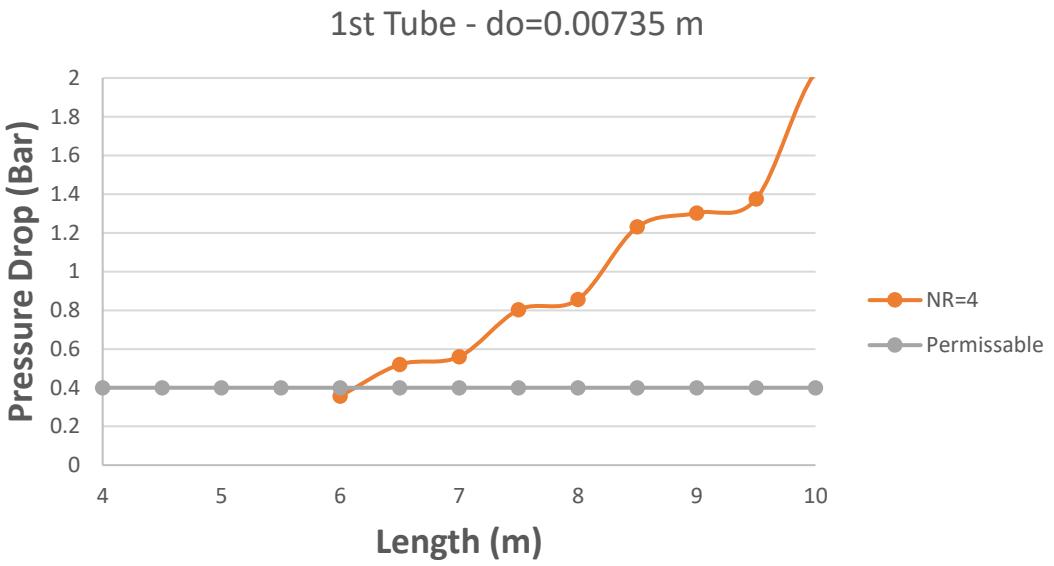

Figure 4.15: Pressure drop according to the length of the tube for the 1st tube and NR=4 – No - Inverter.

The 1st tube with 6 m length of the tube has a significantly smaller bundle area than the others. For that reason, the optimal gas cooler design for the no-inverter system uses the 1st tube. The design of the gas cooler has been performed based on that tube. Specifications about the final gas cooler's design are provided in the Table 4.3 below.

Table 4.3: Gas cooler specifications – No-inverter system.

Gas Cooler Specifications	
Total Length of Tube [m]	6
Number of Passes per tube	5
Number of Passes	35
Length of each pass [m]	1.2
Number of Rows	4
Number of Tubes per Row	7
Bundle Area [m²]	1.17
Refrigerant Pressure Drop [bar]	0.36
Air Pressure Drop [Pascal]	3.01
Air Finned Tube Specifications	
Outside diameter [mm]	7.35
Wall thickness [mm]	0.25
Fin height [mm]	10
Fin Pitch [mm]	3.2
Tube Pitch [mm]	27.85

4.4. Summary

An appropriate gas cooler's design has been defined for each concept (inverter, no-inverter system), based on the on-design point. Furthermore, a compromise between the bundle area and the pressure drop has been achieved. The results show that the bundle area has not linear correlation with the length of the tube as the Figures 4.5, 4.6 and 4.7 for inverter system and the Figures 4.11, 4.12 and 4.13 for no-inverter depict. This not-linear correlation is justified by the different phases of the flow (laminar, transition, turbulent). In addition, an investigation for different numbers of rows took place and the results show that the heat exchanger with 4 number of rows has lower bundle area than with 3 number of rows. The results are depicted in the Figures 4.5, 4.6 and 4.7 for the inverter system and the Figures 4.11, 4.12 and 4.13 for no-inverter. In continue, an investigation for potential finned tube took place and shows that the finned tube with the smallest diameter has the lowest bundle area as the Figure 4.8 for inverter and the Figure 4.14 for no–inverter show. On the other hand, the pressure drop works in a reverse way. That means the smallest diameter has the highest pressure drop and, in that way the lowest bundle area cannot be achieved due to the high pressure drop. Finally, a gas cooler with a bundle area of 2.106 m^2 and a finned tube with an outside diameter of d_o=18.5 m was defined for the system including an inverter while for the no-inverter system a gas cooler with a bundle area of 1.17 m^2 and a finned tube with an outside diameter of d_o=7.35 mm was defined (Tables 4.2 and 4.3, accordingly).

Chapter 5. Off-design model validation

As the detailed design for the gas cooler has been found the off-design for it should be performed. A script was created in Matlab R2019a so as the off-design analysis would be performed. An off-design model is a model in which the geometry of the component and the boundary conditions are specified. This kind of model enables to compute how this specified component (gas cooler) behaves if it leaves the on-design point. In this chapter, a validation of the off-design script and a comparison of heat transfer correlations are presented.

5.1. Validation

Being difficult to construct a test rig with CO_2 as a working fluid, a test rig using water was constructed. The water is a well-known working fluid and its properties have already been investigated and studied thoroughly. The purpose of this experiment is to acquire a realistic overview of a condenser and based on that, to validate the off-design model. In that way, deviations between the model and the experiments could be extracted. For the experiments, an already existed test rig was modified at the University of Bayreuth, Energy department. The main component was the condenser which is a Panasonic heat exchanger, data specifications are provided in the Appendix A. Specific details about the experiments are described below. The used test rig is depicted in the Figure 5.1 below.

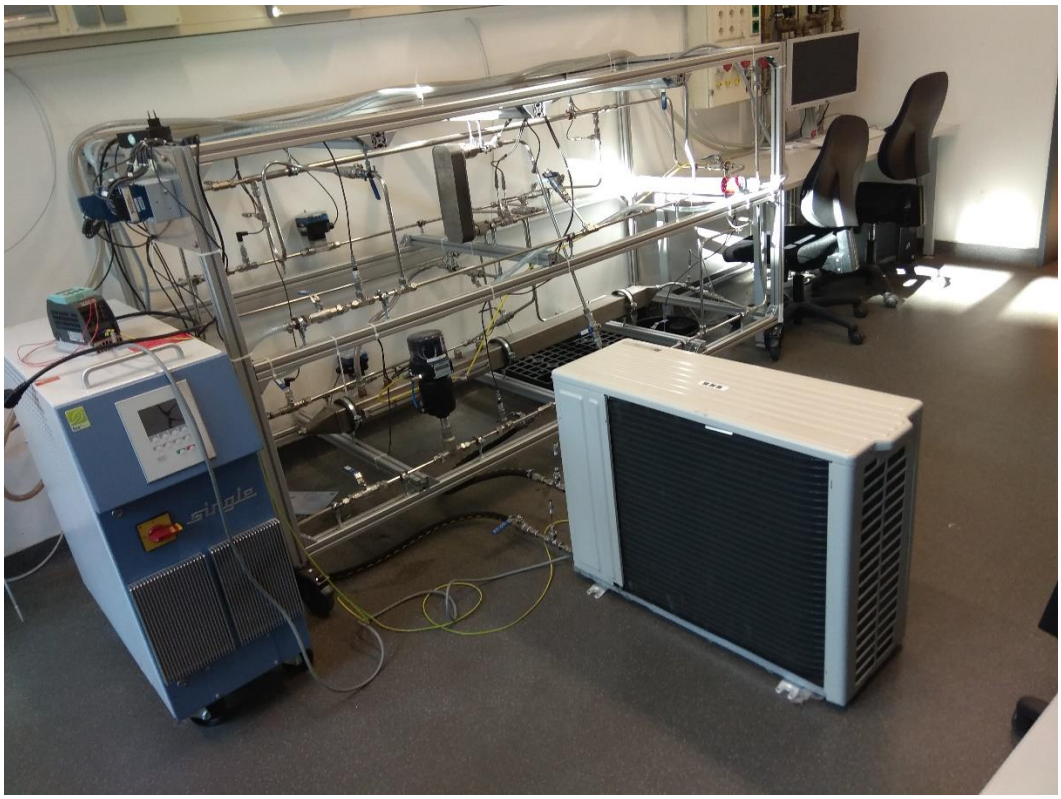

Figure 5.1: The test rig at the University of Bayreuth.

5.1.1 Experiments

The test rig already existed but some modifications were considered necessary in order to adjust the condenser and the measurement equipment into the rig. The test rig consisted of the water operated system (heater) in order to increase the water temperature. The system could increase the water temperature to 90 °C while the maximum pressure was about 4 bar. Based on that, it was concerned that the system needed only temperature and pressure measurements. The test rig for the pressure measurements used pressure transducers before and after the condenser. As far as the temperature is concerned, it was used thermocouples before and after the condenser. Experiments for different water mass flows, different inlet water temperatures and different fan frequencies have been carried out. For that reason, a mass flow valve, a fan frequency controller and a heater were used. The test rig sketch is depicted in the Figure 5.2 below. More detailed data about the experimental components are shown in the Appendix A.

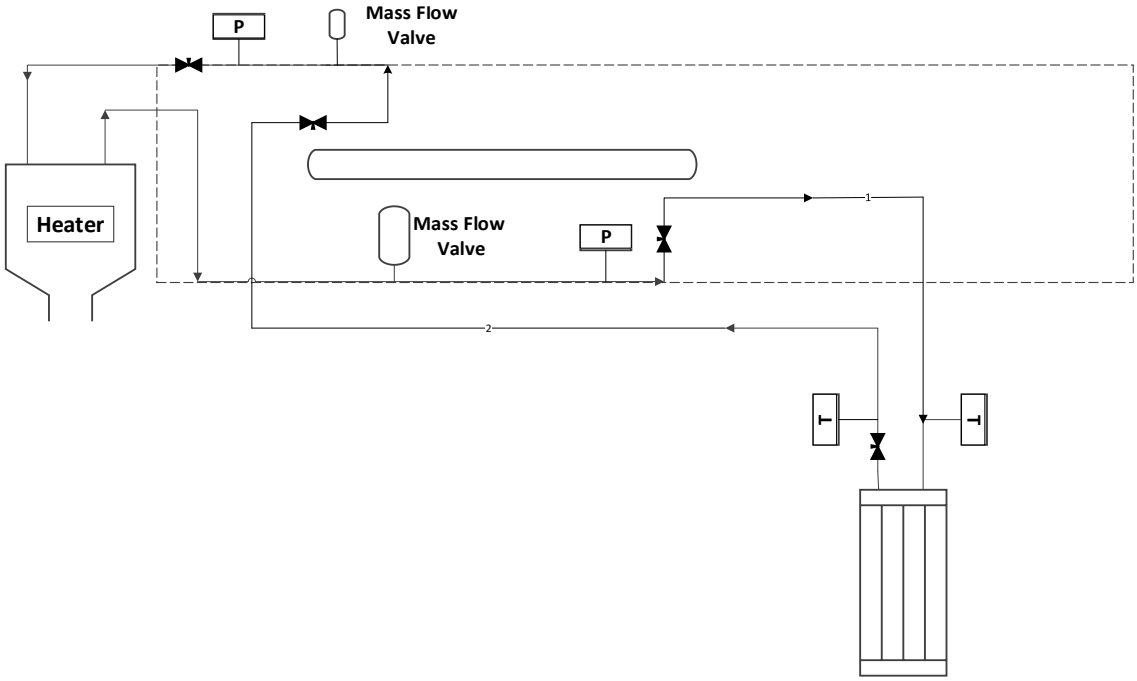

Figure 5.2: Test rig monogrammic sketch.

The range of each variable is depicted in the table 5.1 below.

Table 5.1: The range of the experimental variables.

Water Mass Flow [l/min]	Inlet Water Temperature [°C]	Fan Frequency [Hz]
5	35	30
5.5	40	40
6	45	50
6.5	50	60
7	55	70
7.5	60	80
8	65	
8.5	70	
9	75	

5.1.2 Off-design validated model.

As it has been mentioned the off-design model has two basic inputs. One is the design of the heat exchanger and the other is the thermodynamic properties of the fluids (air inlet temperature, air pressure, water inlet, and outlet temperature and pressure).

The design of the condenser is depicted in the Figures 5.3 and 5.4 below. More details about the condenser are provided in the Appendix A. The properties of the fluids were measured from the measurements into the test rig. Below the calculations of the off-design model are described.

As the mass flow of the water and its thermodynamic properties before and after the condenser were measured, the exchanged heat energy could be found from the following equation:

$$\dot{Q} = \dot{m}_{wa} \cdot Cp_{wa} \cdot (\Delta T_{wa}) \quad 5.1$$

In continue, the air temperature could be found as the Q and the inlet temperature of air were calculated from the following equation:

$$T_{ao} = \frac{\dot{Q}}{\dot{m}_a \cdot Cp_a} + T_{ai} \quad 5.2$$

As far as the air mass flow is concerned, it was given the correlation between the rpm of the fan and the fan air flow rate from the manufacturer as the following equation shows:

$$\dot{V}_a = (0.0381 \cdot n - 4.4704) \quad 5.3$$

Where n is the fan frequency.

In that case, it was controlled the frequency of the fan speed. The fan air flow rate was found by using this correlation. The air density is approximately constant for these temperatures so the mass flow of the air could be calculated from the equation below:

$$\dot{m}_a = \dot{V}_a \cdot \rho_a \quad 5.4$$

In that point, the experimental overall heat transfer coefficient of the condenser could be calculated from the following equation:

$$U_{exp} = \frac{Q}{A_R \cdot \Delta T_{LM}} \qquad 5.5$$

Where:

- Q =calculated from the equation 5.1
- A_R=is given from the manufacturer (Appendix A)
- ΔT_{LM}= equation 4.29

The model overall heat transfer coefficient, however, was calculated according to the equation 4.23. In order to find out the required variables, some assumptions for the design of the condenser should be made.

The condenser consisted of several long bending tubes. Some of them had equal length while others have different. The total mass flow of the refrigerant is separated into 12 long tubes with different lengths each tube. Each tube had several passes into the condenser. Due to the complicated design of the condenser, its modeling was highly difficult. The condenser is depicted in the following Figures 5.3 and 5.4.

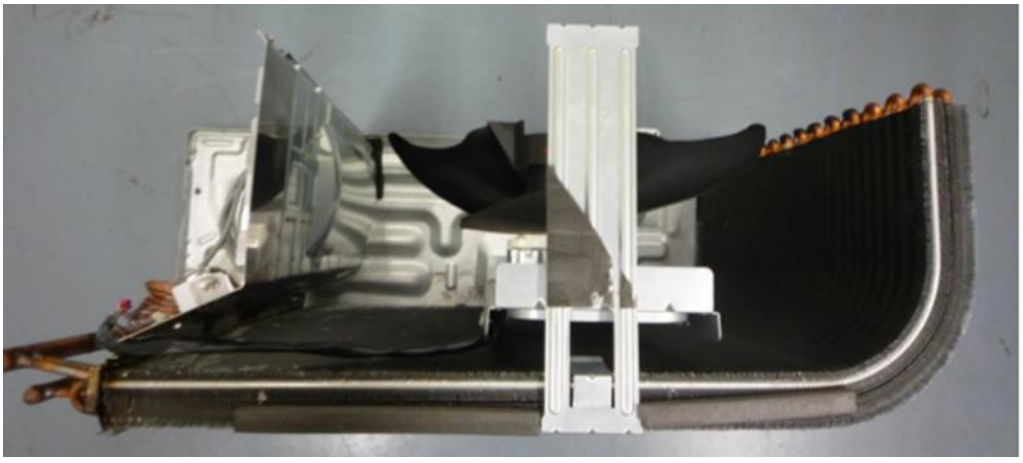

Figure 5.3: The condenser used for the experiments at the University of Bayreuth.

Figure 5.4: The condenser used in the experiments at the University of Bayreuth.

The condenser's design included several long bending tubes. If the tubes are assumed as they are not bending then it will occur a cross-flow design with different lengths of tubes as the Figure 5.5 shows.

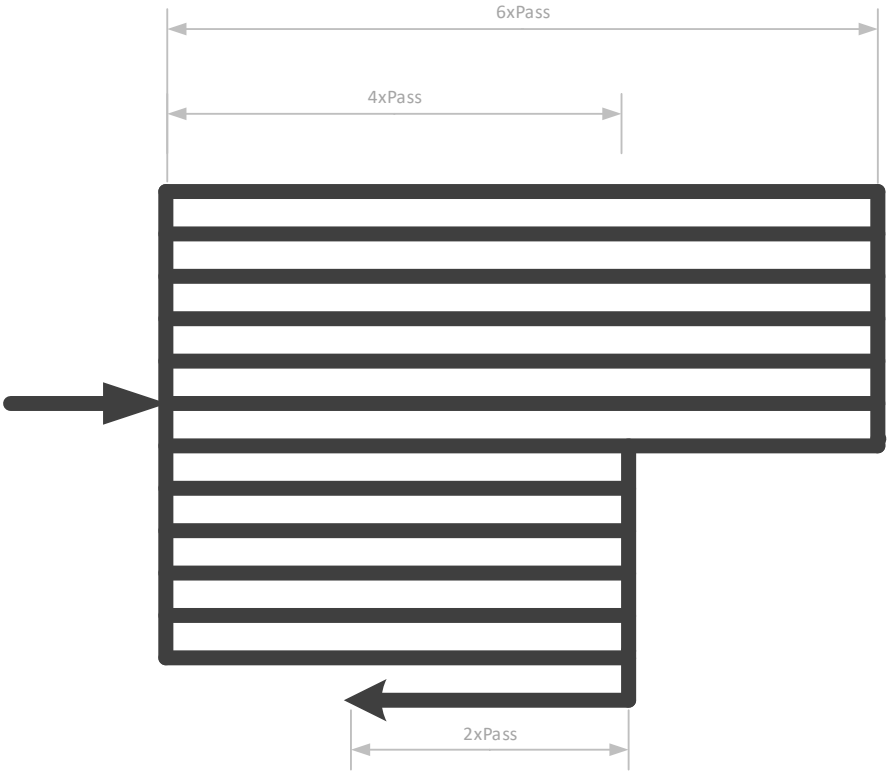

Figure 5.5: The design of the condenser as a crossflow configuration.

The condenser consisted of 3 parts. The first part included 7 tubes with 6 passes each tube. The second part includes 5 tubes with 4 passes each tube while the last part was the outlet of the condenser with only one tube with 2 passes. In continue, in order to calculate the air side heat transfer coefficient circular fins and in line arrangement were assumed due to too small results for the smallest cross section as the VDI-Heat Atlas suggests [16]. Knowing the total surface of the fins and the number of the tubes the total surface of the fins could be calculated corresponding to one tube. Moreover, the number of fins was given (Appendix A) so the surface of one fin can be found. Considering circular fins the only unknown variable is the diameter of fin. The following equation calculates this value;

$$D_f = \sqrt{A_{fin} \cdot \frac{4}{\pi} + {d_o}^2} \qquad 5.6$$

Considering these assumptions for the design of the condenser the model overall heat transfer coefficient could be calculated from the equation 4.23 using the same equation with on-design model (Chapter 4) for the air and refrigerant heat transfer coefficients. Furthermore, for the refrigerant side the Gnielinski and Dittus Boelter and for the air side the VDI-Heat Atlas, Schmidt and Gianolio and Cut correlations were used ([18], [20], [16], [22], [21]).

A comparison between the experimental and model overall heat transfer coefficient and between different heat transfer correlations has been carried out. The results are presented below.

5.2. Results and discussion

Refrigerant side heat transfer coefficient

The following Figures show the model based on two different refrigerant heat transfer correlations compared to the experiments and the differences between the two different heat transfer correlations. For this investigation, the correlation from VDI-Heat Atlas was used for the air side heat transfer coefficient [16]. The deviations between the model and the experiments for 30 Hz fan frequency were significantly larger than they were expected, approximately 45 % for water inlet temperature of 45 °C. The deviations between the two refrigerant heat transfer correlations are about 1 %. The Figure 5.6 shows these deviations.

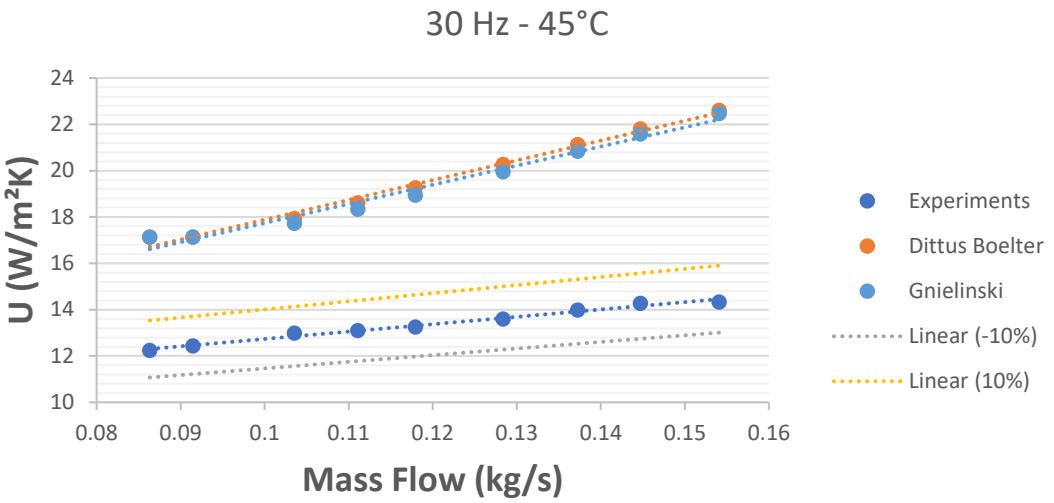

Figure 5.6: Overall heat transfer coefficient according to the refrigerant mass flow 30 Hz – 45 °C.

With 40 Hz fan frequency, the deviations were a little bit smaller. As the Figure 5.7 below shows even though the model can approach the experimental results better, the deviations obviously are still large. More specifically, the average deviations are approximately 20 %.

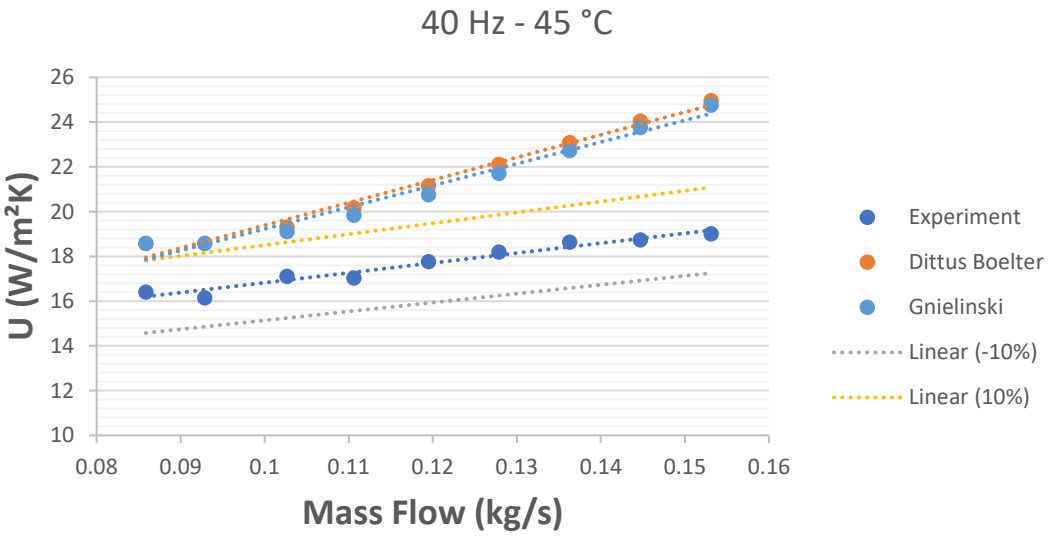

Figure 5.7: Overall heat transfer coefficient according to the refrigerant mass flow 40 Hz – 45 °C.

With 50 Hz the improvement of the deviations is noticeable. The range of the deviations is 5 - 10 % regarding the inlet water temperature. The deviations up to 10 % could be considered acceptable.

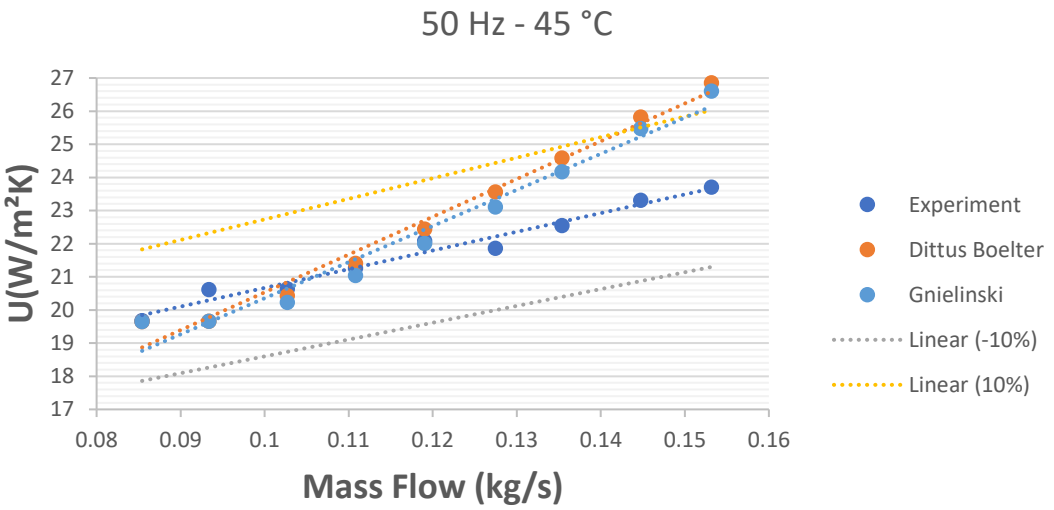

Figure 5.8: Overall heat transfer coefficient according to the refrigerant mass flow 50 Hz – 45 °C.

At that point, it is highly noticeable that when the fan frequency increases the accuracy of the model increases. The Figures below show the deviations from 60 to 80 Hz fan frequency for water inlet temperature of 45 °C. The average deviations were 4 %.

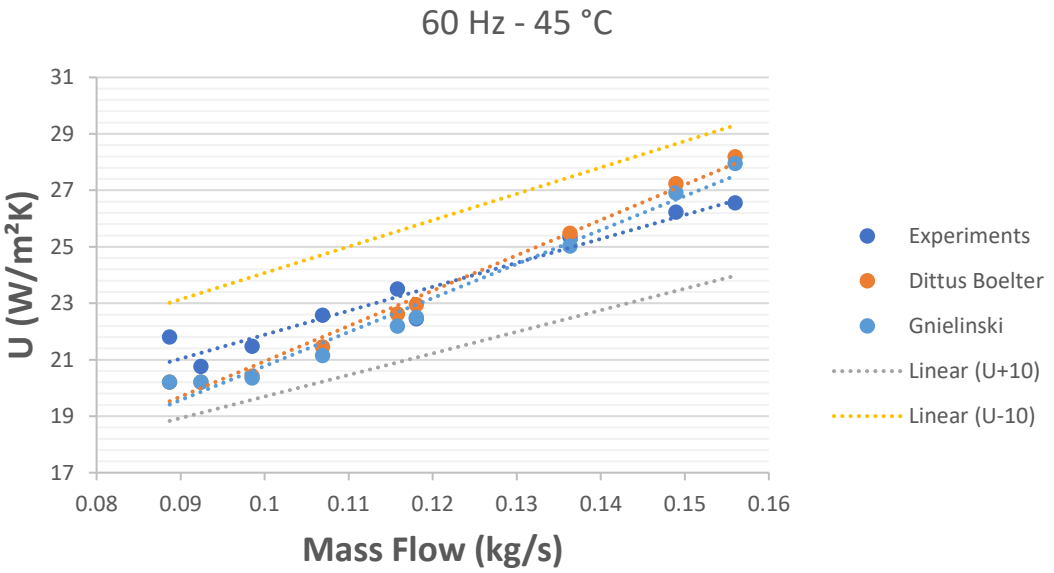

Figure 5.9: Overall heat transfer coefficient according to the refrigerant mass flow 60 Hz – 45 °C.

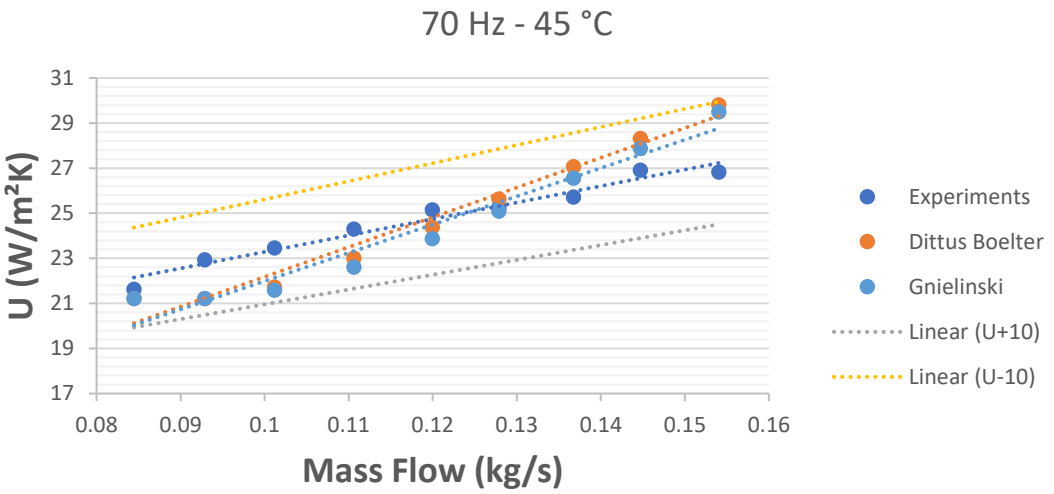

Figure 5.10: Overall heat transfer coefficient according to the refrigerant mass flow 70 Hz – 45 °C.

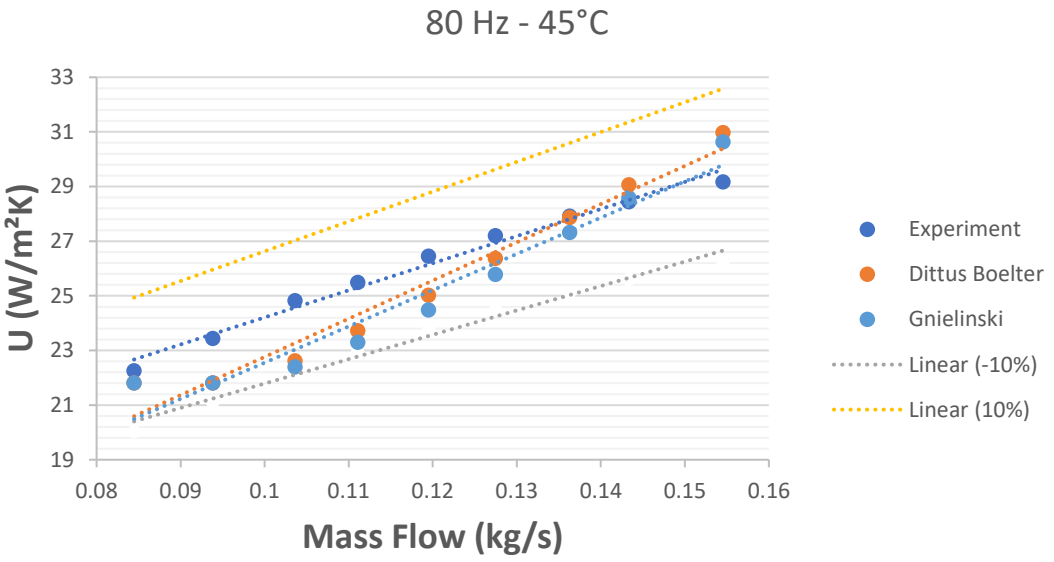

Figure 5.11: Overall heat transfer coefficient according to the refrigerant mass flow 80 Hz – 45 °C.

As it was mentioned before the differences between the refrigerant heat transfer correlations are about 1 %, Figure 5.12 and 5.13 below show the differences between the two refrigerant heat transfer correlations.

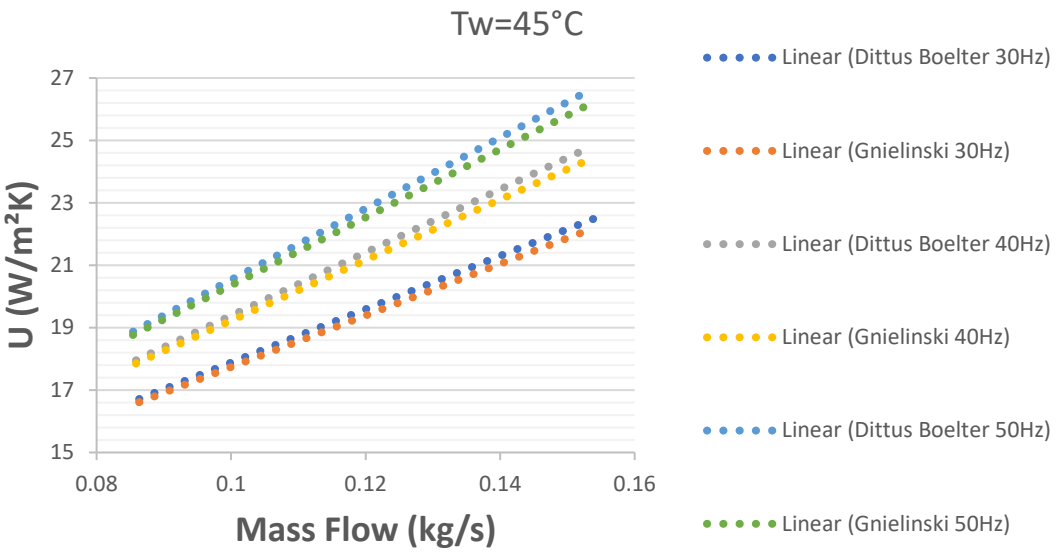

Figure 5.12: Overall heat transfer correlation according to the refrigerant mass flow for 30 – 50 Hz and refrigerant heat transfer correlations.

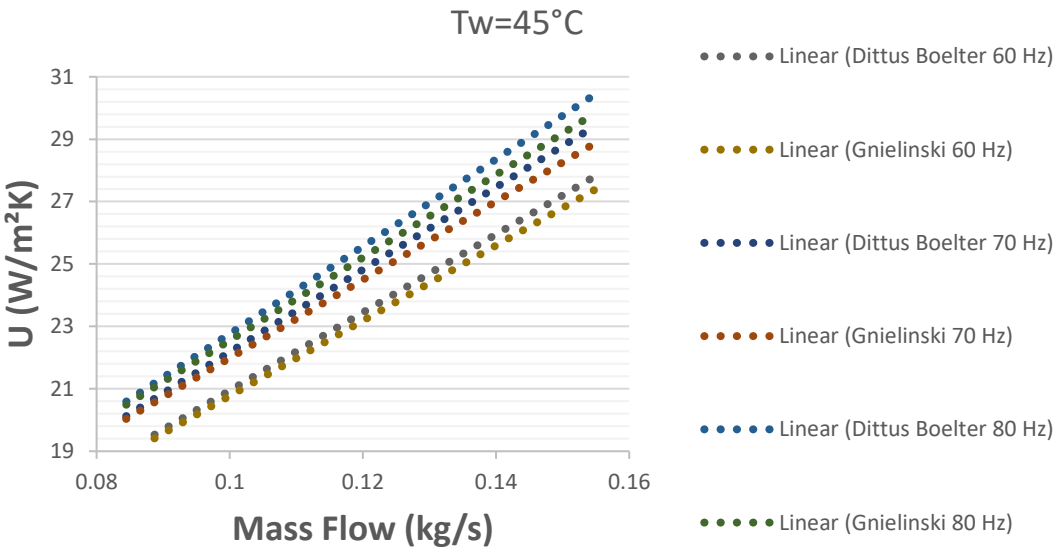

Figure 5.13: Overall heat transfer correlation according to the refrigerant mass flow for 60 – 70 Hz and refrigerant heat transfer correlations.

Air Side Heat Transfer Coefficient

Furthermore, different air side heat transfer correlations were investigated. More specifically, the VDI-Heat Atlas, Gianolo and Cuti and Schmidt correlations were investigated while for the refrigerant heat transfer coefficient the Gnielinski correlation was used. The Figures below show the deviations between the overall heat transfer coefficients based on different air heat transfer correlations. The differences between the correlations are noticeable.

The deviations for fan frequency of 30 Hz and water inlet temperature of 45 °C are 120%, 45% and 89% for Gianolo and Cuti, Atlas and Schmidt correlations, respectively.

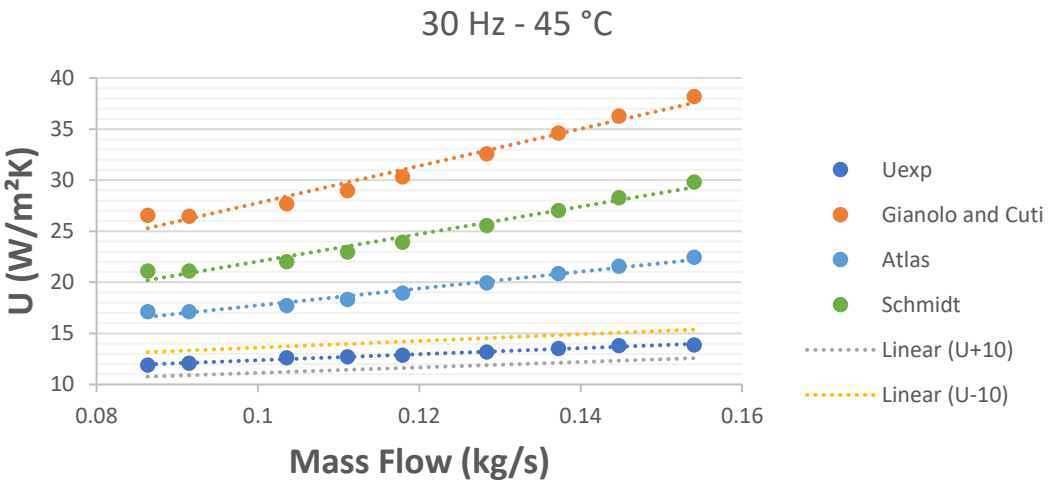

Figure 5.14: Overall heat transfer coefficient according to the refrigerant mass flow 30 Hz – 45 °C.

The deviations for fan frequency of 40 Hz and water inlet temperature of 45 °C are 78%, 20% and 40% for Gianolo and Cuti, Atlas and Schmidt correlations, respectively.

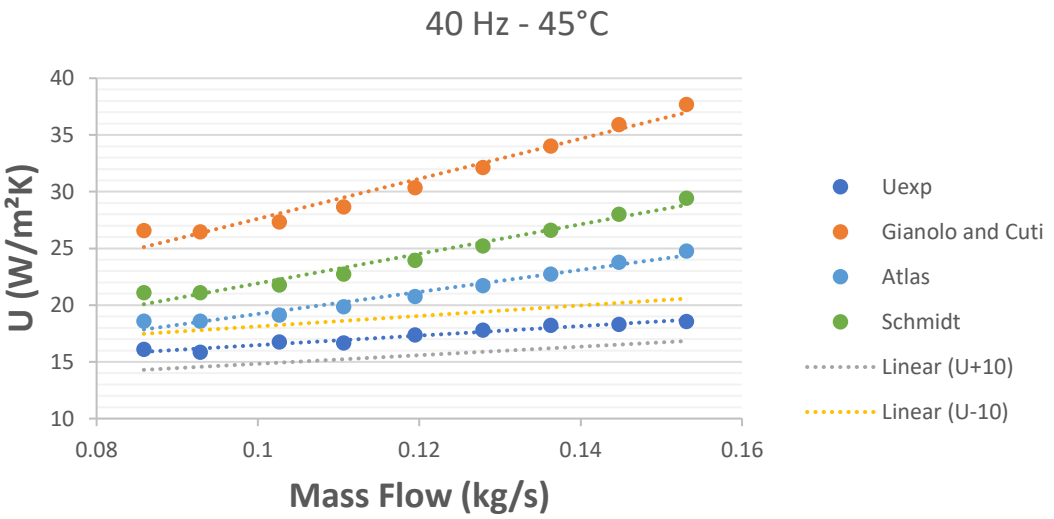

Figure 5.15: Overall heat transfer coefficient according to the refrigerant mass flow 40 Hz – 45 °C.

The deviations for fan frequency of 50 Hz and water inlet temperature of 45 °C are 43%, 5% and 13% for Gianolo and Cuti, Atlas and Schmidt correlations, respectively.

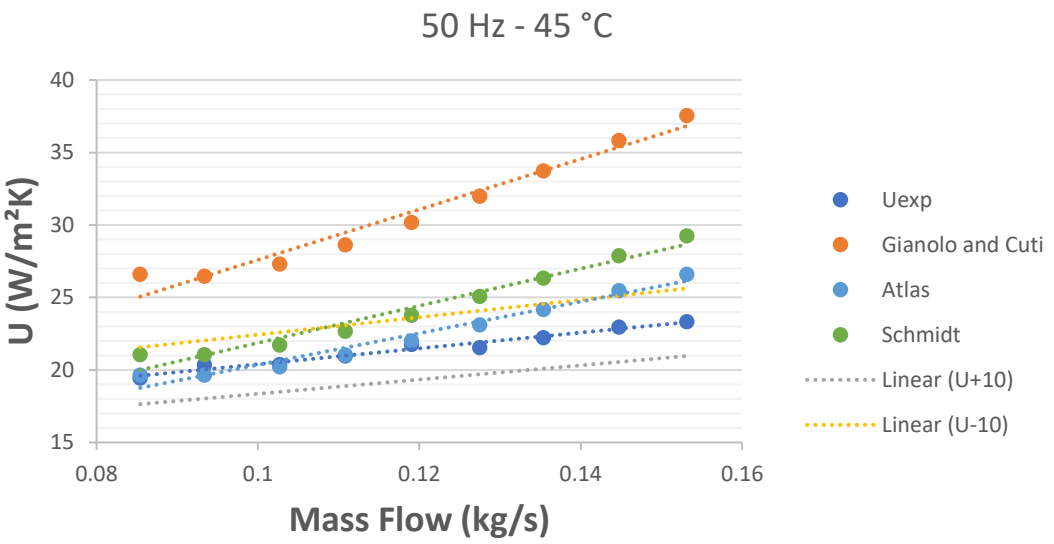

Figure 5.16: Overall heat transfer coefficient according to the refrigerant mass flow 50 Hz – 45 °C.

The deviations for fan frequency of 60 Hz and water inlet temperature of 45 °C are 30%, 5% and 5% for Gianolo and Cuti, Atlas and Schmidt correlations, respectively. The differences between the VDI - Heat Atlas and the Schmidt correlation are not significantly large.

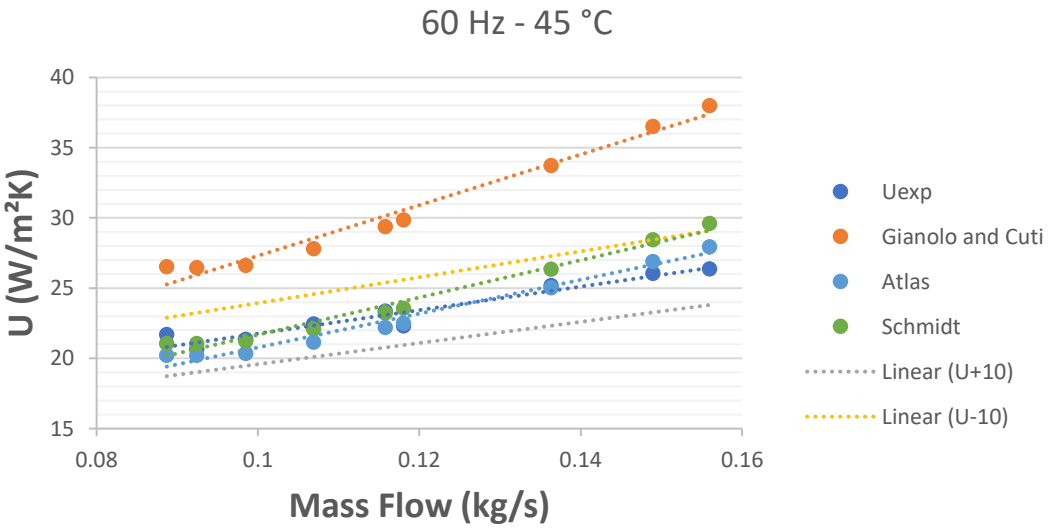

Figure 5.17: Overall heat transfer coefficient according to the refrigerant mass flow 60 Hz – 45 °C.

The deviations for fan frequency of 70 Hz and water inlet temperature of 45 °C are 23%, 5% and 5% for Gianolo and Cuti, Atlas and Schmidt correlations, respectively.

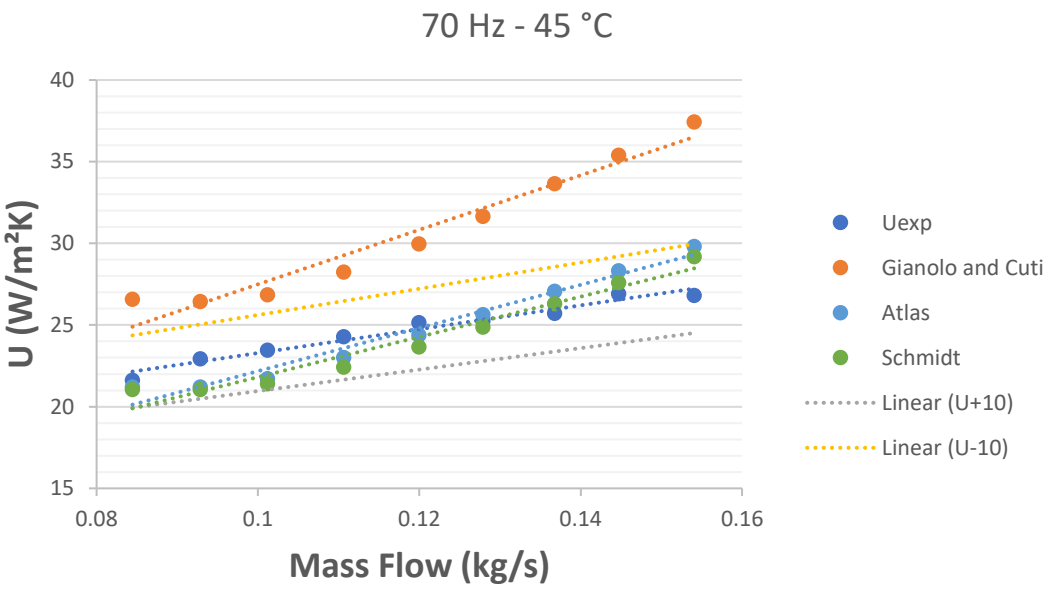

Figure 5.18: Overall heat transfer coefficient according to the refrigerant mass flow 70 Hz – 45 °C

The deviations for fan frequency of 80 Hz and water inlet temperature of 45 °C are 16%, 5% and 8% for Gianolo and Cuti, Atlas and Schmidt correlations, respectively.

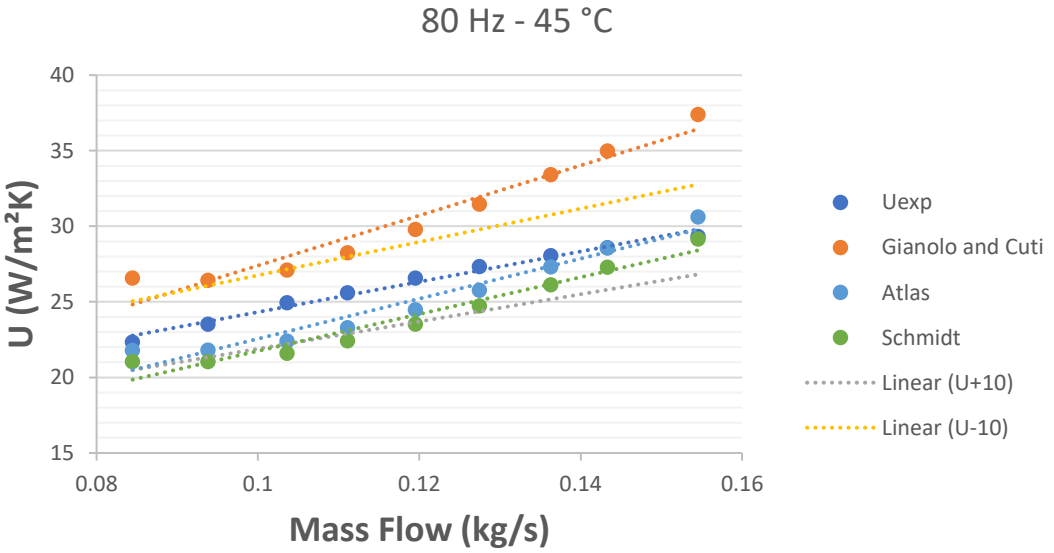

Figure 5.19: Overall heat transfer coefficient according to the refrigerant mass flow 80 Hz – 45 °C.

As it was mentioned before the differences between the heat transfer correlations are noticeable, especially, for low values of fan frequencies as the Figures 5.20, 5.21, 5.22, 5.23, 5.24 and, 5.25 show below.

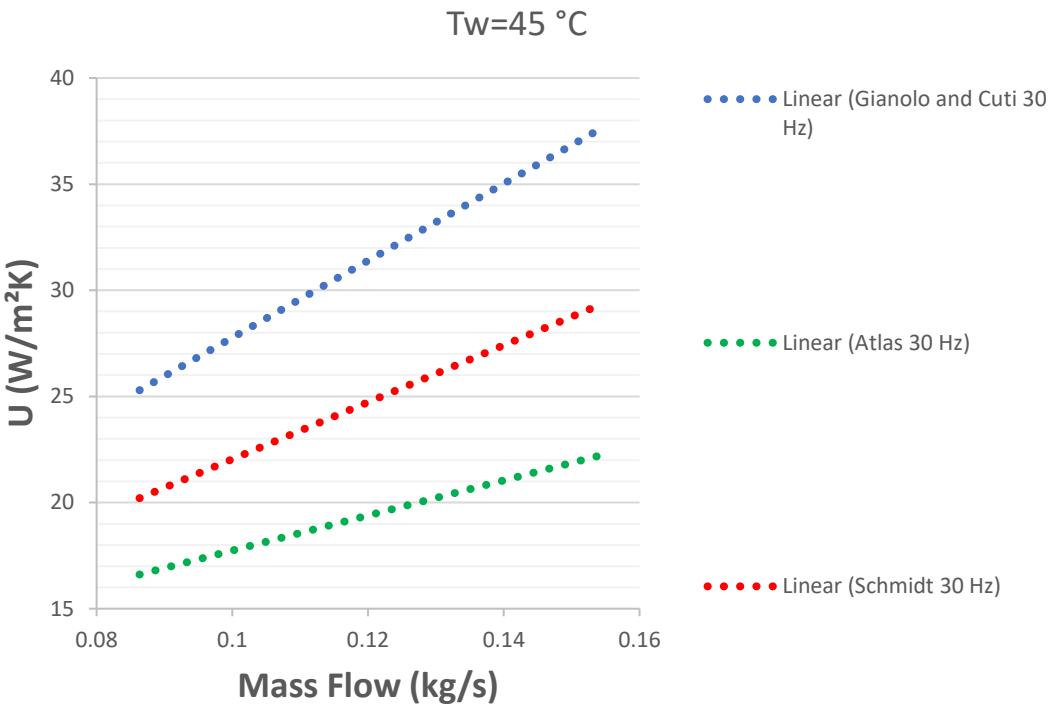

Figure 5.20: Overall heat transfer coefficient according to the refrigerant mass flow for 30 Hz.

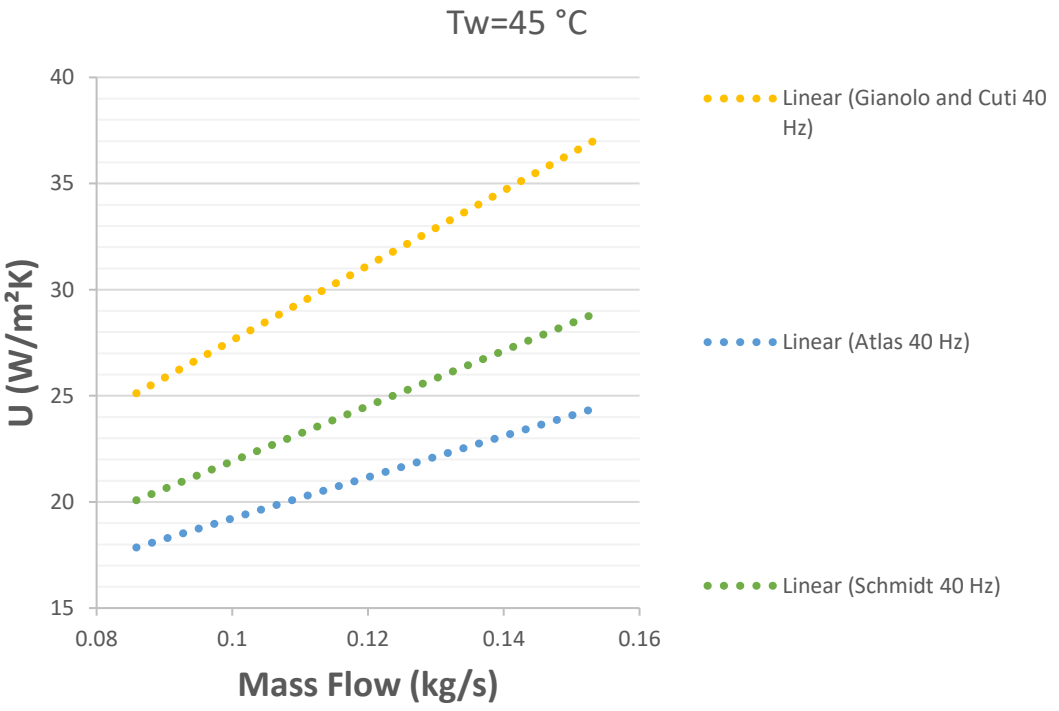

Figure 5.21: Overall heat transfer coefficient according to the refrigerant mass flow for 40 Hz.

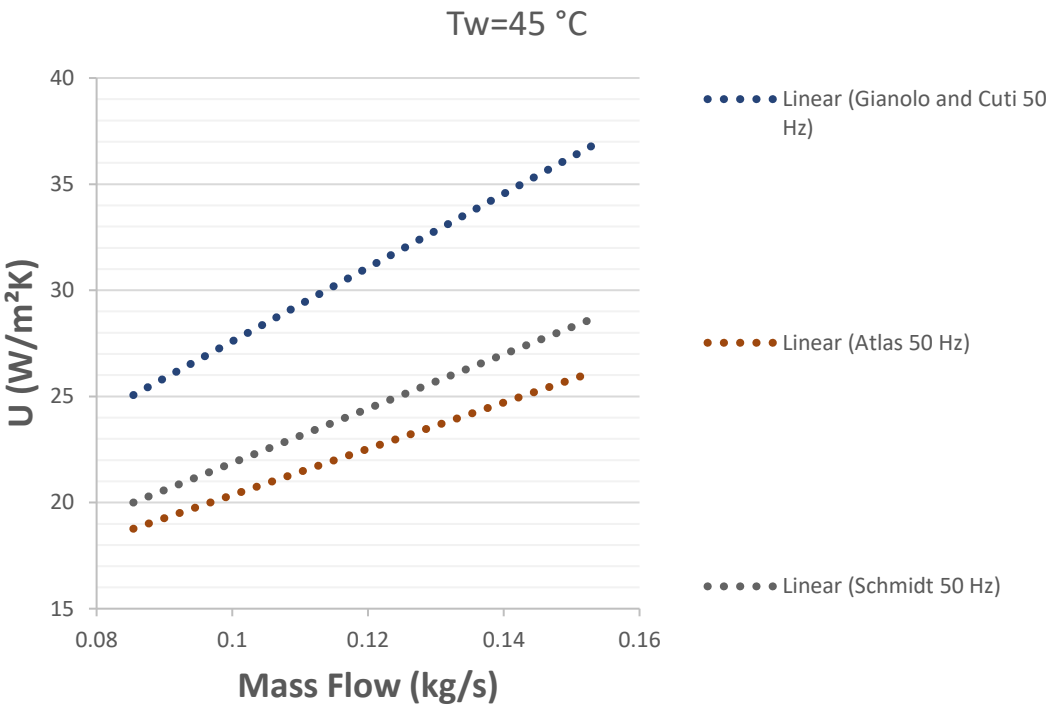

Figure 5.22: Overall heat transfer coefficient according to the refrigerant mass flow for 50 Hz.

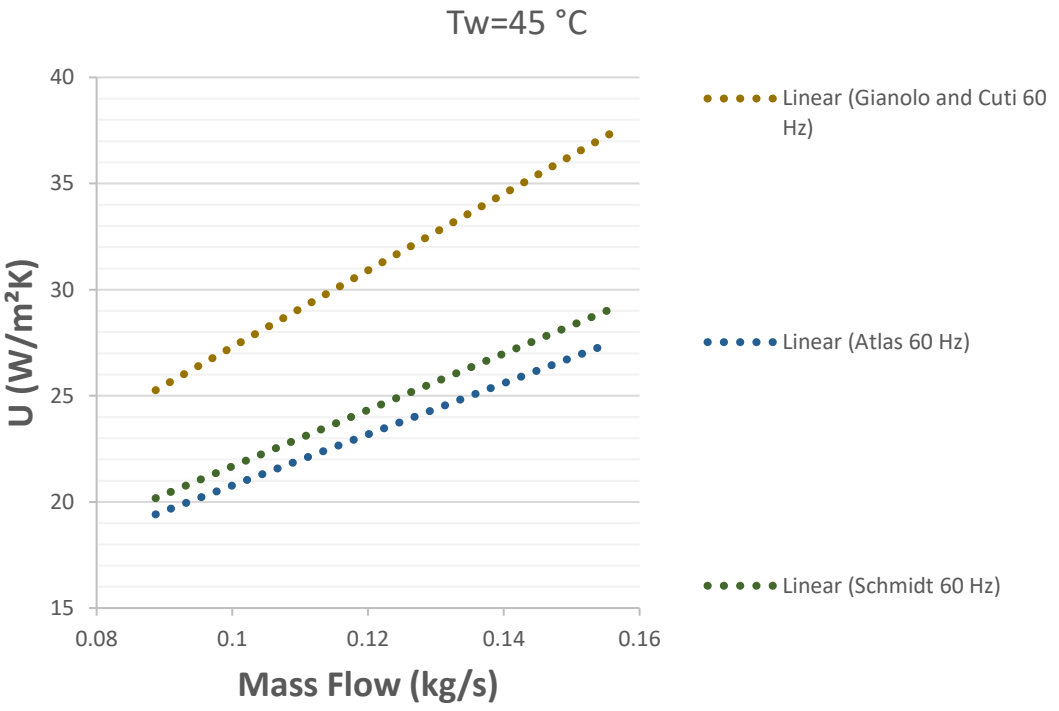

Figure 5.23: Overall heat transfer coefficient according to the refrigerant mass flow for 60 Hz.

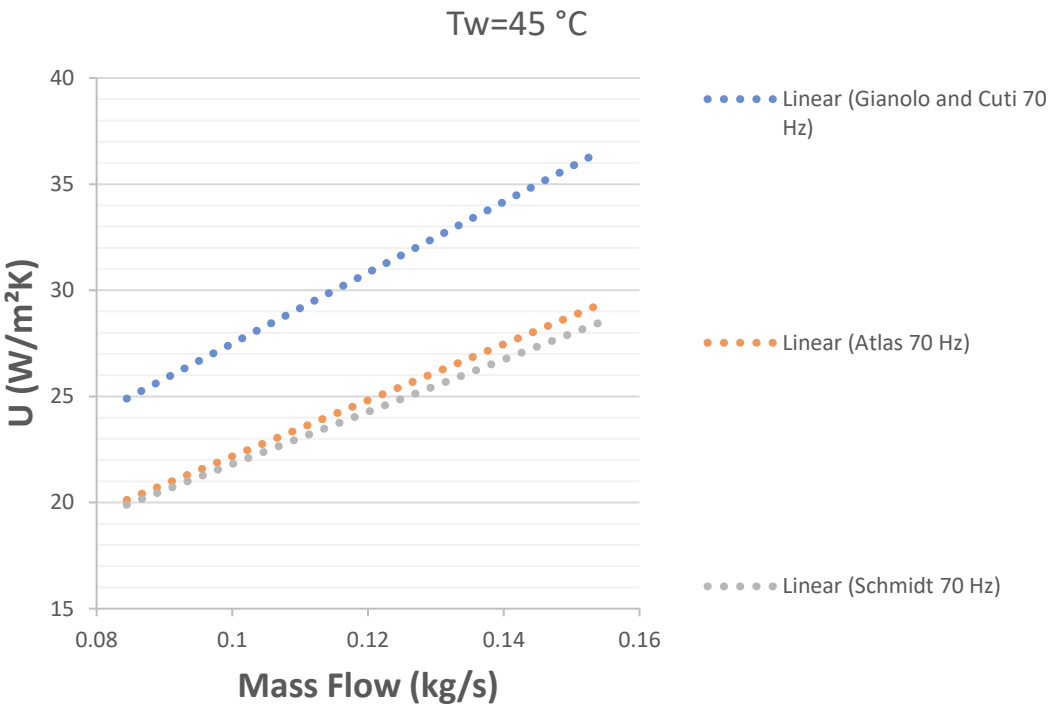

Figure 5.24: Overall heat transfer coefficient according to the refrigerant mass flow for 70 Hz.

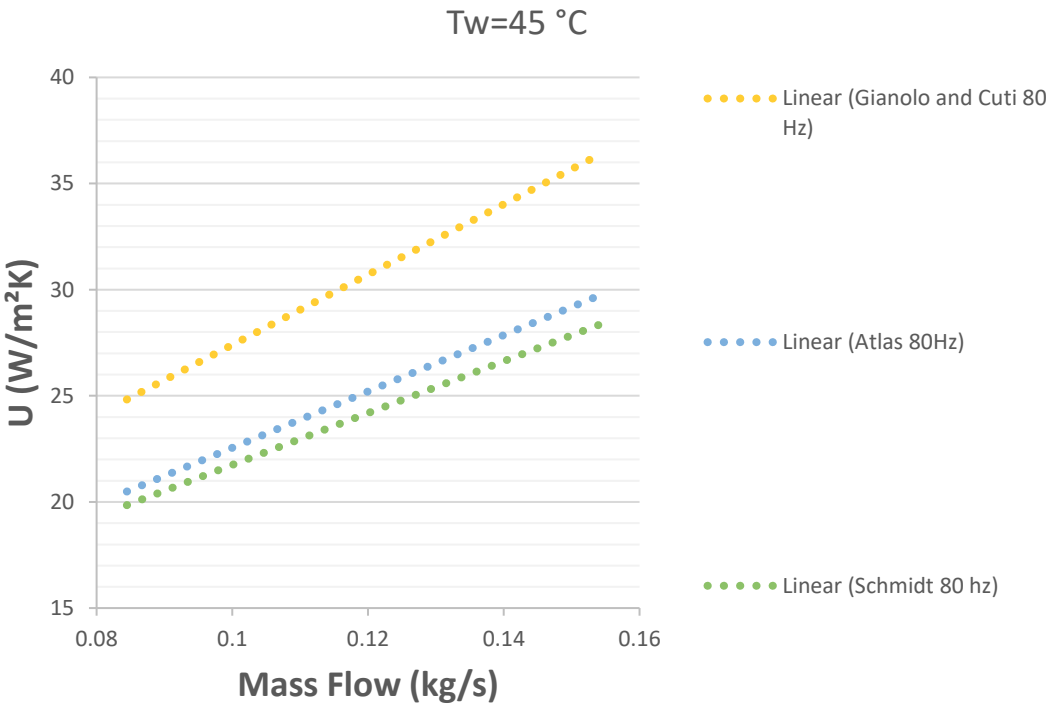

Figure 5.25: Overall heat transfer coefficient according to the refrigerant mass flow for 80 Hz.

Overall Heat Transfer Coefficient

The overall heat transfer coefficient is one of the most important variables of the heat exchanger. How it is affected by the fan frequency, water mass flow and water inlet

temperature were considered necessary to find out. First and foremost, with the increase of the fan frequency the overall heat transfer coefficient increases. In addition, when the water mass flow increases the overall heat transfer coefficient increases. The Figure 5.26 below shows how the overall heat transfer coefficient increases according to fan frequency and the water mass flow for 45 °C inlet water temperature. The Figure 5.27 below shows the impact of the water inlet temperature on the overall heat transfer coefficient. The results are based on the Gnielinski and VDI-Heat Atlas correlations for water and air side heat transfer coefficient, accordingly.

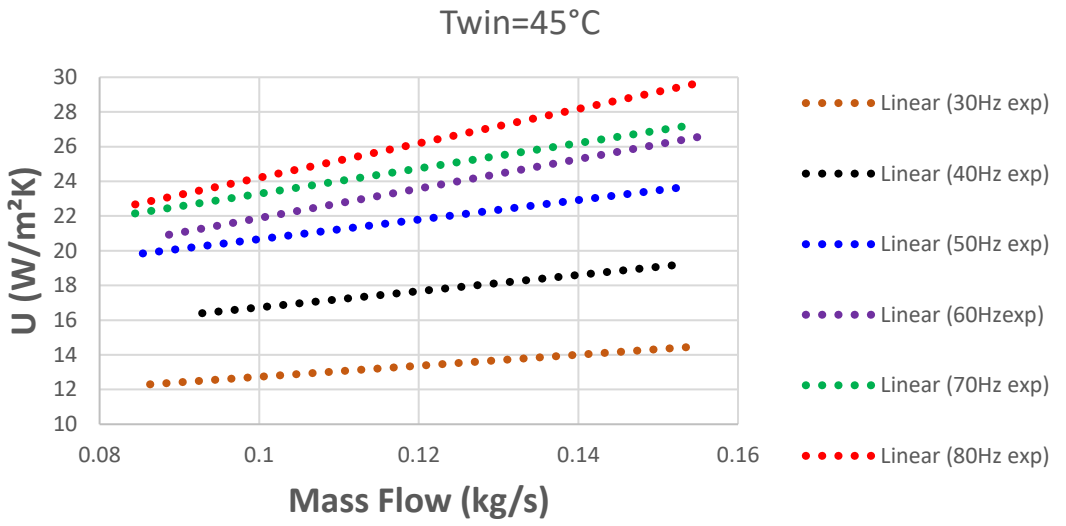

Figure 5.26: Overall heat transfer coefficient according to the refrigerant mass flow for different fan frequencies – 45 °C.

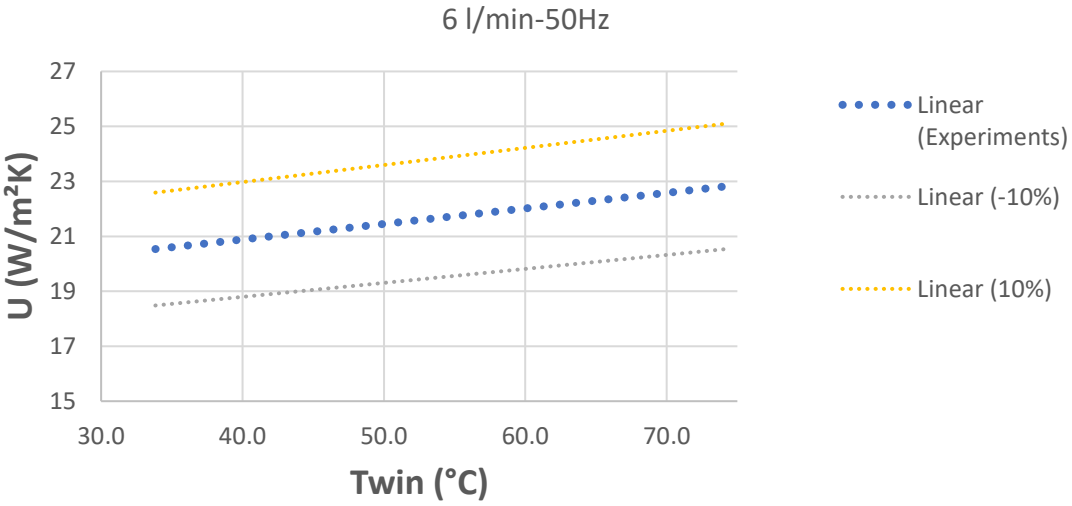

Figure 5.27: Overall heat transfer coefficient according to inlet refrigerant temperature for 6 l/min and 50 Hz.

5.3. Summary

An off-design script has been created in Matlab R2019a based on the on-design model (Chapter 4), using the design of the heat exchanger and the thermodynamic properties of the fluids as an input. The off-design script calculates the behavior of the specific heat exchanger in different off-conditions. A validation of this model based on an experiment using a specific condenser that used water as a working fluid took place at the University of Bayreuth, Energy Department. In that way, deviations between the model and the experiments were extracted. The deviations are varied according to different water mass flows, water inlet temperatures and different fan frequencies. Furthermore, different heat transfer correlations have been investigated for the refrigerant and air side heat transfer coefficient. It could be mentioned that the Gnielinski with VDI-Heat Atlas for refrigerant and air side heat transfer correlation for the refrigerant and air transfer coefficient accordingly, have the best results. Based on those correlations, the average deviations for 60 – 80 Hz are less than 13 % for different water inlet temperatures. As far as the refrigerant heat transfer correlations, it could be mentioned that the differences are about 1 % while for the air side the differences are noticeable.

Chapter 6. Off-design CO_2 performance

An off-design model as it has been referred and previously gives the capability to know how an existing machine, designed on the design point, will operate if this machine leaves this point. Into this model, the geometry and the boundary conditions of the system are specified. In this chapter, the off-design performance of each of the gas coolers in different conditions has been investigated and the results are presented below. The Tables 6.1 and 6.2 show the off-design boundary conditions for the inverter and no-inverter systems, accordingly.

Table 6.1: Boundary off-design conditions – Inverter system

T_{ai}	T_{co2i}	T_{co2o}	P_{co2}	m_{co2}	m_a
[°C]	**[°C]**	**[°C]**	**[bar]**	**[kg/h]**	**[kg/h]**
20	78.3	20.02	93	184	93.15
21	79.3	21.03	93	184	92.79
22	80.3	22.03	93	184	92.29
23	81.2	23.04	93	184	91.80
24	82.2	24.05	93	184	91.30
25	83.2	25.07	93	184	90.60
26	84	26.12	93	208	101.67
27	84.7	27.2	93	233	112.59
28	88.6	28.31	93	257	125.66
29	85.9	29.48	93	282	132.37
30	86	30.71	93	306	141.14
31	86	32.01	93	330	148.68
32	85.8	33.52	93	379	165.14
33	85.5	35.09	93	428	179.17
34	85.3	36.61	93	476	190.51
35	85.1	38	93	525	199.50

Table 6.2: Boundary off-design conditions – No - inverter system

T_{ai}	T_{co2i}	T_{co2o}	P_{co2}	m_{co2}	m_a
[°C]	[°C]	[°C]	[bar]	[kg/h]	[kg/h]
20	78.1	20.38	93	331	166.77
21	79	21.43	93	331	165.78
22	79.9	22.5	93	331	164.58
23	80.9	23.58	93	331	163.31
24	81.8	24.67	93	331	162.12
25	82.7	25.79	93	331	160.72
26	83.7	26.92	93	331	159.25
27	84.6	28.08	93	331	157.64
28	85.2	29.28	93	331	155.49
29	85.6	30.5	93	331	152.78
30	85.8	31.76	93	331	149.59
31	85.9	33.04	93	331	145.77
32	85.9	34.34	93	331	141.89
33	85.9	35.63	93	331	137.11
34	85.9	36.86	93	331	132.19
35	85.9	38	93	331	126.73

6.1. Results and discussion

Inverter

The Figure 6.1 shows how the overall heat transfer coefficient changes according to the ambient temperature. It is noticeable that from 20 °C to 25 °C the overall heat transfer remains almost constant and then increases rapidly. The reason is the capability of the compressor. More specifically, there is a range that the compressor can work. For that case, the compressor works from 30 Hz to 75 Hz and in terms of refrigerant mass flow that means from 184 kg/h to 525 kg/h. As there is a limitation for the range of the compressor from 20 °C to 25 °C the system operates with constant refrigerant mass flow.

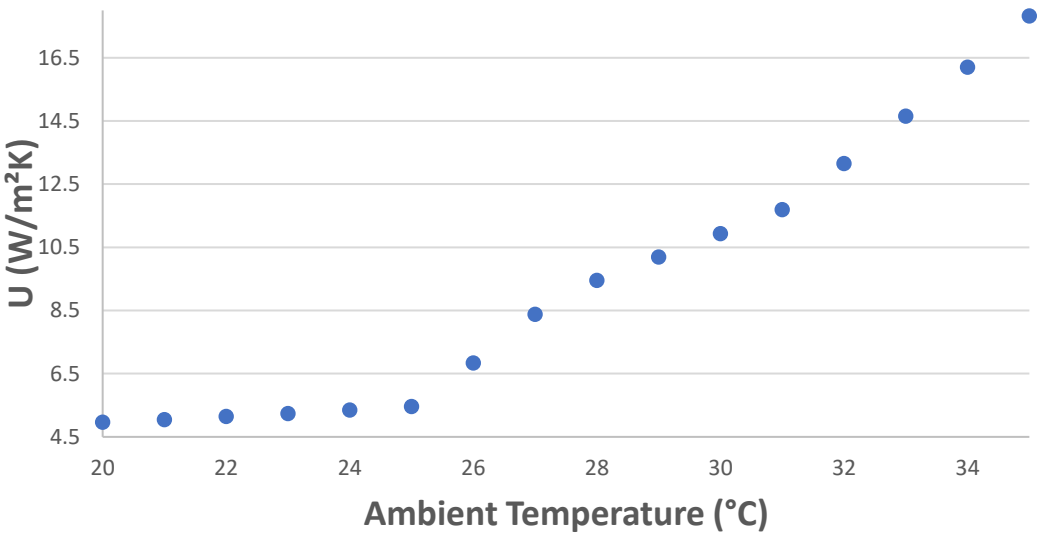

Figure 6.1: Overall heat transfer coefficient according to the ambient temperature - Inverter.

The reason why the overall heat transfer coefficient increases as the ambient temperature increases are because of the increase of the refrigerant mass flow (Table 6.1) and as a result the heat transfer efficiency is increased due to the higher Reynolds number.

The Figure 6.2 below shows how the pressure-drop changes according to the ambient temperature. The pressure drop increases as the increase of the refrigerant flow cause an increase to the Reynolds number and in turn, in pressure losses.

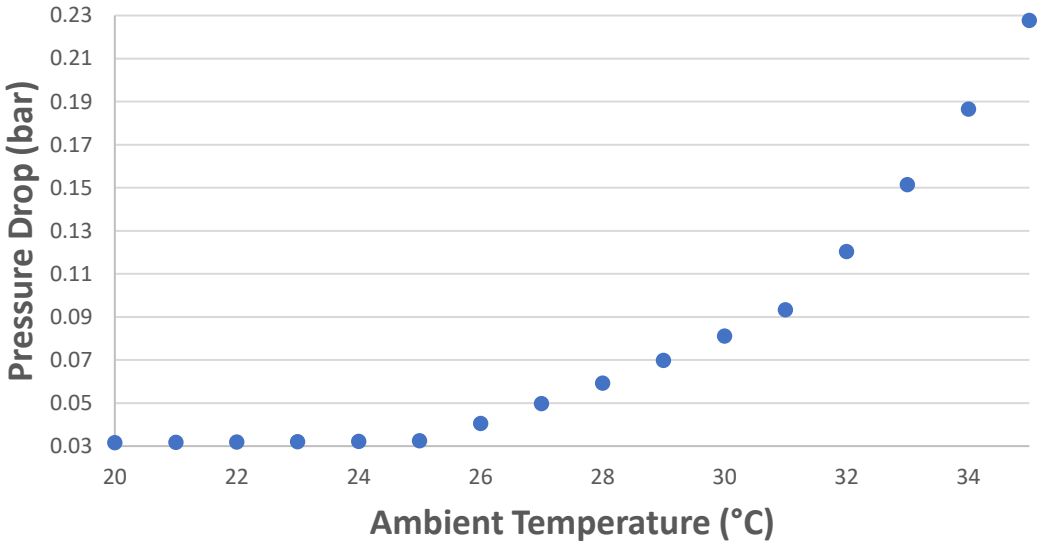

Figure 6.2: Pressure-drop according to ambient temperature - Inverter.

While the ambient temperature increases, the capability of the system to reject heat energy to the environment becomes a more difficult process. The contribution of the fan power is crucial and that is why the fan power consumption is increased. How the fan power is affected by the ambient temperature is depicted in the Figure 6.3 below.

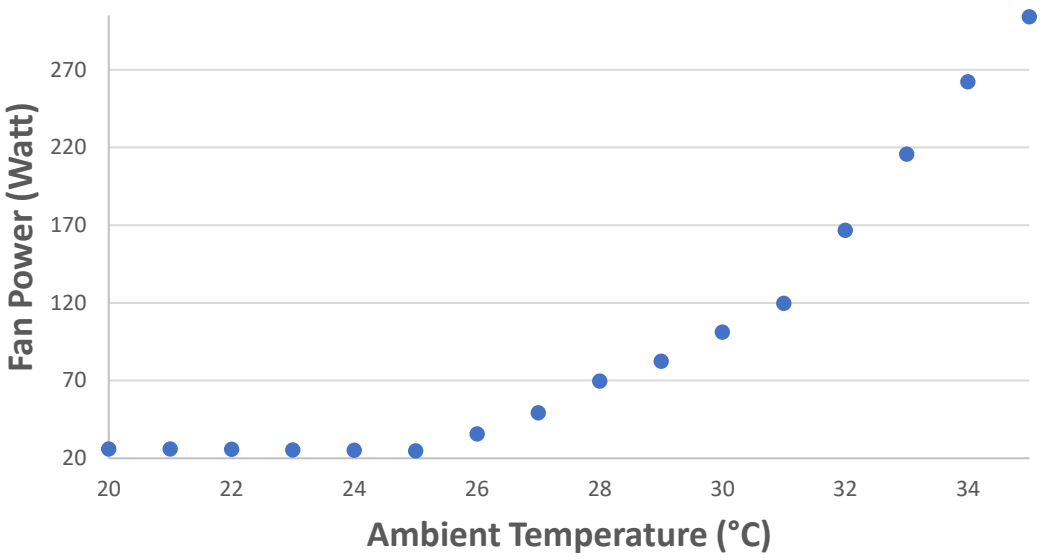

Figure 6.3: Fan power according to the ambient temperature - Inverter.

The COP of the system reasonably declines with the increase of the ambient temperature as with the increase of the ambient temperature the system rejects heat energy to the environment more difficultly. Furthermore, the new COP taking into consideration the pressure drop is calculated. The differences are negligible and that means the gas cooler design can work properly. The COP of the system according to the ambient temperature taking into consideration and without the pressure drop is depicted in the Figure 6.4 below.

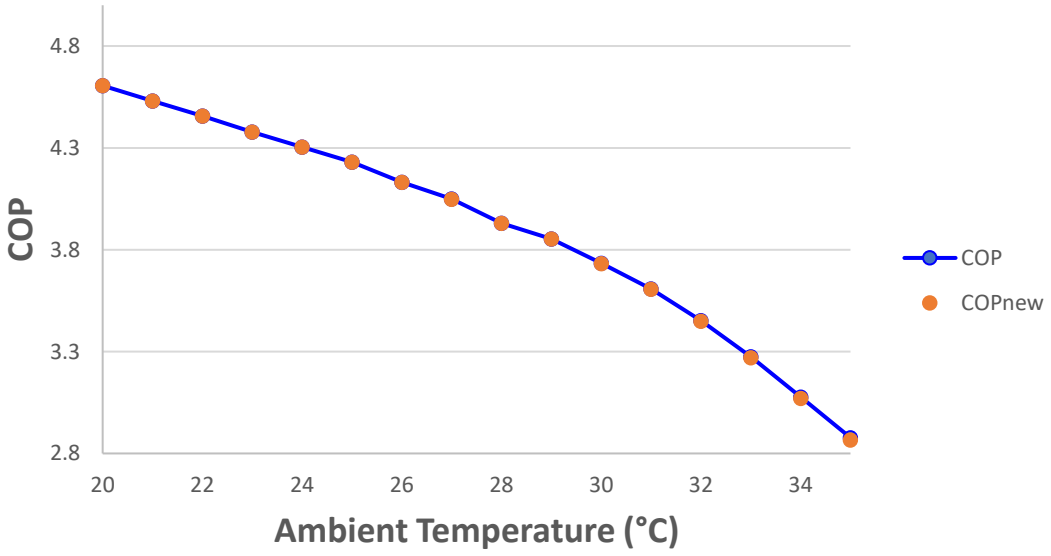

Figure 6.4: Coefficient of performance according to the ambient temperature - Inverter.

The Figure 6.5, 6.6, 6.7, 6.8 and 6.9 show how the ambient temperature, overall heat transfer coefficient, power fan, air pressure-drop and air flow velocity change regarding the air flow velocity. The air flow velocity remains constant from 20 °C to 25 °C and when the inverter starts up increases.

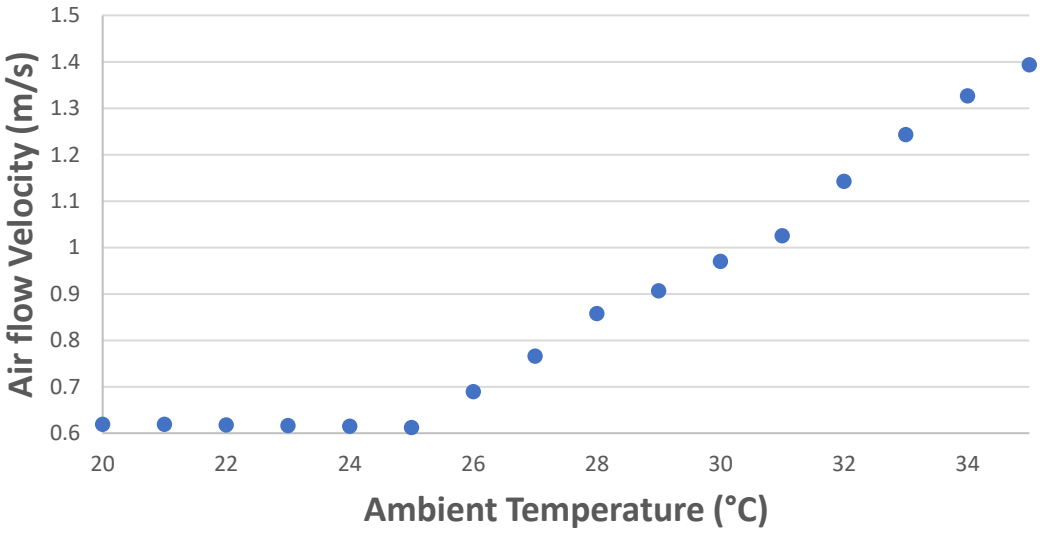

Figure 6.5: Air flow velocity according to the ambient temperature - Inverter.

The overall heat transfer coefficient increases with the increase of the air flow velocity as the Figure 6.6 displays.

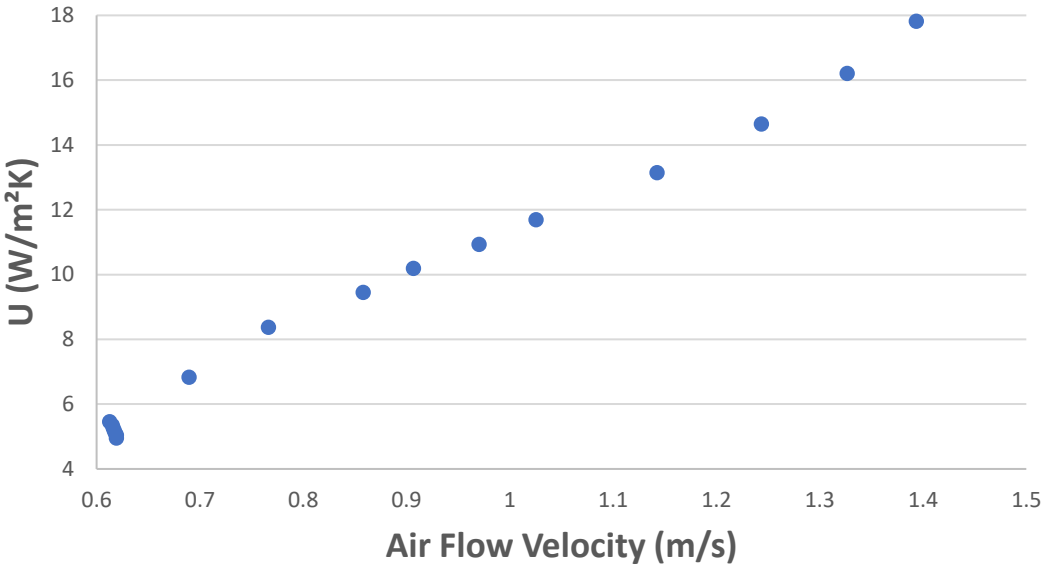

Figure 6.6: Overall heat transfer coefficient according to the air flow velocity - Inverter.

The power fan consumption obviously increases with the increase of the air flow velocity. The figure 6.7 displays how the fan power is affected by the air flow velocity.

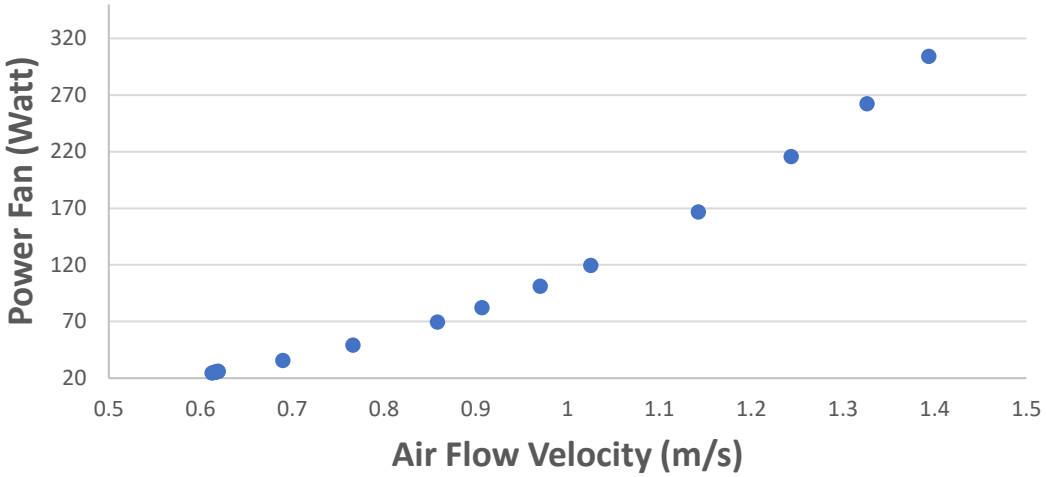

Figure 6.7: Power fan according to the air flow velocity - Inverter.

Furthermore, it is reasonable that the air pressure-drop increases when the air flow velocity increases as the Figure 6.8 shows below.

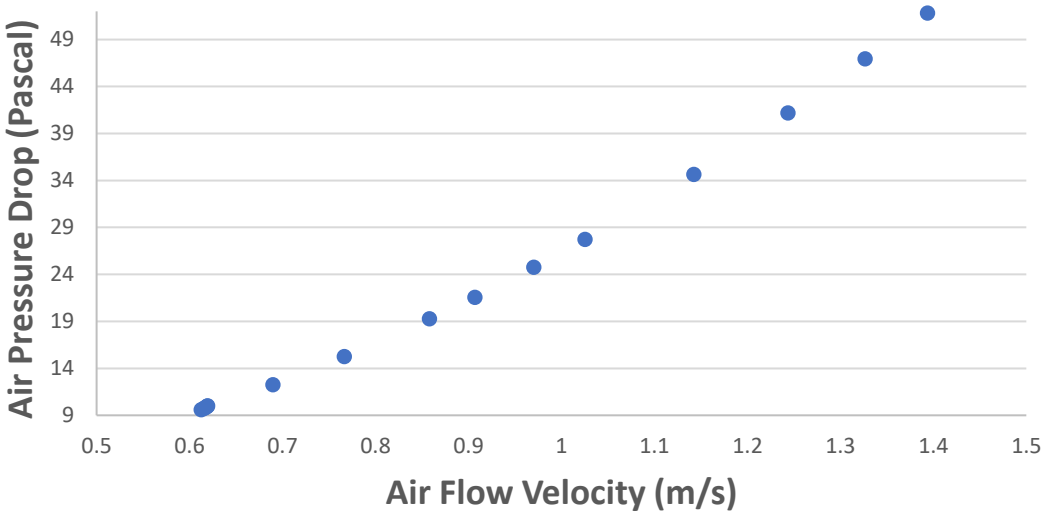

Figure 6.8: Air pressure-drop according to the air flow velocity.

The Figure 6.9 below shows how the COP changes regarding the air flow velocity.

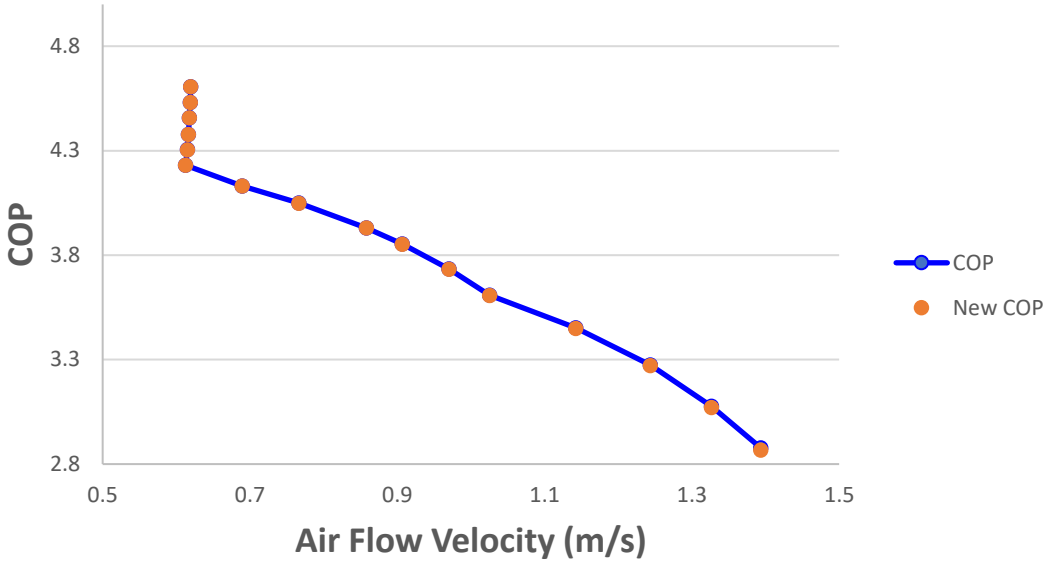

Figure 6.9: Coefficient of performance according to the air flow velocity - Inverter.

As it was mentioned previously, even though the system rejects heat energy more difficultly as the ambient temperature is increased, the refrigerant mass flow increases in a way that the evaporator and gas cooler duties are increased. The Figure 6.10 shows how the ambient temperature affects the evaporator duty.

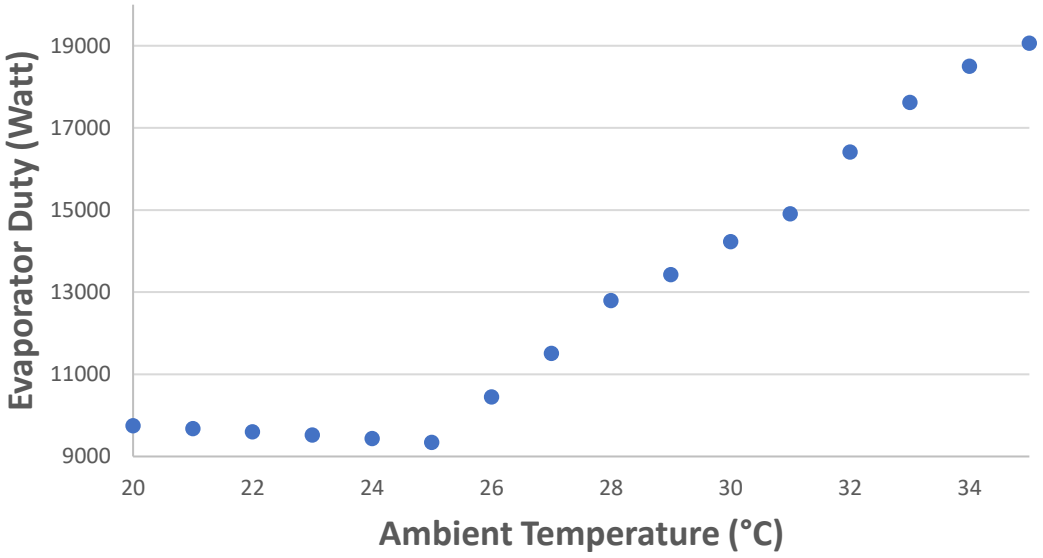

Figure 6.10: Evaporator duty according to the ambient temperature - Inverter.

No Inverter

The no-inverter system operates with constant refrigerant mass flow. The Figure 6.11 displays that the overall heat transfer coefficient decreases as the ambient temperature increases. The system rejects heat to the environment more difficultly as the ambient temperature increases.

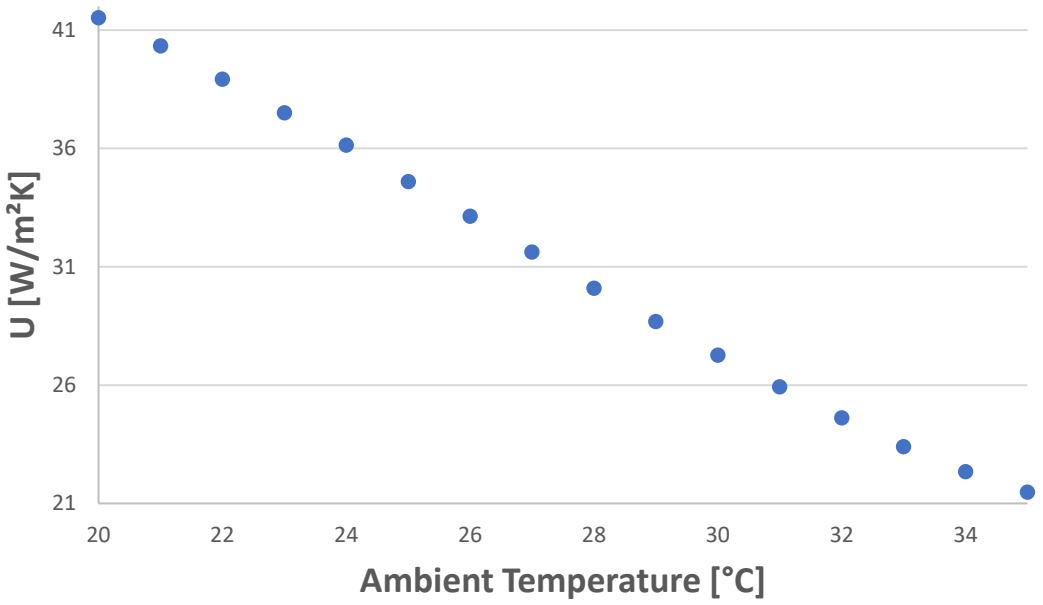

Figure 6.11: Overall heat transfer coefficient according to the ambient temperature – No - Inverter.

The pressure drop increases with the increase of the ambient temperature as the Figure 6.12 displays.

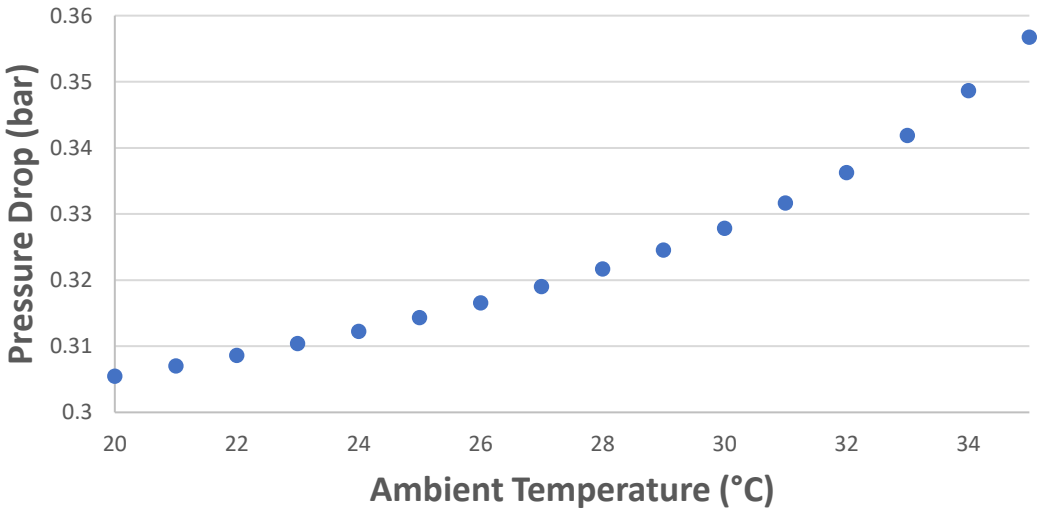

Figure 6.12: Pressure-drop according to the ambient temperature – No - Inverter.

The fan consumption is decreased while the ambient temperature increases because even if the system rejects more difficultly heat energy to the environment the air mass flow decreases remarkably. How the fan power changes according to the ambient temperature is depicted in the Figure 6.13 below.

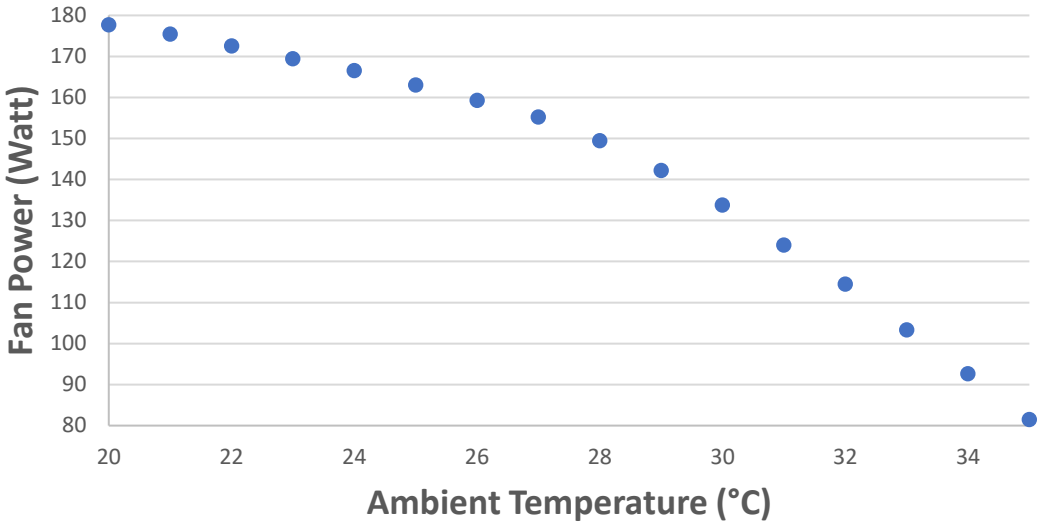

Figure 6.13: Fan power according to the ambient temperature – No - Inverter.

As far as the COP of the system is concerned, it decreases with the increase of the ambient temperature due to the difficulties to reject heat energy to the environment. Taking the pressure drop into consideration, the COP does not change significantly. That means the gas cooler design can work properly. The Figure 6.14 below shows the impact of the ambient temperature on the COP.

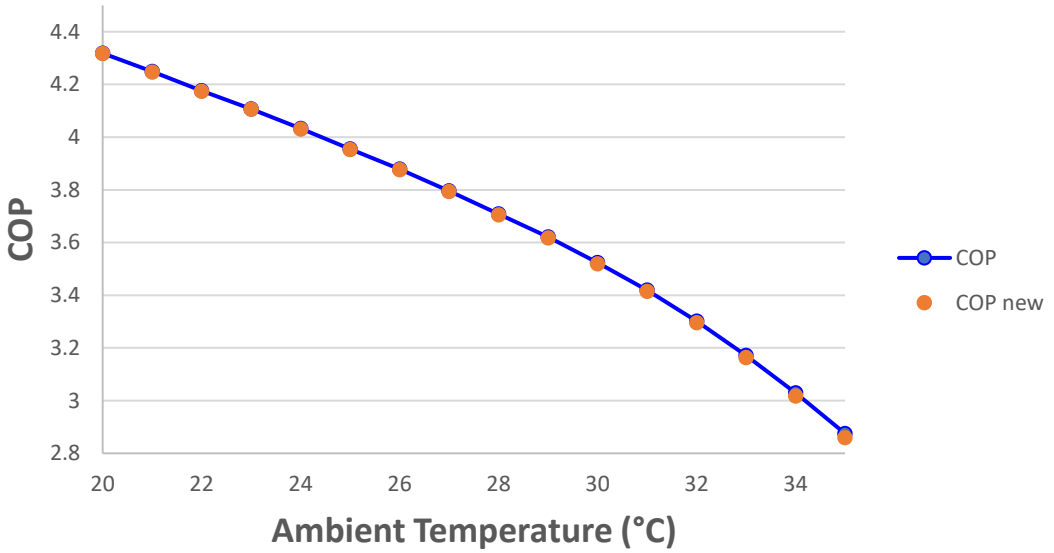

Figure 6.14: Coefficient of performance according to the ambient temperature – No - Inverter.

The no-inverter system remains the refrigerant mass flow constant during the ambient temperature changes. In addition, the system rejects heat energy more difficultly and in turn, absorbs heat energy from the inside place more difficultly. Consequently, it is reasonable that the evaporator duty decreases with the increase of the ambient temperature.

The Figures 6.15, 6.16, 6.17, 6.18 show how the overall heat transfer coefficient, power fan consumption, air pressure drop and the COP change regarding the air flow velocity.

The air flow velocity decreases as the ambient temperature increases. The duty of the gas cooler decreases and as a consequent the air mass flow and the air flow velocity decreases. The Figure 6.15 displays how the air flow velocity changes according to the ambient temperature.

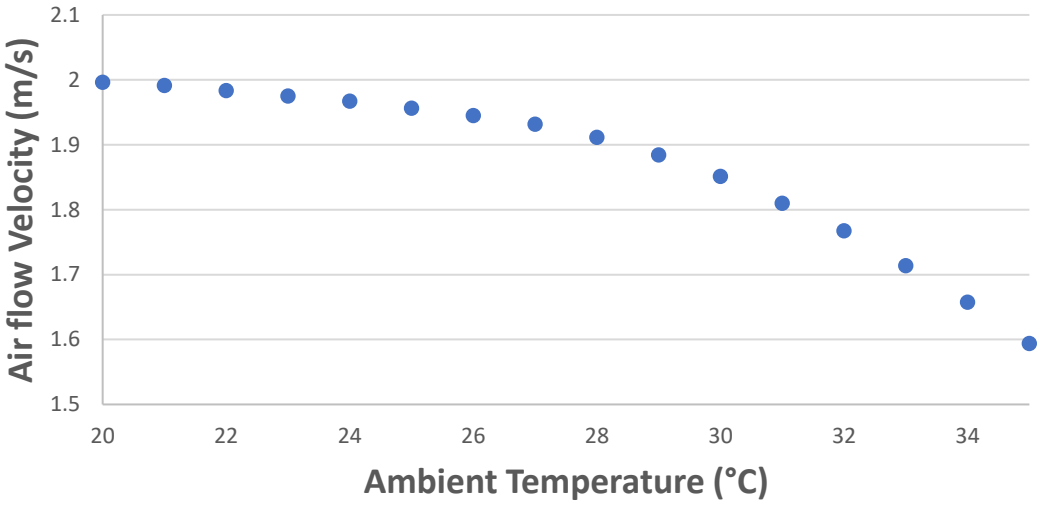

Figure 6.15: Air flow velocity according to the ambient temperature – No - Inverter.

The overall heat transfer coefficient increases as the air flow velocity increases as the Figure 6.16 shows below.

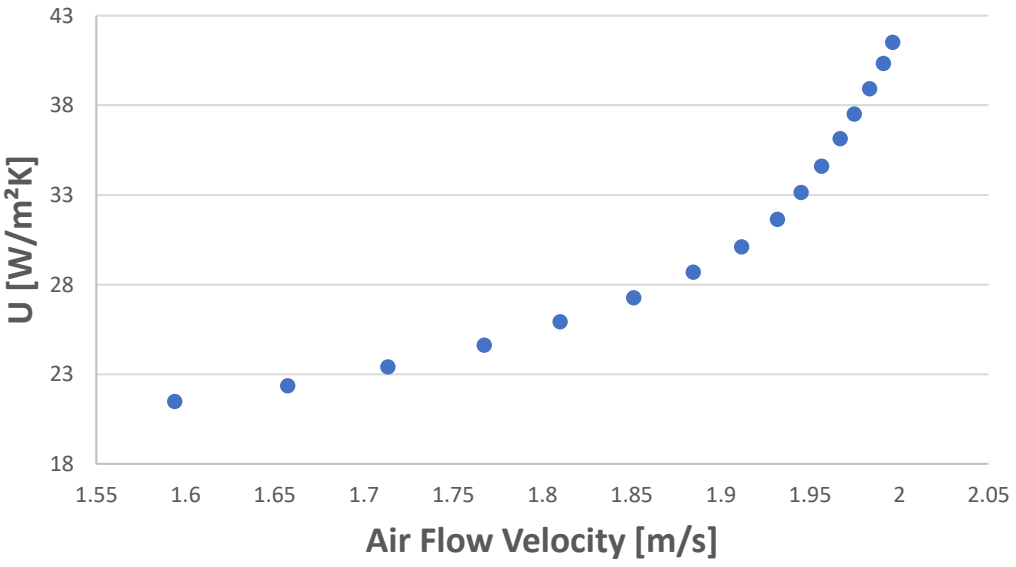

Figure 6.16: Overall heat transfer coefficient according to the air flow velocity – No - Inverter.

Reasonably, the air pressure drop and the fan power increase with the increase of the air flow velocity as the Figures 6.17 and 6.18 show, respectively.

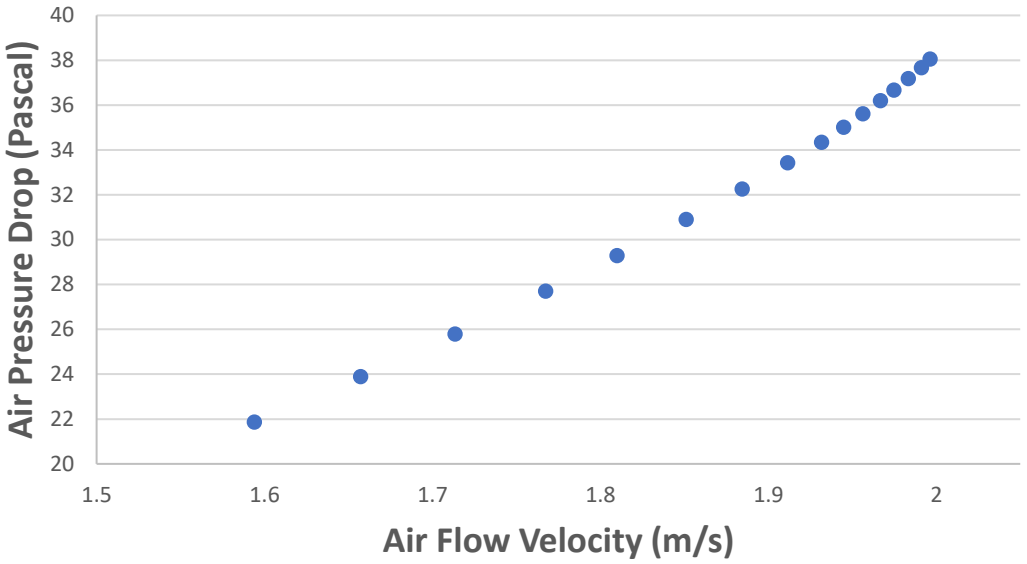

Figure 6.17: Air pressure-drop according to the air flow velocity – No - Inverter.

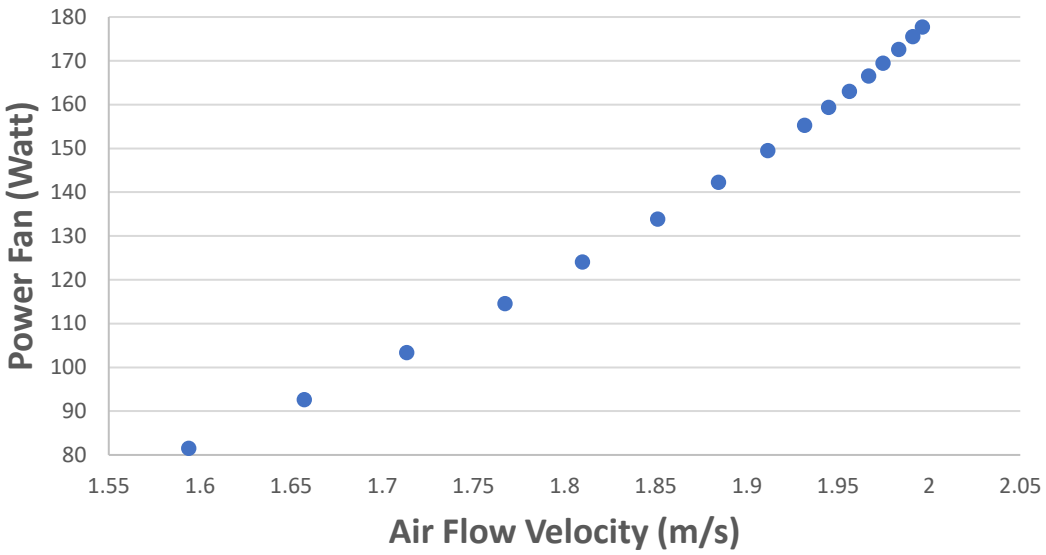

Figure 6.18: Power fan according to the air flow velocity – No - Inverter.

The COP of the system increases with the increase of the air flow velocity as the Figure 6.19 shows.

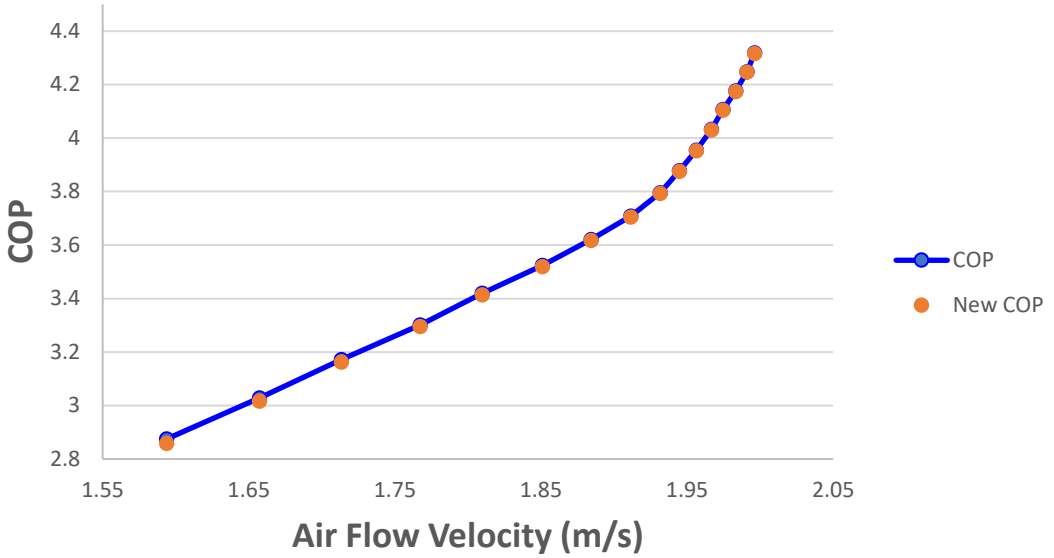

Figure 6.19: Coefficient of performance according to the air flow velocity – No - Inverter.

The evaporator duty decreases while the ambient temperature increases. The system cannot reject heat energy to the environment properly and at the same time, it cannot absorb heat energy from the inside room. The Figure 6.20 shows how the ambient temperature affects the evaporator duty.

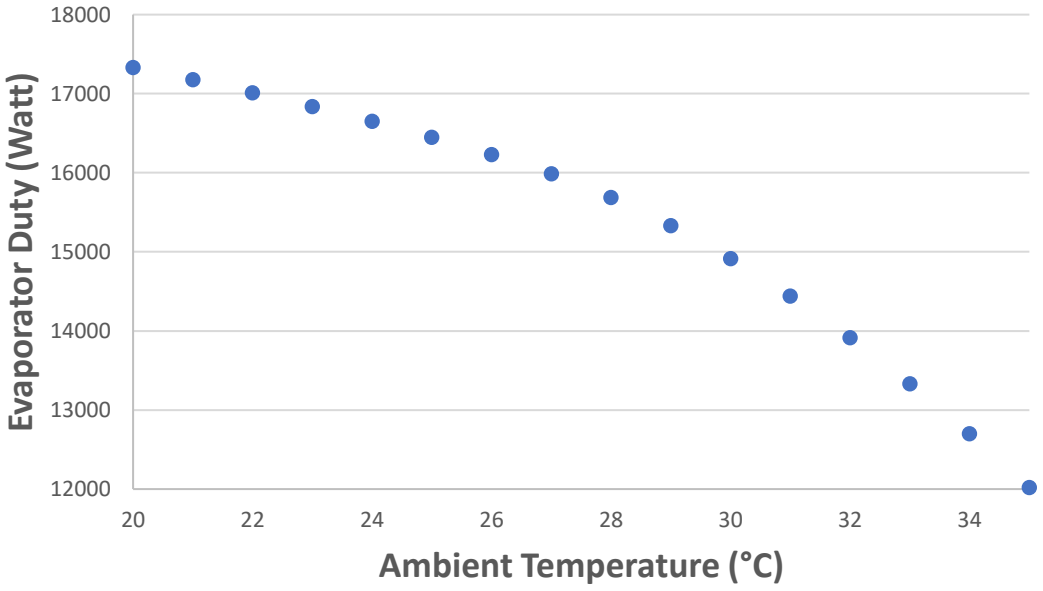

Figure 6.20: Evaporator duty according to the ambient temperature – No - Inverter.

The Figure 6.21 below shows a comparison between the inverter and no-inverter system. It is remarkable that in the inverter system the evaporator duty is increased with the increase of the ambient temperature while in the no-inverter system it decreases.

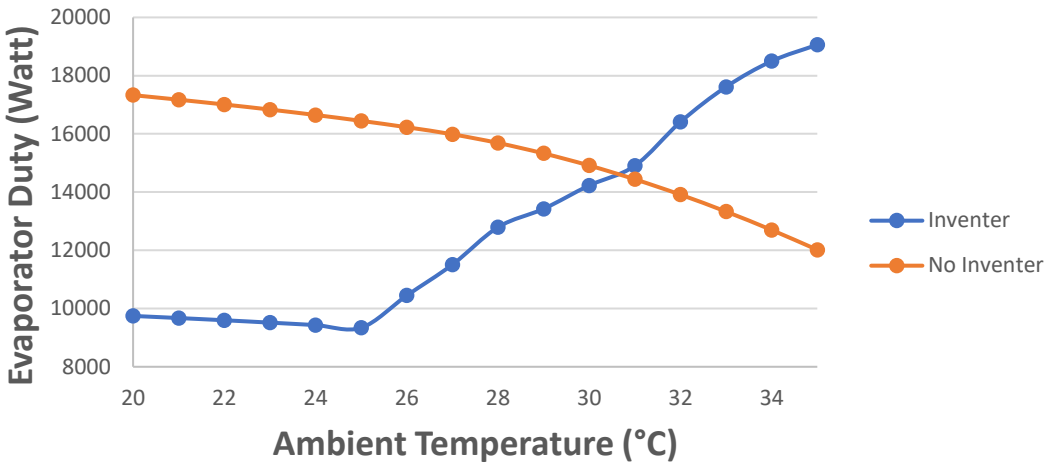

Figure 6.21: A comparison of the evaporator duty.

The Figure 6.22 below shows a comparison between the power fan consumptions. The power fan for the inverter system increases with the increase of the ambient temperature while for the no–inverter system the fan power decreases.

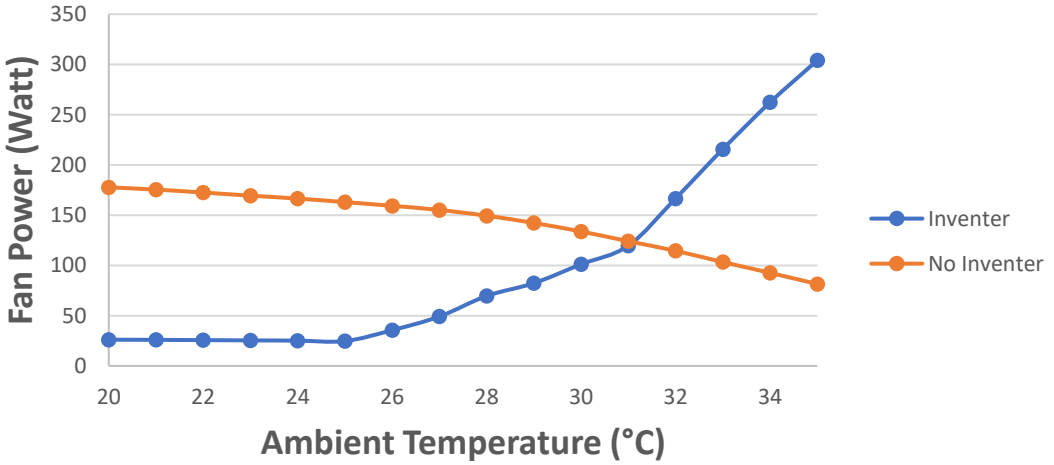

Figure 6.22: A comparison of the fan power.

The Figure 6.23 below depicts the COP of those systems. It is noticeable that the system including inverter has always better COP than without. As it is referred, the inverter system has the capability to regulate the refrigerant mass flow regarding the ambient temperature. In that way, the system works more efficiently.

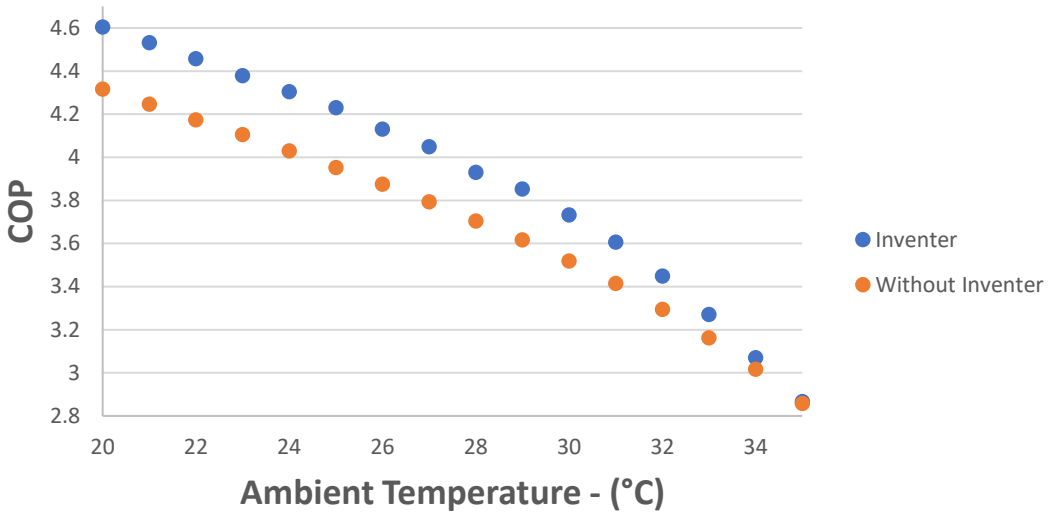

Figure 6.23: A comparison of the coefficient of performance.

It is crucial to refer that the performance of the overall system takes into consideration only the off-design performance of the gas cooler and not from the other components.

6.2. ESEER – European seasonal energy efficiency ratio

The design of the inverter system was carried out according to the European seasonal energy efficiency ratio. On the other hand, the no-inverter system cannot follow the European Standards in this context. However, the no–inverter systems can follow the European Standards with other methods such as regulating the pressure process of the system, but this method is not included in the scope of this thesis so it will not be investigated. The ESEER is calculated by equation including full and part load operating Energy Efficiency Ratio (EER) for different seasonal air temperatures including for appropriate weighting factors and it gives an idea about the overall energy efficiency of the system. The table 6.3 below shows these values.

Table 6.3: European Seasonal Energy Efficiency [28].

	Partial Load Factors	**T_{ai} [°C]**	**T_{wi} [°C]**	**Weighting Factor**
EER A	100%	35	30	3%
EER B	75%	30	26	33%
EER C	50%	25	22	41%
EER D	25%	20	18	23%

The formula for ESEER is [28]:

$$ESEER = (3 \cdot EER_{100\%} + 33 \cdot EER_{75\%} + 41 \cdot EER_{50\%} + 23 \cdot EER_{25\%})/100 \qquad 6.1$$

6.2.1 ESEER of the inverter system

According to the European Standards, the inverter system has been designed in order to achieve an ESSER as high as possible. In our case, the systems are able to achieve till 50 % of the partial load. For each partial load, the energy efficiency ratio found out. As the system is not able to achieve the 25 % of the partial load, in the formula for the ESSER a partial load of 50 % was used, instead. The results are shown in the Table 6.4 below.

Table 6.4: Inverter - European seasonal energy efficiency.

	Tai	Partial Load	EER	Weighting Factor
EER A:	35	100%	2.86	0.03
EER B:	30	75%	3.73	0.33
EER C:	25	50%	4.23	0.41
EER D:	20	51%	4.60	0.23
ESEER:	4.11			

The ESSER is a number that indicates how much energy efficient a mechanical system is. According to the European Standards, based on the ESSER a mechanical system can be classified by a letter that indicates its efficient class. Table 6.5 below shows the letters according to the ESSER number.

Table 6.5: Energy Efficient Class [28].

Energy Efficient Class	
A	3.20<ESEER
B	3.20>ESEER>3.00
C	3.00>ESEER>2.80
D	2.80>ESEER>2.60
E	2.60>ESEER>2.40
F	2.40>ESEER>2.20
G	2.20>ESEER

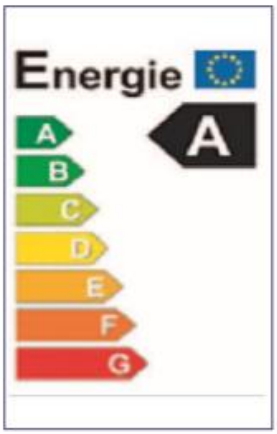

The inverter system has ESSER number higher than 3.20. That means the energy efficiency of the system can be described from the letter A.

6.3. Summary

An overview of the gas cooler performance and its impact on the COP of the overall system in different off-design conditions has been carried out. Furthermore, a comparison of the off-design performance of the two systems (inverter, no-inverter) has been conducted in terms of COP. It is noticeable that the gas cooler's design works properly since the pressure drop does not affect the COP of the system as the Figure 6.4 and 6.14 show for the inverter and no-inverter, accordingly. Moreover, the COP of the systems (inverter, no-inverter) decreases while the ambient temperature increases due to the difficulties of the system to

reject heat energy to the environment. The inverter system has significantly higher COP than the no-inverter due to its capability to regulate the refrigerant mass flow according to the ambient temperature (Figure 6.23). A system including an inverter is a way in order to follow the European Standards and enhance the efficiency of the system. The inverter system follows the European Standards acceptable with a number of ESSER of 4.11 (Table 6.4) and based on that number the system classified in the energy efficient class A (Table 6.5). In a no-inverter case, the system cannot follow the European Standards without other processes taking place such as regulation of the process pressure according to the ambient temperature.

Chapter 7. Conclusions and recommendations for future work

The use of carbon dioxide (CO_2) has emerged as a nature refrigerant to replacing HFCs as it is non-flammable, non-toxic with good thermophysical properties. Refrigeration systems using CO_2 should take into consideration the unique thermophysical properties of CO_2 which impose special design considerations.

In this thesis, a comprehensive investigation of the gas cooler was conducted. On- and off-design analysis of the gas cooler took place and also an experiment was carried out so as to validate the calculations and the heat transfer correlations.

In more detail, the research involved:

- An introduction in refrigeration and air-conditioning systems. A literature review of the CO_2 as a refrigerant and, the different CO_2 refrigeration systems.
- A literature review of the types of gas coolers and the heat transfer and pressure drop correlations.
- Introduction to the residential CO_2-air conditioning project which took place at the University of Bayreuth, Energy Department. Definition of its boundary conditions and based on that, a definition of the on-design point with respect to the use of an inverter.
- On-design analysis of the gas cooler based on the design point and a detailed analysis of the design of the gas cooler.
- Validation of the model and quantification of the deviations in the context of different heat transfer correlations.
- Off-design performance and thermodynamic analysis of the gas cooler according to the European Seasonal Energy Efficiency Ratio (ESEER).

7.1. Conclusions

- The investigation between potential air-conditioning systems revealed that the system with two expansion valves and an internal heat exchanger operates more properly than the others (Chapter 3).
- A compromise between the bundle area and the pressure drop has been achieved. The heat exchanger with 4 number of rows has lower bundle area than with 3 number of rows (Figures 4.5, 4.6 and 4.7 for inverter system and the Figures 4.11, 4.12 and 4.13 for no-inverter). The investigation for potential finned tube showed that the finned tube with the smallest diameter has the lowest bundle area (Figure 4.8 for inverter and Figure 4.14 for no – inverter). On the other hand, the pressure drop works in a reverse way, the smallest diameter has the highest pressure drop (Figures 4.9, 4.10 for inverter and 4.15 for no-inverter). Finally, a gas cooler with a bundle area of 2.106 m^2 and a finned tube with an outside diameter of d_o=18.5 mm was defined for the system including an inverter while for the no-inverter system a gas cooler with a bundle area of 1.17 m^2 and a finned tube with an outside diameter of d_o=7.35 mm (Tables 4.2 and 4.3, accordingly).

- Validation of the off-design calculations based on an experiment using a specific condenser that used water as a working fluid and, took place at the University of Bayreuth, Energy Department. The results showed that the deviations are varied according to different water mass flows, water inlet temperatures and different fan frequencies. Furthermore, different heat transfer correlations have been investigated for the refrigerant and air side heat transfer coefficient. It could be mentioned that the Gnielinski with VDI-Heat Atlas for refrigerant and air side heat transfer correlation for the refrigerant and air transfer coefficient accordingly, have the best results. Based on these correlations, the average deviations for 60 – 80 Hz are less than 13% for different water inlet temperatures. As far as the refrigerant heat transfer correlations, it could be mentioned that the differences are about 1% while for the air side the differences are noticeable.
- An overview of the gas cooler performance and its impact on the COP of the overall system in different conditions was carried out. A comparison of the off-design performance of the two systems (inverter, no-inverter) was conducted in terms of COP. It is noticeable that the gas cooler's design works properly since the pressure drop does not affect the COP of the system as the Figure 6.4 and 6.14 show for the inverter and no – inverter, accordingly. Moreover, the COP of the systems (inverter, no-inverter) decreases while the ambient temperature increases due to the difficulties of the system to reject heat energy to the environment. The inverter system has significantly higher COP than the no-inverter due to its capability to regulate the refrigerant mass flow according to the ambient temperature (Figure 6.23). A system including an inverter is a way in order to follow the European Standards and enhance the efficiency of the system. The inverter system follows the European Standards acceptable with a number of ESSER of 4.11 (Table 6.4) and based on that number the system classified in the energy efficient class A (Table 6.5). In a no-inverter case, the system cannot follow the European Standards without other processes taking place such as a regulation of the process pressure according to the ambient temperature.

7.2. Recommendations for future work

As the no-inverter system cannot follow the European Standards (Table 6.3) without other processes taking place, it is recommended an investigation for how a no-inverter system can follow them. No-inverter systems regulate the pressure in order to follow these Standards. This investigation would give the potential for a more comprehensive and complete comparison between the inverter and no-inverter system.

References

1. Danfoss, *Danfoss_ARTICLE_Transcritical Refrigeration Systems with Carbon Dioxide (CO2)*.
2. Torrella, E., et al., *Energetic evaluation of an internal heat exchanger in a CO2 transcritical refrigeration plant using experimental data.* International Journal of Refrigeration, 2011. **34**(1): p. 40-49.
3. Joneydi Shariatzadeh, O., et al., *Comparison of transcritical CO2 refrigeration cycle with expander and throttling valve including/excluding internal heat exchanger: Exergy and energy points of view.* Applied Thermal Engineering, 2016. **93**: p. 779-787.
4. Kadam, A.D., A.S. Padalkar, and V.U. Walekar, *Comparative Study of trans-critical CO2 cycle with and without suction line heat exchanger at high ambient temperature*. Vol. 3. 2013.
5. Yang, W.-w., et al., *Theoretical study of a high-temperature heat pump system composed of a CO2 transcritical heat pump cycle and a R152a subcritical heat pump cycle.* Applied Thermal Engineering, 2017. **120**: p. 228-238.
6. Llopis, R., et al., *Subcooling methods for CO2 refrigeration cycles: A review.* International Journal of Refrigeration, 2018. **93**: p. 85-107.
7. Elbel, S. and N. Lawrence, *Review of recent developments in advanced ejector technology.* International Journal of Refrigeration, 2016. **62**: p. 1-18.
8. Ge, Y.T. and S.A. Tassou, *Performance evaluation and optimal design of supermarket refrigeration systems with supermarket model "SuperSim". Part II: Model applications.* International Journal of Refrigeration, 2011. **34**(2): p. 540-549.
9. Elbel, S. and P. Hrnjak, *Experimental validation of a prototype ejector designed to reduce throttling losses encountered in transcritical R744 system operation.* International Journal of Refrigeration, 2008. **31**(3): p. 411-422.
10. Lin, C., et al., *Experimental study on the separator in ejector-expansion refrigeration system.* International Journal of Refrigeration, 2019. **100**: p. 307-314.
11. Lucas, C. and J. Koehler, *Experimental investigation of the COP improvement of a refrigeration cycle by use of an ejector.* International Journal of Refrigeration, 2012. **35**(6): p. 1595-1603.
12. Nakagawa, M., A.R. Marasigan, and T. Matsukawa, *Experimental analysis on the effect of internal heat exchanger in transcritical CO2 refrigeration cycle with two-phase ejector.* International Journal of Refrigeration, 2011. **34**(7): p. 1577-1586.
13. https://emergentcoils.com/pages/micro-condenser-coils.
14. Solutions, W.T. http://www.wieland-thermalsolutions.com/internet/en/products/finned_tubes/hochberippte_rohre/Hochberippte_Rohre.jsp.
15. http://www.wermac.org/equipment/air-cooled_heatexchanger.html.
16. Atlas, V.H., *VDI Heat Atlas*.
17. Pitla, S.S., E.A. Groll, and S. Ramadhyani, *New correlation to predict the heat transfer coefficient during in-tube cooling of turbulent supercritical CO2.* International Journal of Refrigeration, 2002. **25**(7): p. 887-895.
18. Gnielinski, V., *On heat transfer in tubes.* International Journal of Heat and Mass Transfer, 2013. **63**: p. 134-140.
19. Jackson, J.D., *Fluid flow and convective heat transfer to fluids at supercritical pressure.* Nuclear Engineering and Design, 2013. **264**: p. 24-40.
20. Incropera, *Fundamentals of heat and mass transfe*.
21. Schmidt, E.F., *Wärmeübergang und Druckverlust in Rohrschlangen.* Chemie Ingenieur Technik, 1967. **39**(13): p. 781-789.
22. Gianolio, E. and F. Cuti, *Heat Transfer Coefficients and Pressure Drops for Air Coolers with Different Numbers of Rows Under Induced and Forced Draft.* Heat Transfer Engineering, 1981. **3**(1): p. 38-48.

23. Tsamos, K.M., et al., *Energy analysis of alternative CO2 refrigeration system configurations for retail food applications in moderate and warm climates.* Energy Conversion and Management, 2017. **150**: p. 822-829.
24. Ge, Y.T. and R.T. Cropper, *Simulation and performance evaluation of finned-tube CO2 gas coolers for refrigeration systems.* Applied Thermal Engineering, 2009. **29**(5): p. 957-965.
25. Han, D.H. and K.-J. Lee, *Single-phase heat transfer and flow characteristics of micro-fin tubes.* Applied Thermal Engineering, 2005. **25**(11): p. 1657-1669.
26. Mori, K., et al., *Cooling Heat Transfer Characteristics of CO2 and CO2-Oil Mixtures at Supercritical Pressure Conditions*. Vol. 20. 2011. 407-412.
27. Kuang, G., M. Ohadi, and Y. Zhao, *Experimental Study of Miscible and Immiscible Oil Effects on Heat Transfer Coefficients and Pressure Drop in Microchannel Gas Cooling of Supercritical CO2*. Vol. 2003. 2003.
28. Müller, C., *Leistungszahlen für Kälte-, Klima- und Wärmepumpensysteme.*

Appendix A: Panasonic condenser and experimental equipment

Entire Geometry	Width	mm	37.8
	Height	mm	586
	Depth	mm	770
Tube Side Geometry	Material		Copper (A1050)
	Shape		L-shaped pipe
	Outer Diameter	mm	7.35
	Wall Thickness	mm	0.25
	Length	mm	Front:750 Back:770
	Rows	-	32
	Columns	-	2
Fin side Geometry	Material		Aluminum (C1220T)
	Shape		Corrugated fin
	Width	mm	18.9
	Height	mm	586
	Thickness	mm	0.1
	Number of sheet		Front:563 Back:585 Total:1,148

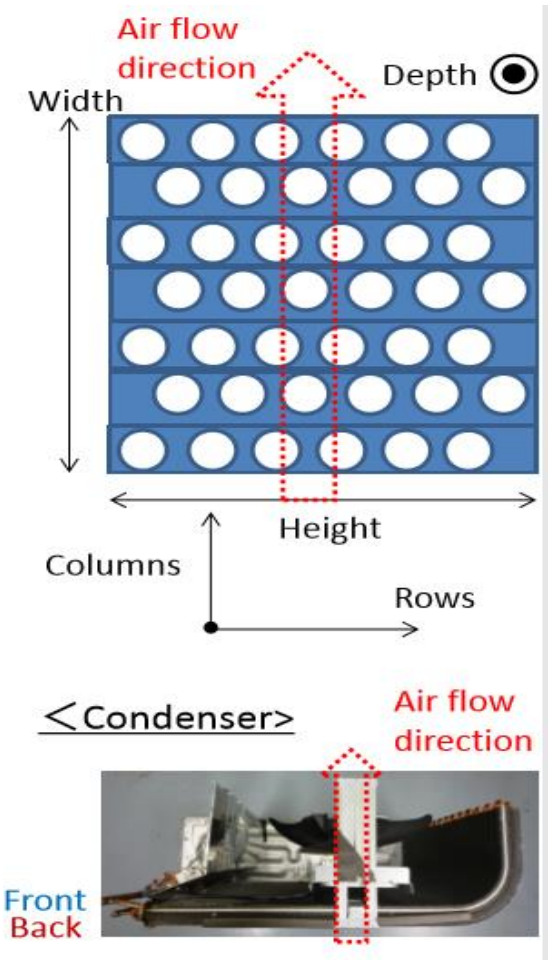

Condenser: Panasonic CU – 713CX2

Pipes: Germany – Bund '' 61537

Heater: Single – STW 150/1 – 18 -45 – KS7

Pressure sensors: PAA21Y – C – 6 – M12 OMEGA

Temperature sensors: M12JSS-M3-U-200-A OMEGA

Mass Flow valve: Burkert 8630

Appendix B: Off – design performance tables

Off-design performance - inverter system

P_{CO2i}	P_{CO2o}	T_{ai}	T_{ao}	T_{co2i}	T_{co2o}	Q_{ev}	Q_{gc}	$Comp_{Power}$	m_{co2}	m_a	w_o	COP	COP_{new}
[bar]	[bar]	[°C]	[°C]	[°C]	[°C]	[Watt]	[Watt]	[Watt]	[kg/h]	[kg/h]	[m/s]	-	-
93	92.969	20	27	78.3	20.02	9747	11836	2089	184	93.15	0.62	4.61	4.61
93	92.968	21	28	79.3	21.03	9674	11782	2108	184	92.79	0.62	4.53	4.53
93	92.968	22	29	80.3	22.03	9598	11725	2127	184	92.29	0.62	4.46	4.46
93	92.968	23	30	81.2	23.04	9517	11663	2146	184	91.80	0.62	4.38	4.38
93	92.968	24	31	82.2	24.05	9432	11596	2164	184	91.30	0.62	4.30	4.30
93	92.968	25	32	83.2	25.07	9341	11523	2182	184	90.60	0.61	4.23	4.23
93	92.960	26	33	84	26.12	10447	12934	2487	208	101.67	0.69	4.13	4.13
93	92.950	27	34	84.7	27.2	11509	14305	2795	233	112.59	0.77	4.05	4.05
93	92.941	28	35	88.6	28.31	12794	15978	3184	257	125.66	0.86	3.93	3.93
93	92.930	29	36	85.9	29.48	13426	16837	3411	282	132.37	0.91	3.85	3.85
93	92.919	30	37	86	30.71	14228	17939	3711	306	141.14	0.97	3.73	3.73
93	92.907	31	38	86	32.01	14905	18912	4007	330	148.68	1.03	3.61	3.61
93	92.880	32	39	85.8	33.52	16409	20999	4589	379	165.14	1.14	3.45	3.45
93	92.849	33	40	85.5	35.09	17615	22783	5168	428	179.17	1.24	3.27	3.27
93	92.813	34	41	85.3	36.61	18498	24244	5746	476	190.51	1.33	3.08	3.07
93	92.772	35	42	85.1	38	19062	25383	6322	525	199.50	1.39	2.88	2.87

Off-design performance - no-inverter system

P_{CO2i}	P_{CO2o}	T_{ai}	T_{ao}	T_{co2i}	T_{co2o}	Q_{ev}	Q_{gc}	$Comp_{Power}$	m_{co2}	m_a	w_o	COP	COP_{new}
[bar]	[bar]	[°C]	[°C]	[°C]	[°C]	[Watt]	[Watt]	[Watt]	[kg/h]	[kg/h]	[m/s]	-	-
93	92.695	20	27	78.1	20.38	17330	21163	3834	331	166.77	2.00	4.32	4.32
93	92.693	21	28	79	21.43	17174	21040	3866	331	165.78	1.99	4.25	4.25
93	92.691	22	29	79.9	22.5	17009	20908	3899	331	164.58	1.98	4.18	4.17
93	92.690	23	30	80.9	23.58	16835	20766	3931	331	163.31	1.97	4.11	4.11
93	92.688	24	31	81.8	24.67	16648	20611	3963	331	162.12	1.97	4.03	4.03
93	92.686	25	32	82.7	25.79	16447	20442	3995	331	160.72	1.96	3.95	3.95
93	92.683	26	33	83.7	26.92	16228	20256	4027	331	159.25	1.94	3.88	3.88
93	92.681	27	34	84.6	28.08	15986	20044	4058	331	157.64	1.93	3.80	3.79
93	92.678	28	35	85.2	29.28	15688	19768	4080	331	155.49	1.91	3.71	3.71
93	92.675	29	36	85.6	30.5	15329	19422	4092	331	152.78	1.88	3.62	3.62
93	92.672	30	37	85.8	31.76	14913	19012	4099	331	149.59	1.85	3.52	3.52
93	92.668	31	38	85.9	33.04	14440	18541	4101	331	145.77	1.81	3.42	3.41
93	92.664	32	39	85.9	34.34	13912	18013	4101	331	141.89	1.77	3.30	3.29
93	92.658	33	40	85.9	35.63	13330	17431	4101	331	137.11	1.71	3.17	3.16
93	92.651	34	41	85.9	36.86	12698	16799	4101	331	132.19	1.66	3.03	3.02
93	92.643	35	42	85.9	38	12018	16119	4101	331	126.73	1.59	2.88	2.86